POLITECNICO DI MILANO

Scuola di Ingegneria Industriale e dell'Informazione
Dipartimento di Chimica, Materiali e Ingegneria Chimica "Giulio Natta"
Master's Degree in Materials Engineering and Nanotechnology

Functionalized carbon black for elastomeric composites with improved crosslinking efficiency and lower dissipation of energy

Supervisor: Prof. Maurizio Stefano Galimberti
Advisor: Francesco Moriggi

Master's Thesis by:
Marco Mondovì
ID number: 918988

Academic year 2019-2020

To my
Beautiful
Family

Table of contents

List of Figures

List of Tables

List of Abbreviations

6PPD: (1,3-dimethyl butyl)-N'-Phenyl-p-phenylenediamine

BR: Synthetic poly (1,4-butadiene)

CB: Carbon Black

CB-PyC: adduct between carbon black and pyrrole compound

CB/EAP: adduct between carbon black and mono-ethanolammine pyrrole

CB/p-PDAP: adduct between carbon black and p-phenylenediamine pyrrole

CB/TETAP: adduct between carbon black and triethylenetetramine pyrrole

CNT: Carbon Nanotubes

CVD: chemical vapor deposition

DA: Diels-Alder

DM: different mixing

DPG: dipropylene glycol

GC: gas chromatography

GC-MS: gas chromatography-mass spectrometry

HD: 2,5-hexanedione

HSP: Hansen solubility parameter(s)

M_H: highest achievable torque

M_L: lowest achievable torque

MS: mass spectrometry

MWCNT: Multi Walled Carbon Nanotubes

NMR: Nuclear magnetic resonance

NR: Natural rubber

phc: parts per hundred carbon

phr: parts per hundred rubber

PyC: Pyrrole compound(s)

SBR: Styrene-Butadiene rubber

SWCNT: Single Walled Carbon Nanotubes

T_{90}: optimal vulcanization time

T_g: polymer's glass transition temperature

T_{S1}: scorch time

TBBS: N–tert-butyl-2-benzothiazyl sulfenamide

TESPT: bis(3-triethoxysilylpropyl) tetrasulfide

TESPD: bis(3-triethoxysilylpropyl) disulfide

TGA: Thermogravimetric analysis

Abstract

Rubber composites need to be efficiently crosslinked and reinforced to achieve the dynamic-mechanical properties required by tyre application.

In this thesis, carbon black was functionalized with pyrrole compounds and was used in rubber composites with only carbon black or with carbon black/silica as the filler system.

A sustainable, facile, versatile, not expensive method was applied for the carbon black functionalization with pyrrole derivatives. Pyrrole compounds were synthesized in the absence of solvents or catalysts from the Paal-Knorr reaction between a primary amine and 2,5-hexanedione.

Carbon black adducts were investigated through the evaluation of Hansen solubility parameters and via pH measurements in water dispersions.

Elastomeric compounds were prepared with natural rubber and butadiene rubber and were characterized by means of dynamic-mechanical and tensile properties.

The behavior of functionalized carbon black, in total or partial replacement of the pristine filler, alone or in a filler system carbon black/silica, was studied.

Properties variation due to the presence of functionalized carbon black were registered. In particular, faster vulcanization kinetics, higher stiffness and increased viscosity were common characteristics of all the compounds with functionalized carbon black. In some cases, lower hysteresis and filler network were registered, thus contributing to a lower fuel consumption and CO_2 emissions.

Riassunto

Questa tesi è focalizzata su compositi elastomerici basati su polimeri dienici e carbon black funzionalizzato con composti pirrolici, utilizzato come carica rinforzante da solo o in un sistema di cariche ibride carbon black/silice.

La funzionalizzazione del carbon black con i derivati pirrolici è avvenuta attraverso un metodo sostenibile, facile, versatile e non costoso. I composti pirrolici sono stati sintetizzati in assenza di solventi o catalizzatori tramite la reazione di Paal-Knorr tra un'ammina primaria e 2,5-esanedione.

Gli addotti di carbon black sono stati studiati attraverso la stima dei loro valori di pH in dispersioni acquose e dei parametri di solubilità di Hansen.

I compositi elastomerici sono stati preparati con gomma naturale e gomma butadiene e sono stati caratterizzati attraverso lo studio delle proprietà dinamico-meccaniche e di trazione.

È stato studiato il comportamento del carbon black funzionalizzato, in sostituzione totale o parziale della carica rinforzante pura, da solo o in un sistema di cariche rinforzanti ibride carbon black/silice.

La presenza del carbon black funzionalizzato ha portato a dei cambiamenti nelle proprietà dei compositi elastomerici. In particolare, le seguenti caratteristiche erano comuni a tutti i compositi con carbon black funzionalizzato: una cinetica di vulcanizzazione più rapida, una maggiore rigidità e un aumento nella viscosità. In alcuni casi è stata registrata anche una riduzione dell'isteresi ed una migliore interazione carica rinforzante-polimero, contribuendo così a un minor consumo di carburante ed emissioni di CO_2.

Chapter 0

Introduction

Rubbers: fundamental materials

Rubbers are fundamental materials for the life of human beings. They are used for many and important applications, from gaskets to compounds for tyre. The latter one is the most important application for rubbers and accounts for about 70-75% of their consumption.

Charles Goodyear said: "There is probably no other inert substance the properties of which excite in the human mind an equal amount of curiosity, surprise and admiration. Who can examine and reflect upon this property of gum-elastic without adoring the wisdom of the Creator?" [1]. Elasticity is indeed a fascinating property and the vulcanization, discovered by Goodyear, plays the key role of crosslinking the polymer chains, thus allowing the occurring of entropic elasticity.

However, the dynamic-mechanical properties of rubbers, even after crosslinking, are not enough for the applications of rubber materials: rubbers have to be reinforced. Hence, the so-called reinforcing fillers are added to the rubber compounds, in order to achieve the required values for properties such as stresses at different elongations, tensile strength, dynamic modulus, tear, fatigue and abrasion resistance.

In conclusion, the best properties of a rubber compound are achieved upon crosslinking and reinforcing and this requires the accurate tuning of the crosslinking and reinforcing systems.

The crosslinking systems

Many types of crosslinking systems exist. The most important ones are based either on peroxides or on sulphur and sulphur-based chemicals. For tyre compounds, the sulphur-based systems are almost exclusively used. Besides sulphur, they contain chemicals, typically sulphenamides, which promote the formation of covalent bonds with the polymer chains and faster vulcanization reactions. They are named accelerators and are or form bases in the rubber matrix. In compounds with an acidic filler such as silica, amines (named secondary accelerators) are added on purpose to offset the effect of silica and thus to allow an efficient vulcanization. Indeed, an efficient vulcanization reaction is mandatory, to ensure high productivity and reproducibility of rubber compounds, particularly in the case of demanding dynamic-mechanical applications such as those for tyres. Frequently, the accelerators, in particular the secondary accelerators, have critical safety data sheets and research is in progress to replace them with safer substances. It would be highly desirable to have an efficient vulcanization reaction avoiding the addition of chemicals, particularly if such chemicals are critical for the impact on the human health and the environment.

The reinforcing fillers

Carbon black (CB) and silica are the most important reinforcing fillers for rubber composites. These are used on a large scale, particularly in tyre compounds: CB since the beginning and silica since the 1990's of the last century. In particular, silica is the preferred filler nowadays, because it allows to pursue and to achieve low dissipation of energy. This is due to the fact that silica is able to establish a link with the elastomer chains, due to the chemical reaction with a coupling agent. A carbon material, chemically reactive with the rubber chains, could be in principle able to reproduce the properties of a silica-based compound. The silica-based compounds are increasingly used in tyres and silica is replacing, completely or partially, carbon black. Compounds are made with the carbon black / silica binary filler system, though the lack of compatibility between the two fillers does not allow to achieve their real potential. It would be clearly desirable to improve the compatibility between carbon black and silica. A way to achieve such a goal could be the modification of the surface of carbon black.

The functionalization of sp^2 carbon allotropes

It is worthwhile to dwell upon the functionalization of CB and, more in general, of sp^2 carbon allotropes. Oxidation of CB dates back to the late 1800's and, in the last decade, has been applied to graphite for the preparation of graphene oxide. Methods are documented also for the introduction on the CB surface of sulphur and nitrogen containing groups. The mentioned reactions require different chemicals, follow different pathways and are often characterized by the use of dangerous and noxious reagents.

The research groups where this thesis was done has recently developed a functionalization method able to modify the surface of sp^2 carbon allotropes with a variety of functional groups, by performing the same reaction, which can be defined sustainable, as it occurs by simply mixing the functionalizing agent and the carbon material, donating then either mechanical or thermal energy, in the absence of solvents or catalysts. The functionalizing agent is a pyrrole compound of the general chemical structure shown in Figure 0.1.

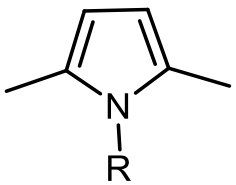

Figure 0.1 The general chemical structure of the pyrrole compound.

The mechanism of the functionalization has been elucidated [2] and it is shown in Figure 0.2.

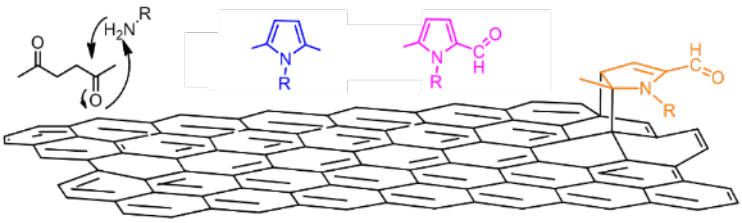

Figure 0.2 Mechanism proposed for the functionalization of graphene layers with pyrrole compounds.

This functionalization method has been named as "pyrrole methodology". In the light of the above reported mechanism, the pyrrole compound forms a covalent bond with the carbon substrate. Moreover, by changing the R group, a variety of substituents are introduced onto the carbon surface.

Objectives of the thesis and description of the research activity

The main objectives of the present thesis were:

- to achieve faster and efficient vulcanization reactions
- to promote better compatibility between carbon black and silica

thanks to the chemical modification of the surface of carbon black and thus without the addition of any further chemical to the rubber compound.

An important objective of the research was to achieve the abovementioned objectives without adding any secondary accelerators. As mentioned above, chemicals such as the secondary accelerators are often characterized by critical safety data sheets. Their use in factories as well as their leakage from the compounds is a source of concerns. Moreover, the migration of the accelerators in a multi-phase material, such as a tyre, leads to alter the vulcanization kinetics and to damage the properties of the compounds.

It is worth underlining the objective of performing functionalization reactions in the light of the principles of green chemistry, avoiding the use of dangerous and noxious reagents, applying a simple functionalization method, made by few steps, achieving high atom efficiency, in particular carbon efficiency.

The pyrrole methodology was used for the functionalization of furnace carbon black.

To achieve the above reported objectives, new pyrrole compounds were synthesized. Pyrrole derivates used for the functionalization were obtained from the Paal Knorr reaction of 2,5-hexanedione with the primary amines shown in Figure 0.3 a and 0.3 b.

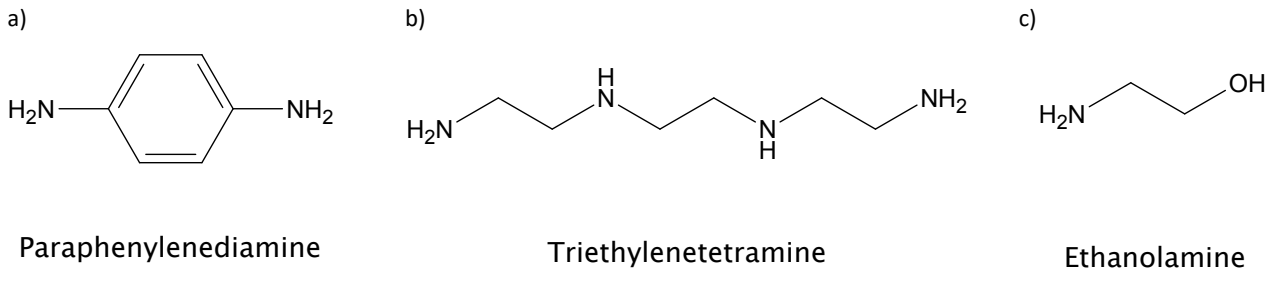

Figure 0.3. a) paraphenylenediamine, b) triethylenetetramine, c) ethanolamine.

The structure of these primary amines reveal that they were selected in order to add bases onto the CB surface. Such bases should be able to promote

- a more efficient vulcanization.
- a better compatibility of CB with silica.

A further pyrrole compound was prepared, starting from ethanol amine, shown in Figure 0.3.c. The objective was to compare the behaviors of the adducts containing the bases and of the adduct containing the OH group, which should be able, in principle, at least to establish an interaction with the silanols of silica.

The functionalization reactions were performed by donating thermal energy to the CB/PyC mixture, determining then the yield of functionalization.

The adducts were investigated, estimating their Hansen solubility parameters and the pH of water dispersions.

The CB/PyC adducts were used in rubber compounds:

- with CB as the only filler, to investigate the effect of the adduct on the vulcanization reaction
- with the hybrid CB/silica filler system, to investigate the effect of the adduct on the compatibility of CB with silica.

The compounds were prepared by melt blending, using a brabender® type internal mixer.

Vulcanization reaction was studied by performing a rheometric test.

Dynamic-mechanical properties were determined by applying sinusoidal stresses in the shear and in the axial mode.

Quasi static measurements were used to assess the tensile properties.

References

[1] Goodyear, C. “Gum elastic and its variation with a detailed account of its applications and uses” **1855**, 1, New Haven.

[2] Barbera, V., Brambilla, L., Milani, A., Palazzolo, A., Castiglioni, C., Vitale, A., ... & Galimberti, M. (2019). Domino Reaction for the Sustainable Functionalization of Few-Layer Graphene. Nanomaterials, 9(1), 44.

Section I – State of art

Chapter 1
Overviews on rubber

1.1. Introduction

A rubber is a natural or synthetic polymer which has a very high deformability and the capability to recover completely. Being a common elastomer, the typical value of the Young modulus is in the order of 10^6 Pa and its strain at break is 10^3 % [1]. In order to be considered as a rubber, a material has to show the following properties:

- The material must be macromolecular and therefore a high molecular weight is required with the presence of many entanglements.
- In order to guarantee the right flexibility to the chains, the material's Tg must be below room temperature. Elastomers generally have Tg in the range of 233K/253K in order to show rubberlike behavior at room temperature.
- The elastomer must have low secondary forces between the molecules to show the right flexibility.
- The material has to be slightly crosslinked.
- The material has to be essentially amorphous. It is characterized by a random coil conformation in its undeformed state.

There are two main types of rubbers: natural rubbers (NR) and synthetic rubbers (SR). The main industrial applications for rubbers are in the tires industries (75%), in chemical industries (12.4%), and as latex (12.3%).[2]

Thailand, Indonesia, Malaysia and India are the world leading manufactures for the natural rubber. The world's rubber consumption in 2017 accounted more than 28 millions tons, of which 47% of natural type. It is estimated that in 2023 the consumption will reach 34.6 millions of tons.[3]

1.2. Natural rubber

Natural rubber can be found in *Taraxacum Kok-Saghyz (Russian dandelion)*, *Guayule* and majorly in *Hevea Brasiliensis*. The raw NR polymer is obtained by coagulation of the latex extracted by the above reported trees. Natural rubber is a natural macromolecular compound, containing cis-1,4-

polyisoprene comprising 94 % and the remaining 6% is composed by impurities such as lipids, proteins and other low molecular weight carbohydrates [4].

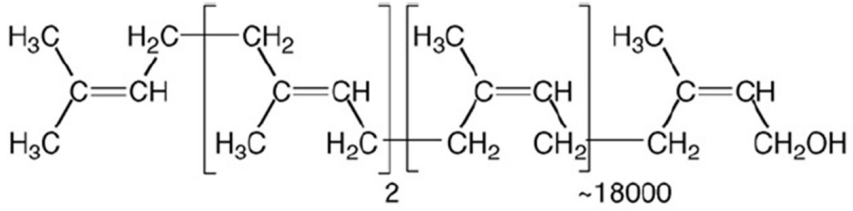

Figure 1.1 Chemical structure of natural rubber.

Natural rubber is characterized by high elasticity, good mechanical strength, high resilience and abrasion resistance. The good mechanical properties at high elongation are a consequence of the controlled stereochemistry (more than 99.9% 1,4 cis). It shows good electrical insulation too. Regarding chemical properties, these are mainly related to the presence of unsaturated double bonds which lead to a good reactivity towards heat, light, ozone and oxygen.
Natural rubber also shows a low impermeability and aging resistance. This is also characterized by a difficult processability. All the unsaturated rubbers can be vulcanized by sulfur.

1.3. Synthetic rubber

Synthetic rubbers derive from various Petroleum-based monomers. Although synthetic rubbers have worse properties with respect to natural rubber, their production is needed because natural rubber resources are becoming scarce and cannot sustain alone the world rubber demand. Anyway, synthetic rubbers show a high degree of flexibility and mobility.
Synthetic rubber production became very important during the second world war in order to provide tires to the war machines. Its production also increased in the 1950s due to a development of the petrol-chemical industries. Today, the annual production of synthetic rubbers is at 15 millions tons per year.[5]
Synthetic rubbers include general purpose synthetic rubbers and specialty elastomers. General purpose synthetic rubbers are those polymers which contain only Carbon and Hydrogen. Polybutadiene (BR) and styrene-butadiene random copolymers (SBR) belong to this family. Specialty elastomers can also contain heteroatoms. This leads to a different solubility parameter and hence they show a better chemical and thermal stability. BR and SBR are going to be described more in detail in the next paragraphs because of their use in tire manufacture. [6]

1.3.1. Styrene-butadiene rubber

SBR results to be the most important synthetic rubber. It can be obtained in a twofold way: through radical polymerization (Emulsion-SBR, E-SBR) and with anionic polymerization (Solution-SBR, S-SBR).[7]

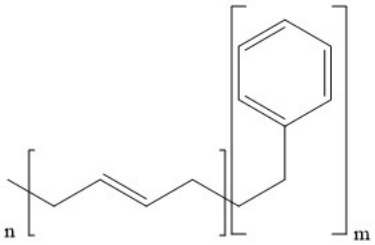

Figure 1.2 Chemical structure of SBR.

Emulsion SBR shows a better processability and minor costs with respect to S-SBR. Emulsion processes guarantee a good control on the composition of the formed copolymer. [8]

The reaction process is reported in the Figure 1.3:

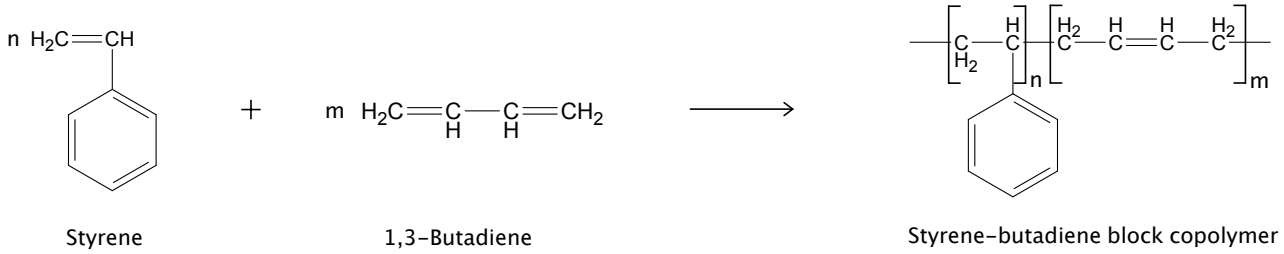

Figure 1.3 Emulsion polymerization of SBR.

The polymerization takes place in presence of mercaptan, which enables to control the molecular weight thanks to the chain transfer mechanism. Hydroperoxide, iron sulphate and EDTA (ethylenediamine tetra-acetic acid) are used as initiators. EDTA's purpose is to increase the solubility of iron salts in water. E-SBR production process has a conversion of about 60%. [6]

Solution SBR (S-SBR) is a living anionic polymerization and the control of the molecular weight is determined by the monomer/initiator ratio. Reactions take place on the chain ends. The first step consists in the synthesis of the first polystyrene block. The solvent is pure and not water based. In this way the polystyrene block end only when all the styrene monomers are consumed. Now the polybutadiene block can be attached. Again, this process ends only when all the butadiene monomers are finished. This process is characterized by a conversion of about 100 %. [6]

S-SBR is preferred respect to E-SBR because it is characterized by a higher conversion, a more controlled and a narrower distribution of molecular weight.

When increasing the styrene content, the rubber becomes stronger. The T_g is also influenced by the relative amount of styrene and butadiene. Glass transition temperature increases proportionally to styrene content.

SBR is mainly used for tires, for technical goods and for latexes.

1.3.2. Butadiene rubber

Polybutadiene rubber (BR) is the second largest synthetic polymer after SBR, and 70 % of its production is used for tire manufacturing.[4] The polybutadiene monomeric unit can arrange in three different configurations that will influence the final properties. These are reported in Figure 1.4:

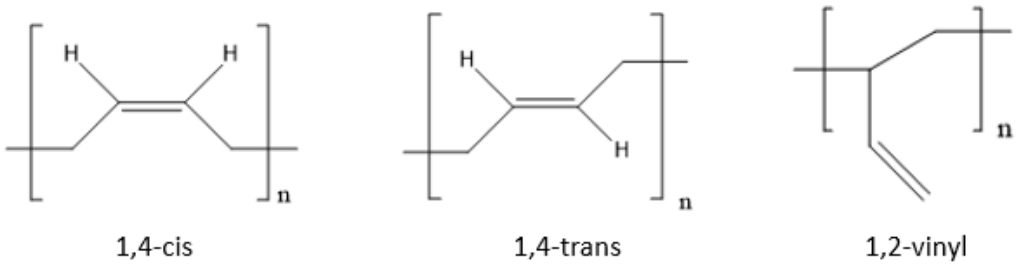

Figure 1.4 Possible molecular configuration for polybutadiene monomeric units.

The type of butadiene that is obtained is determined by the catalyst used for polymerization. The catalysts employed are transition metals and they are: neodymium, nickel, cobalt, titanium and rare earth. Ziegler-Natta catalysts are used to obtain a high stereoregularity. [8,9]

Tire production requires high-cis polybutadiene. Due to its high stereoregularity, the material is able to crystalize under stretching, improving its mechanical properties, in particular its tensile strength, fracture and fatigue behavior. Neodymium and Nichel guarantee the largest cis percentage, respectively 98% and 96%, while alkyl-lithium catalyst is used to obtain low-cis polybutadiene.

Vulcanized polybutadiene rubbers show a better wear resistance and elasticity compared to SBR and natural rubber. Since its Tg is lower than SBR, tire compounds produced with BR are characterized by a longer life and by a lower fuel consume.[10]

1.4. Rubber elasticity theory

Rubber elasticity can be defined as the capability of rubbers to be deformed with a complete recoverability. When applying an external deformation on a material, most of solids show an enthalpic-elastic behavior. The external applied force induces little shifts on the atomic positions and

increases the enthalpic energy. The little atomic displacements do not provide a significant increase in entropy, that can be neglected. In order to restore the equilibrium condition, characterized by a minimum in energy, the system is going to decrease its enthalpy and hence the driving force for the elastic recovery is enthalpic in nature. This behavior, represented in the Figure below, is characteristic of crystalline solids.

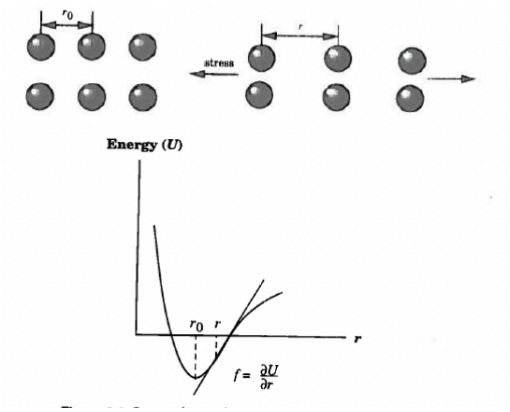

Figure 1.5 Energy-driven elasticity typical of crystalline solids.

Rubbers, instead, present entropic elastic behaviors which are related to the random coil conformation of polymers and to the presence of crosslinks. When an external force is applied, it induces an alignment of the polymeric chains, increasing the order of the system and so decreasing its entropy. Once the external force is removed, the system comes back to the equilibrium state, decreasing its energy. It is made possible by increasing the disorder in order to restore the random coil conformation.[6,11] This mechanism is shown in Figure 1.6:

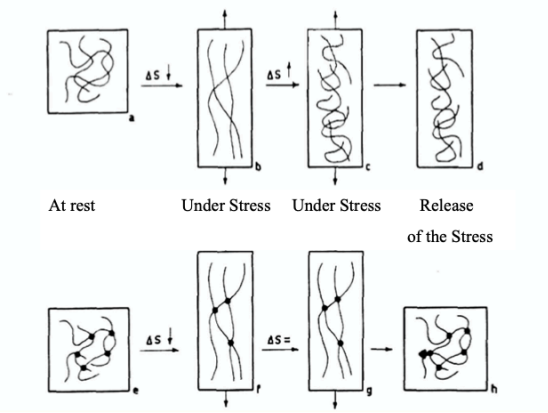

Figure 1.6 Entropic-elastic behavior: without crosslinks (a,b,c,d) ; with crosslinks (e,f,g,h).

The Figure underlines the importance of crosslinks for the elasticity of rubbers. Rubbers show the elastic-recovery only in the presence of crosslinks, which guarantee that polymeric chains do not slip independently.

Several approaches are used to describe the rubber elasticity. Thermodynamic and statistical approaches are reported below. The thermodynamic method is focused on the macroscopic behavior while the statistical approach is based on the molecular structure of rubbers.

1.4.1 Thermodynamic approach

Considering a rubber strip subjected to tension, it is possible to write the following expression related to the work done on the system:

$$dW = -PdV + fdL$$

Where f is the externally imposed force. The applied force induces a change in the internal energy:

$$dU = dW + dQ = -PdV + fdL + TdS$$

It leads to a change in the Gibbs free energy:

$$dG = fdL + VdP - SdT$$

It is possible to write:

$$f = \left(\frac{\partial G}{\partial L}\right)_{T,P} = f_H + f_S = \left(\frac{\partial H}{\partial L}\right)_{T,P} - T\left(\frac{\partial S}{\partial L}\right)_{P,L} = \left(\frac{\partial H}{\partial L}\right)_{T,P} + T\left(\frac{\partial f}{\partial T}\right)_{P,L}$$

The elastic retraction force is given by the sum of two different contributions, one enthalpic and the other entropic. The above-reported equation is known as the equation of state of elasticity at constant pressure. Considering an ideal rubber, it is possible to neglect the enthalpic term and obtain:

$$f \sim -T\left(\frac{\partial S}{\partial L}\right)_{P,L} \sim +T\left(\frac{\partial f}{\partial T}\right)_{P,L}$$

On this basis, in the f/T plot it should be expected a linear behavior in which the restoring force increases with the temperature. However, experimental data show that it is not always true. For low

deformations there is an anomalous behavior, characterized by a negative slope in the σ/T curve. This behavior is reported in the Figure below:

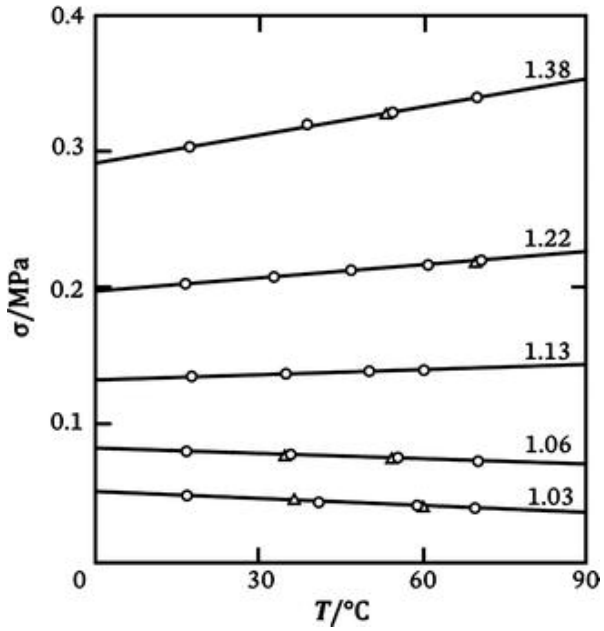

Figure 1.7 Stress at constant length as function of T for different elongations.

It is called thermoelastic inversion. It is possible to put in evidence, from the equation of state of elasticity, the dependence of the restoring force with respect to the temperature:

$$\left(\frac{\partial f}{\partial T}\right)_{P,L} = \frac{f - \left(\frac{\partial H}{\partial L}\right)_{T,P}}{T}$$

For small deformations, ∂L is very low and so the enthalpic term is predominant, leading to a negative slope. Increasing the applied strain, the entropic term becomes more important until the enthalpic term should be neglected. The ideal rubber approximation is valid if small deformations are not taken into account.[6]

1.4.2 Statistical approach

Rubber elasticity can also be explained by means of a statistical description and it is based on the following assumptions:

- The entropic term depends only on the conformations available to the system.
- Conformations of the system are described by a Gaussian distribution function. Chains are considered as volume-less, and so the polymeric chain is defined as a “phantom chain”.

- Affine deformation assumption: the deformation of the single polymeric chain is proportional and coherent to the macroscopic deformation.
- Volume remains constant during the deformation.

Under these assumptions, the following formulation is attained for the force per unit area:

$$\sigma = G\left(\lambda - \frac{1}{\lambda^2}\right), (1)$$

Where λ is the extension ratio in the direction of the uniaxial deformation. G is called modulus of the rubber and it depends on the density of crosslinks (ν') and on the temperature:

$$G = \nu' RT$$

With R as the gas constant. Equation (1) is known as the constitutive equation of elasticity of the rubber. It is relevant to outline the following two properties that emerge from the constitutive equation:

1. For a given strain, when increasing the temperature there is an increase in the stress. Conformations' compactness becomes less probable, and this leads to a raise in entropy. For crystalline solids, the opposite trend is presented due to the different elastic behavior.
2. When the strain is kept constant, an increasing of the crosslinks densities results in an increase in the stress. Mechanical properties are therefore enhanced with an increase of crosslinks.

In the Figure below, a comparison between the real behavior and the predicted one is reported under uniaxial tension conditions:

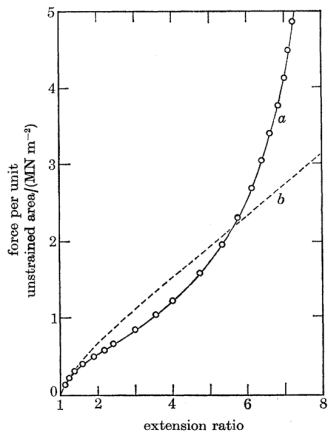

Figure 1.8 Comparison between the stress/strain curve for the real rubber and the theoretical predicted one.[12]

It is possible to notice that the two curves fit quite well for low deformations ($\lambda<1.5$) while the fitting is not precise for bigger values. This discrepancy between real and theoretical behavior is related to the following factors:

- Inadequacy of the Gaussian statistics in the description of the rubber real behavior at high strains.
- Affine assumption hypothesis is not applicable for high deformations.
- The statistical approach disregards crystallization under strain which happens instead in real rubbers.
- Entanglements, loops, sol fraction or dangling bonds are not taken into account.

Statistical approach is quite accurate for the compression behavior of rubbers.[6,12] Figure 1.9 reports the comparison between real and theoretical behavior:

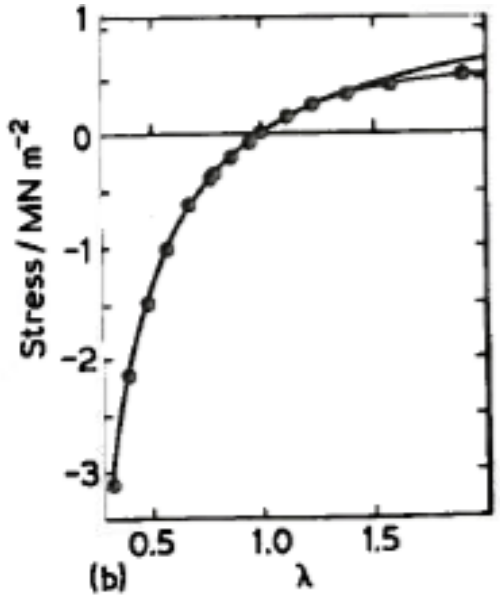

Figure 1.9 Comparison of the stress/strain curve for the real (continuous line) and the theoretical behavior (dots).[6]

References

[1] P. M.Visakh et. Al. *Advances in elastomers I: Blends and interpenetrating networks, 2013.*

[2] M. Galimberti, Course of *"Chemistry for elastomer composites"*, Polytechnic University of Milan, 2020.

[3] https://www.plastmagazine.it/gomma-mercato-internazionale-e-applicazioni/ (last access on 26/03/2021).

[4] A.D. Robets, *Natural rubber science and technology*, Oxford University Press, 1988.

[5] https://www.statista.com/statistics/1097029/global-market-size-of-synthetic-rubber-by-region/ (last access on 26/03/2021).

[6] S. E. Turri, Course of "Advanced chemistry for materials engineering", Polytechnic University of Milan, 2018.

[7] W. Obrecht, J.P. Lambert, M. Happ, C. Oppenheimer-Stix, J. Dunn, R. Krüger, *Ullmann's Encyclopedia of Industrial Chemistry*, *Rubber, 4. Emulsion*, Weinheim: Wiley-VCH, 2012.

[8] H.D. Brandt et al., *Encyclopedia of Industrial Chemistry*, 2012.

[9] W.C. White, *Chemico-Biological Interactions*, 2007, 166 (1–3), 10-14.

[10] J.A. Kent, *Handbook of Industrial Chemistry and Biotechnology (11th Ed.)*, 2006.

[11] Mark JE. Rubber elasticity. J Chem Educ. 1981;58(11):898.

[12] L. R. Treloar, The mechanics of rubber elasticity. *The royal society publishing, 1976, 301-330.*

Chapter 2
Carbon allotropes

2.1. Introduction

Carbon is the fourth most abundant element in the universe and the second in the human body by mass.[1] It can bind with other elements or with itself thanks to three different types of hybridization. Electronic ground state configuration of carbon is $1s^2 2s^2 2p^2$ and it can form sp^1, sp^2 and sp^3 hybridized orbitals. It is possible because 2s-orbitals and 2p-orbital are similar in terms of energy. The sp^3 hybridization is characterized by four identical σ bonds which are tetrahedrally oriented. Sp^2 hybridization is characterized by three equivalent sp^2 orbitals, which can form both σ and π bonds. Sp^2 hybridization leads to a trigonal planar geometry. In the sp hybridization, an s orbital interacts with a lone p orbital generating a sp orbital. The remaining two p orbitals are unaltered. Sp hybridized carbon allotropes are completely planar, such as carbyne.

Solid carbon exists in different allotropic forms, depending on the type of hybridization involved and on the spatial configuration. The work here presented is focused on carbon black, a material based on sp^2 carbon. These concepts are summarized in Figure 2.1.

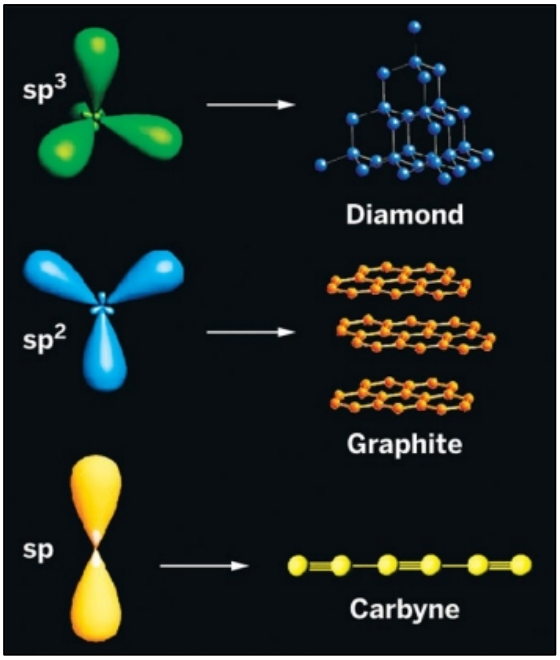

Figure 2.1 Carbon hybrids orbitals associated to carbon allotropes.[2]

2.2. sp^3 hybridization-diamond

Diamond is an allotrope of carbon characterized by sp^3 hybridization. Each carbon atom in diamond is surrounded by other four carbon atoms connected together by strong covalent σ bonds.

Diamond is a metastable form of carbon, which means that it is thermodynamically unstable but kinetically stable. Due to its strong covalent bonds, diamond is the natural mineral characterized by the strongest hardness, equal to ten in the Mohs scale. [3]

Although diamond is an insulator, [4] characterized by a band gap of 5.45 eV, it has the highest thermal conductivity (2200 W/mK). Thanks to its high chemical inertia and hydrophobicity, diamond is able to resist in very aggressive environments.

2.3. sp^2 hybridization

2.3.1. Carbon black

Carbon black (CB) is the most popular reinforcing filler in elastomeric composites because of its ability to increase tensile strength, rolling and abrasion resistance. Nearly 90% of carbon black production is exploited in tire manufacture. [5]

CB is formed by nanometric particles of carbon and it is characterized by a very high surface area that is responsible of the filler-filler and filler-polymer interactions, which are related to the reinforcement in elastomers. Carbon black particles range between 20 and 300 nm.[6] Smaller particles lead to a higher surface area. This is related to the following formula:

$$SA = \frac{surface}{mass} = \frac{(4\pi r^2)}{\left(\frac{4}{3}\pi r^3 \rho\right)} = \frac{6}{\rho r}$$

Where SA stands for surface area, r is the particle radius and ρ is the density. Smaller particles are characterized by higher darkness. Carbon black particles are constituted by overlapping graphitic layers in an onion-like structure, as reported in the Figure below:

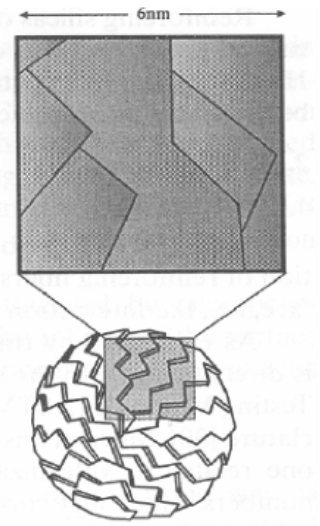

Figure 2.2 Surface morphology of a carbon black nanoparticle.

Carbon black has a structure similar to the graphite but with a random orientation between different layers and so it is characterized by short-range order and long-range disorder [7].

Primary particles group together forming aggregates. They constitute the smallest dispersible unit of carbon black. They are unbreakable and they are considered as the reinforcing objects. For these reasons, aggregates' structure is maintained during rubber processing and cannot be separated during mixing. Aggregates are formed by the coagulation of particles and their structure determine the strength of the reinforcement. Occluded rubber phenomenon is related to the aforementioned structure and it is explained later in detail.

Interaction of aggregates leads to agglomerates, bigger structures that can be broken during processing. Van der Waals forces are the interactions responsible for the strength of the agglomerates, and, because of the weakness of these forces, agglomerates can be easily broken.[8,9] Carbon black morphology is reported in Figure 2.3:

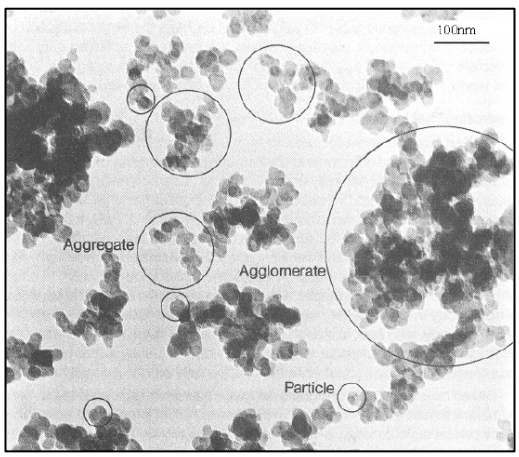

Figure 2.3 Carbon black morphology.

Carbon black is produced by combustion of gas or oil inside large furnaces. Particles' size and structure can be modified controlling the temperature and the pressure inside the furnace.

From the chemical point of view, there are two main production processes: thermal oxidative decomposition and thermal decomposition. The difference relies on either the presence or absence of oxygen. Thermal oxidative processes are, by far, the most used, being responsible for 95% of carbon black production. The principals CB manufacturing processes are summarized in the Table as follows:[10]

Table 2.1 Carbon black manufacture processes.

Chemical Process	Features	Production Process	Feedstock
Thermal Oxidative Decomposition	Closed system	Furnace process black	Aromatic oils based on coal tar or crude oil, natural gas
	Open system	Gas black process	Coal tar distillates
		Channel black process	Natural gas
Thermal Decomposition	Discontinuous	Thermal black process	Natural gas (oil)
	Continuous	Acetylene black process	Acetylene

2.3.2. Fullerenes

Fullerene is constituted by carbon atoms arranged in a quasi-spherical configuration through the sp^2 hybridization. It is constituted by hexagons (like in the graphite) and pentagons (which give the curvature). It is possible to estimate the number of pentagons and hexagons thanks to the Euler's theorem [11].

Euler's theorem links the number of vertices (n), equal to the number of carbon atoms, to the faces (f), and the edges (e), of a solid in the following way:

$$n + f = e + 2$$

Considering that all atoms are sp^2 hybridized, the formula results in:

$$e = \frac{3}{2}n$$

The following relationship is also important:

$$h + p = f$$

Where p is the number of pentagons and h is the hexagons number. Each pentagon contains five carbon atoms while six carbon atoms belong to each hexagon. n can be computed as follows:

$$n = \frac{(5p + 6h)}{3}$$

The outcome illustrates that p is always equal to 12 for any value of n, hence any fullerene is characterized by twelve pentagons.

There are two different types of carbon-carbon bonds: the one between two hexagons, that measures 1.38 Å, and those between a hexagon and a pentagon, that is long 1.45 Å. [12,13]

C_{60} fullerene is the most stable and it is constituted by twelve pentagons and twenty hexagons. Its representation is reported in the Figure 2.4:

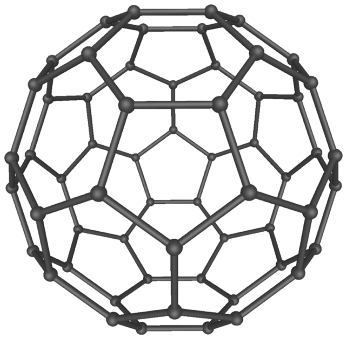

Figure 2.4 Model of the C_{60} fullerene.

Fullerene are formed when an electric arc is established between two carbon electrodes. Soot and C_{60} are the main products, however, also other fullerenes are created in smaller amounts.[14] Due to the high stability of the bonds, similarly to graphitic ones, fullerene is rather stable, and it is insoluble in most of the solvents. Nevertheless, its reactivity can be enhanced through surface functionalization. In nanotechnology, the fullerene's thermal resistance and superconductivity are largely investigated.[15]

2.3.3. Carbon nanotubes

Carbon nanotubes (CNT) are thin, hollow cylinders made of graphitic sheets [16]. As shown in Figure 2.5, there are two main types of carbon nanotubes: Single-Walled Carbon Nanotubes (SWCNTs, d≈1nm) and Multi-Walled Carbon Nanotubes (MWCNTs, d≈10nm).

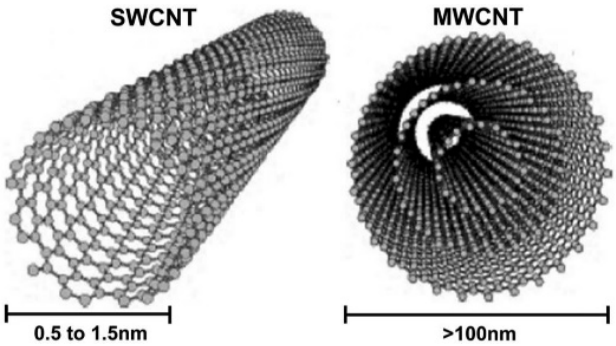

Figure 2.5 Representation of Single-Walled Carbon Nanotubes (SWCNT) and Multi-Walled Carbon Nanotube (MWCNT) [17].

Carbon nanotubes can be imagined as a rolled graphene sheet. Their properties depend on the orientation of the carbon nanotube longitudinal axis with respect to the graphitic plane. According to the relative orientations, reported in the Figure below, carbon nanotubes can behave as metals or semiconductors.

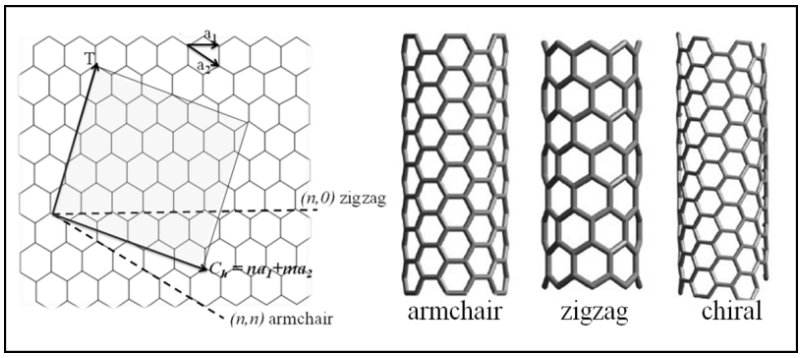

Figure 2.6 Armchair, zigzag and chiral type of CNT's.[18]

The way in which the graphene sheet is wrapped is defined by two integer indices n and m. These indices can define the chiral vector, C, in the following way:

$$C = na_1 + ma_2$$

Where a_1 and a_2 are the unit vectors of the graphene lattice. The chiral vector is related to the Carbon Nanotube diameter according to the following equation:

$$d = \frac{C}{\pi} = \frac{a}{\pi}\sqrt[2]{(n^2 + m^2 + nm)}$$

There are only two directions in which are generated non-chiral nanotubes. These are zigzag nanotubes, obtained for m=0, and armchair nanotubes that correspond at n=m situation. Armchair and zigzag directions differ of a 30° angle [19].

CNT's are characterized by low density and high mechanical strength and, because of this reason, they can be used as reinforcing fillers [20].

Carbon nanotubes also show high electrical and thermal conductivity, thermal stability and excellent electronic properties.

CNT's are produced with two different kinds of methods [21]: high temperature processes, such as arc-discharge or laser ablation, and lower temperature processes (T<800°C), such as chemical vapor deposition (CVD). High temperature processes have been replaced by CVD processes because they guarantee a better control on the growing CNT with consequent better properties.

2.3.4. Graphite

Graphite is the most thermodynamically stable form of carbon. The atoms are disposed hexagonally in a planar condensed ring system. Carbons' atoms in the plane are bonded covalently thanks to three sp^2 orbitals. These layers are stacked on top of each other and bonded by weak Van Der Waals forces established from π electron cloud and the structure can be seen in Figure 2.7.

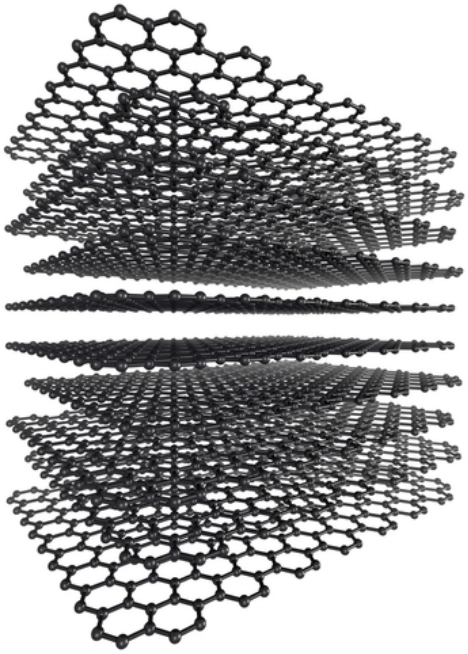

Figure 2.7 Graphite atomic structure.

Layers can be stacked in different ways: ABAB stacking is the more common and leads to hexagonal crystal lattice, while ABCABC leads to a rhombohedral crystal lattice. Turbostratic graphite refers, instead, to a disordered structure. High temperature (3000 °C) treatments favor the ordered systems. Graphite's peculiar properties are [4,22]

- High thermal stability: no thermal degradation or phase change occurs until 4000 K.
- Softness and slipperiness: the weak Van Der Waals forces, established between graphite layers, allow the sliding of the planes, making graphite a good lubricating material.
- Lower density than diamond.
- Chemical resistance: insoluble in both polar and non-polar solvents and attacked only by aggressive oxidizing conditions.
- Electrical conductivity: this property is related to the delocalization of π-electrons.

2.3.4.1. *Nano-graphite:*

As the graphite aggregates dimension decreases, the resulting microstructure begins to lose the long-range properties. The material shows then mixed properties which belongs both to the crystalline and amorphous phases.

Nowadays, nano-graphite is becoming important in rubber technology as reinforcing filler. Associated with a drop in dimension, there is an increase in specific surface area, and thus a higher number of interactions is favored between filler-filler and filler-polymeric matrix.

High surface area is also important as it promotes surface modification reactions. A higher degree of functionalization, and thus a better tailoring of surface properties of the material, can be reached increasing the surface area.

2.3.5. Graphene

Graphene is composed by a monolayer of carbon atoms arranged in a pattern of hexagonal rings [23] and it is the first 2D ordered structure discovered. Graphene is the building block of graphitic materials as the monolayers can be stacked together forming graphite, rolled producing a carbon nanotube [24] or give rise to more complicated allotropes such as fullerenes.

Each carbon atom inside the graphene layer can establish four bonds because of the sp^2 hybridization: three σ bonds with the neighbor atoms, deriving from the interaction of the sp^2 orbitals and, for each carbon, the lone p orbital interacts with each other producing a distributed π bond (conjugation), perpendicular to the graphene sheet. This peculiar electron distribution makes the graphene one of the most electrically and thermally conductive material in the direction parallel to the plane.

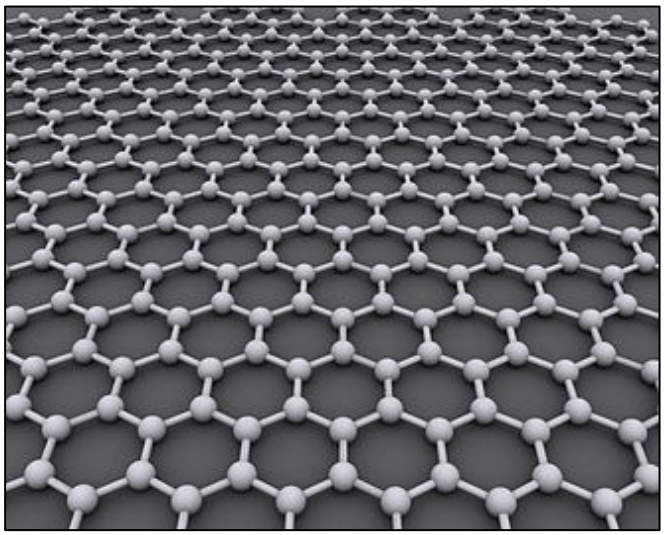

Figure 2.8 Graphene structure.

Graphene (2.8) has gained more and more interest in the last years for its remarkable properties which are reported below [25]:

- Electron mobility of $2.5 \times 10^5 \ \frac{cm^2}{Vs}$.
- Young's modulus of 1TPa and intrinsic strength of 130 GPa.
- Very high thermal conductivity, above $3000 \ \frac{W}{mK}$.
- Complete impermeability to any gas.
- Ability to sustain high density of electric current.

All of these properties are, however, related to the pure graphene and they can be heavily influenced by the presence of defects, that could appear during the production phase, and by the presence of more than one layer. Even only twenty graphene layers stacked together behave very similarly to the bulk graphite.[23,24]

2.3.5.1. *Graphene's production:*

Graphene can be produced either in a bottom-up or in a top-down approach. Exfoliation of graphitic materials is the principle of the top-down approach. There are two main categories of exfoliation: liquid phase and thermal exfoliation.[25] Regarding the liquid phase exfoliation, this is executed by ultrasonication in a suitable solvent and yields to graphene flakes of small dimensions in suspension. Thermal exfoliation, on the other hand, consists in a thermal-shock procedure in order to have exfoliation and reduction simultaneously of graphite oxide. Both procedures are characterized by a low cost of fabrication, but it is ultimately limited by the possible presence of defects and in the dimension control of the obtained product.

A bottom-up approach, that overcomes the aforementioned problems, is the Chemical Vapor Deposition (CVD) in which graphene is grown on a metal surface, that is later etched away, and the film is transferred on a substrate.

Alternatively, graphene could be produced by opening single-wall carbon nanotubes. A visual summary of graphene's production mechanisms can be seen in Figure 2.9:

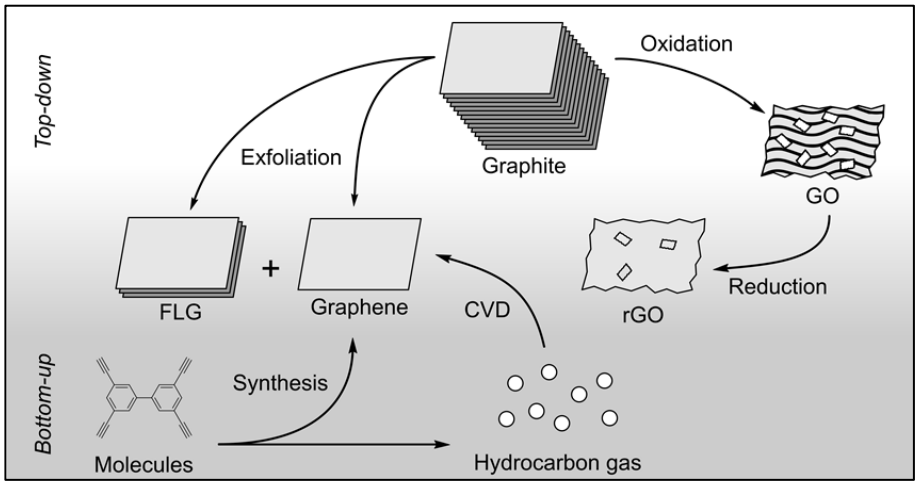

Figure 2.9 Overview on the common methods of Graphene's production. [26]

2.3.5.2. *Graphene related materials:*

Due to the unique and tunable properties of graphene, there are many possible fields for the application of graphene-based materials. The material design is greatly helped by the chemical functionalization and by the tuning of the dimensions: lateral dimensions can be tuned from nm to mm and their thickness can be adjusted from the single monolayer to hundreds of layers.

Graphene can be employed in electronics because of its conductivity and thanks to its flexibility [23]. Research has been brought forward in high-frequency transistors and logic transistors technology.

Graphene can also be utilized in optical applications as photodetectors, optical modulators and optical polarization controllers.[25,27] Opto-electronics applications are based on the fact that electrons in graphene behave as massless particles and this leads to a wavelength-independent absorption which is suitable for a wider spectral range than common semiconductors.

Graphene can also be applied in composites materials and in paints thanks to its chemical resistance and its mechanical properties combined with an intrinsic low density.

Energy storage and production field is investigating the utilization of graphene in solar cells too. [23,25] Nevertheless, there are at the state of the art few graphene-based materials because of many production's processes scale-up difficulties.

2.4. sp^1 hybridization-carbyne

Carbyne is an ideally infinite sequence of carbon atoms forming a one-dimensional chain. The bonds between the carbon atoms define the type of chain. As reported in Figure 2.10, two polymorphs of carbyne are present: α-carbyne and β-carbyne. [28]

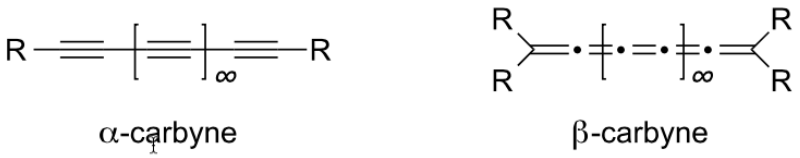

Figure 2.10 Two structural form of carbyne.

β-carbyne is characterized by a sequence of double bonds, all with the same length equal to 1.28 Å. The resulting chain is known as cumulene. α-carbyne, instead, consists of the alternation of single and triple bonds. The chain formed in this manner is called polyyne.[29] In this case there are two types of bonds characterized by different lengths: 1.20 Å for the triple bond and 1.38 Å for the single one. The cumulene chain is characterized by a BLA (bond length alternation) equal to zero, while it is different from zero in the polyyne case. It is possible to understand, on BLA basis, which kind of chain is present in the carbyne.

The π-electron delocalization, present in both types of chains, makes the carbyne highly reactive. In addition, the high conjugation, which increases with an increasing number of carbon atoms, makes carbyne unstable. For these reasons carbyne tends to crosslink and is expected to react with other atoms. Its atoms can also relax to other more stable carbon hybrid forms. It is suggested that the carbyne limit would be a molecule with c.a. 50 consecutives alkynes. [30]

References

[1] J. B. Reece, & Campbell, *Campbell biology*. Boston: Benjamin Cummings / Pearson, 2011.

[2] Bitao Pan et al., Carbyne with finite length: The one-dimensional sp carbon, Science Advances, Vol 1, 2015.

[3] A. V. Rode, E. G. Gamaly, A. G. Christy, J. G. Fitz Gerald, S. T. Hyde, R. G. Elliman, B. Luther-Davies, A. I. Veinger, J. Androulakis, and J. Giapintzakis, Unconventional magnetism in all-carbon nanofoam, Phys. Rev. B 70, 054407 – Published 17 August 2004.

[4] N. Brandt, S. Chudinov, Ya.G. Ponomarev. *Semimetals Graphite and Its Compounds,*Vol. 20.1, 1988.

[5] Nicolaus Probst, Eusebiu Grivei, Structure and electrical properties of carbon black, Carbon, Volume 40, Issue 2, 2002, Pages 201-205.

[6] V. Mittal, *Advanced in Polyolefin nanocomposites*, CRC Press, 2011, 12, 330-332.

[7] G. R. Hamed, *Rubber Chem. Technol*., 2000, 73.

[8] M. Galimberti, Course of *"Chemistry for elastomer composites"*, Polytechnic University of Milan, 2020.

[9] S. E. Turri, Course of "Advanced chemistry for materials engineering", Polytechnic University of Milan, 2018.

[10] J. B. Donnet, R. C. Bansal, M. J. Wang, *Carbon Black - Science and Technology, 2nd ed.*, CRC Press, 1993.

[11] Raos, F., Course of"Advanced chemistry for material engineering", Polytechnic University of Milan, 2018.

[12] W. David, R. Ibberson, J. Matthewman *et al.* Crystal structure and bonding of ordered C_{60}. *Nature* **353,** 147–149,1991.

[13] P.W. Fowler, Electron deficiency of the fullerenes, *J. Phys. Chem.* 1995, 99, 2, 508–510, 1995.

[14] Shriver, D F, Mark T. Weller, Tina Overton, Jonathan Rourke, and F A. Armstrong. *Inorganic Chemistry*, 2014. Print.

[15] K.H. Johnson, M.E. McHenry, D.P. Clougherty, High-Tc superconductivity in potassium-doped fullerene, KxC60, via coupled C60 (pπ) cluster molecular orbitals and dynamic Jahn-Teller coupling, Physica C: Superconductivity, Volume 183, Issues 4–6, 1991, Pages 319-323.

[16] M. S. Dresselhaus, et. Al. *Carbon Nanotubes,* 2001.

[17] Ribeiro, Bruno et al . Carbon nanotube buckypaper reinforced polymer composites: a review. Polímeros, São Carlos, v. 27, n. 3, p. 247-255, Sept.2017.

[18] S. Ghosh, Hydrogen Storage in Single-Walled Carbon nanotubes, 2017.

[19] C. S. Casari, Course of "Physics of nanostructures", Polytechnic University of Milan, 2019.

[20] M. J. Matthews, M. A. Pimenta, G. Dresselhaus, M. S. Dresselhaus, M. Endo. *Phys. Rev. B: Condens. Matter Mater. Phys*. 1999, 59.

[21] N. Karousis, N. Tagmatarchis and D. Tasis, *Chem. Rev*, 2010, 110, 5366.

[22] N. Deprez and D. S. McLachlan, The analysis of the electrical conductivity of graphite conductivity of graphite powders during compaction, *J. Phys. D: Appl. Phys.* **21** 101, 1988.

.[23] K. S. Novoselov, Nobel Lecture: Graphene: Materials in the Flatland, Reviews of Modern Physics, Volume 83, July–September 2011.

[24] K.S. Novoselov, A.K. Geim, The Rise Of Graphene, Nat. Mater. 2007, 6, 183-191.

[25] K. S. Novoselov, V. I. Fal'ko, L. Colombo, P. R. Gellert, M. G. Schwab & K. Kim, A roadmap for graphene, Nature ,Vol 490, 1 1 October 2012.

[26] M. Nordlund,*Carbon Nanostructures – from Molecules to Functionalised Materials, 2017.*

[27] K. Kostarelos, K. S. Novoselov, Graphene devices for life, Nature nanotechnology, 9(10), 744, 2014.

[28] J. A. Januszewski, Chem. Soc. Rev., 2014.

[29] Heimann RB, Evsyukov SE, Kavan L. Carbyne and carbynoid structures. Vol 21. Springer Science & Business Media; 1999.

[30] W. A. Chalifoux, Nat. Chem., 2010.

Chapter 3
Silica

3.1. Introduction

Silica is an inorganic oxide containing four oxygen atoms bonded to the central silicon atom. Its structure is a tetrahedral, with the oxygens located on the edges. Different crystalline polymorphs of silica are present and the most abundant in the earth's crust is the α-quartz phase.[1]

Figure 3.1 Structural motif found in α-quartz, common in almost all forms of silicon dioxide.[2]

Silica is divided in three classes: amorphous, crystalline, and synthetic amorphous silica. Precipitated silica is a subclass of amorphous silica and it is mainly used as filler reinforcement in tire applications.

3.2. Amorphous silica surface

Silica presents an acidic behavior directly related to the amount of -OH moieties on the surface [3] which also characterize silica's hygroscopic behavior: the hydroxyl groups can form hydrogen bonds with water leading to surface hydration. High levels of hydration can negatively impact the final compound physical properties.[4]

3.3. Silica in rubber compounds

The presence of silica in a rubber matrix offers several advantages, such as reduction of rolling resistance, improvement in tear strength and in wet grip. [5,6]

In rubber composites, a homogeneous filler dispersion is correlated to a higher tensile strength and abrasion resistance. Because of the tendency of silica particles to interact with each other, rather than with the polymeric chains, there is a reduction in the polymer-filler interaction and this results in an inhomogeneous filler dispersion inside the polymeric matrix. The low compatibility between the silica and the elastomer relies on their different polarity. [7]

Another problem related to the use of silica as a filler in rubber compounds is the deactivation of vulcanization accelerators. Vulcanization is the process in which a crosslinked network is established,

leading to an increase in the elasticity and a decrease in the plasticity of the rubber compound. Zinc oxide is used as an activator of this process and it is used in combination with stearic acid to decrease the curing time while improving the mechanical properties of the final compound.[5] Due to the presence of silanol groups on the surface, silica shows an acidic behavior, and it adsorbs basic compounds such as ZnO and amine-based accelerators, deactivating them[6] and consequently lowering the vulcanization efficiency.

Organo-silanes are employed both to make compatible the silica with the polymer and to reduce accelerator deactivation. A common silane molecule used in rubber industry is characterized by the presence of two different portions: an apolar group that can establish weak dispersion bonds with the rubber and an organo-silane moiety that can condensate with the silica filler. Silica-silane-rubber system is reported in Figure 3.2:

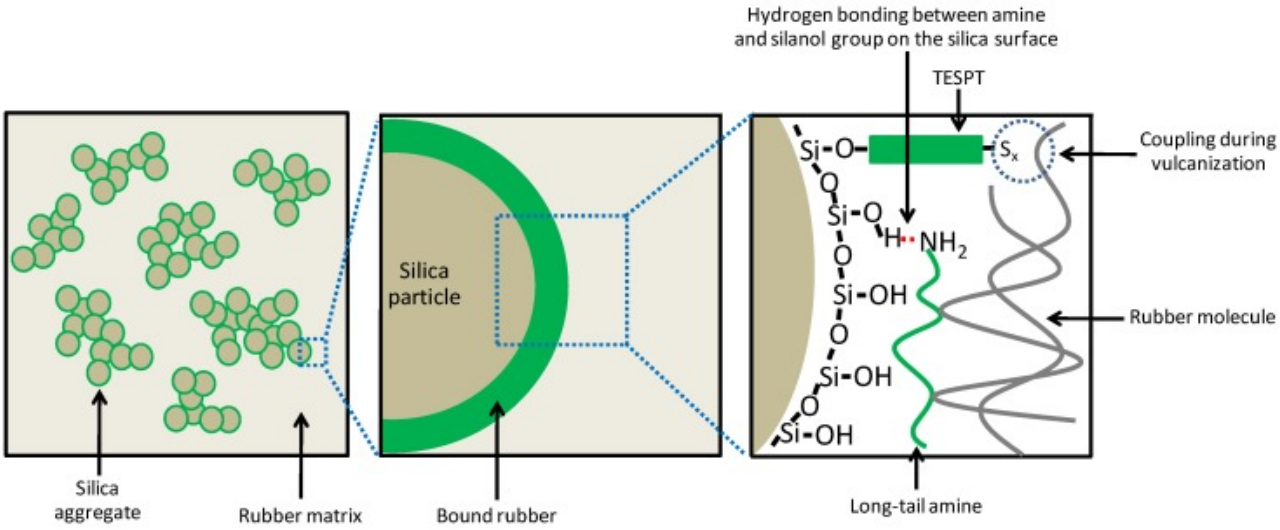

Figure 3.2 Representation of silica-silane-rubber system.[8]

Silanes help decreasing size of the aggregates and of the silica network, improving its dispersion inside the polymeric matrix and the filler-rubber interactions.[6] The introduction of silanes in silica-filled compounds allows to overcome the losses in the composite performances, making silica a competitive reinforcing agent.

References

[1] L. Leviein, C.T. Prewitt and D.J. Weidner. Structure and elastic properties of quartz at pressure P=1 atm.*American Mineralogist, 1908.65:920-930.*

[2] https://commons.wikimedia.org/w/index.php?curid=29397581 (last access 26/03/2021).

[3] L.T. Zhuravlev, *Colloids on Surface A: Physichemical and Engeneering Aspects*, 2000, 173 (1-3), 1-38.

[4] L.T. Zhuravlev, *Reaction Kinetics & Catalysis Letters*, 1993, 50 (1-2), 15-25.

[5] J.E. Mark, B. Erman, F.R. Eirich, *Science and Technology of Rubber*, Academic Press, 2013.

[6] S.M. Hosseini, M. Razzaghi-Kashani, Vulcanization kinetics of nano-silica filled styrene butadiene rubber, Polymer 55, 2014.

[7] M. Castellano, A. Turturro, E. Marsano, L. Conzatti, S. Vicini, *Polymer Composites*, 2014, 35 (8), 1603-1613.

[8] C. Hayichelaeh, L.A.E.M. Reuvekamp, W.K. Dierkes, A. Blume, J.W.M. Noordermeer,K. Sahakaro . Enhancing the Silanization Reaction of the Silica-Silane System by Different Amines in Model and Practical Silica-Filled Natural Rubber Compounds. *Polymers*. 2018; 10(6):584.

Chapter 4
Rubber reinforcement theory

4.1. Types of fillers

Elastomeric composites are composed mainly by vulcanized rubber and reinforcing fillers. They have the function of increasing rubber stiffness while maintaining its strength and elastic properties. In addition, fillers decrease the cost of the final product.

Fillers can be divided by their reinforcing ability, which is strictly correlated to the size of the particles:[1]

- **Reinforcing**: 0.01/0.1 μm
- **Semi-reinforcing**: 0.1/1 μm
- **Diluents**: 1/10 μm
- **Degradants:** dimensions higher than 10 μm

In the rubber industry carbon black and silica are the most used fillers, however, advanced applications can also contain materials such as zinc oxide, silicates, and carbonates. The present work was focused on the functionalization of carbon black and its introduction in both carbon black and carbon black-silica rubber composites.

4.2. Reinforcing fillers

As the name suggests, reinforcing fillers are necessary to improve the mechanical properties of rubber composites.[2] The listed properties are increased up to one order of magnitude in the presence of reinforcing fillers:

- Stress at a given elongation
- Tensile strength
- Modulus
- Tear resistance
- Fatigue and abrasion resistance

Simultaneous increase in both modulus and elongation at break for elastomers is related to the filler-polymer interactions and is described more precisely in the next sections.

Different factors influence the mechanism of reinforcement:[3]

1. Filler morphology
2. Dispersibility
3. Surface physics

4. Surface chemistry

4.2.1. *Filler morphology:*

Reinforcing fillers are constituted by primary particles that combine forming aggregates which cannot be separated through mixing and are the unit base for polymer reinforcement. Different aggregates can interact by means of Van Der Waals forces forming agglomerates. Although primary particles are mostly fused together forming aggregates, their dimensions are very important in the filler reinforcement capability. The lower the particle size, the higher is the surface area and consequently the greater is the possible filler-filler and filler-polymer interactions. More and more attention is thus brought on the study of nanostructured carbon allotropes as reinforcing fillers.

The aggregation of primary particles defines the **structure**, which express the size and bulkiness of the aggregates and agglomerates.[4] It is the degree of disorder of secondary particles and it is fundamental for the determination of the occluded rubber, the elastomer fraction inside the aggregates voids, and the effective volume of the filler.[1] These entangled polymers chains behave similarly to fillers, improving material's properties. Generally, the higher the anisotropicity of the aggregate the greater the reinforcing.

4.2.2. *Dispersibility:*

It is necessary to have a good filler dispersion within the polymeric matrix to provide homogenous properties in the material. Dispersibility is strongly related to the surface energy and to the structure, it is largely influenced by aggregates and agglomerates interactions and it is facilitated when matrix and fillers have similar surface energies. High structure corresponds usually to a high degree of dispersion.

4.2.3. Surface physics:

The polymer-filler interaction is related to the absorption of polymeric chains on the particle's surface.[3]

Carbon black particles show a graphitized surface where defects are also present. Because of the higher anisotropicity, amorphous zones are supposed to give rise to stronger filler-polymer interactions.

4.2.4. Surface chemistry:

Carbon black surface include organic, mineral impurities and oxidized species due to manufacturing processes.[3] While organic and mineral impurities do not have a significant effect on the reinforcement, oxidized species can lead to lesser performances. Nevertheless, mineral impurities influence the reactivity during the vulcanization process, increasing the vulcanization speed.[1]

4.3. Viscosity

The Einstein equation correlates viscosity of a fluid with the fraction of dispersed solid particles, and it is described as [1]

$$\eta = \eta_0(1 + 2{,}5\Phi)$$

Where Φ is the filler volume fraction. This model is however valid for low filler concentration and neglects filler-filler interactions. To overcome the concentration problem, Guth-Gold provides a modified equation of the Einstein model: [5]

$$\eta = \eta_0(1 + 2{,}5\Phi + 14{,}1\Phi^2)$$

Due to the polymer chains absorption on the filler surface and to the filler-filler interactions, the Guth-Gold model is still not valid for a filled-elastomer compound. A modified version of the Guth-Gold model has been proposed where Φ was substituted by Φ_c:

$$\eta = \eta_0(1 + 2{,}5\Phi_c + 14{,}1\Phi_c^2)$$

where Φ_c is the correct filler volume fraction and it is expressed in the following way:

$$\Phi c = \frac{\Phi}{2}\left(1 + \frac{1 + 0{,}02139\ DBP}{1{,}46}\right)$$

The DBP (dibutyl phthalate) is the filler structure term. Φ_c considers thus filler-filler interactions and occluded rubber phenomenon: polymers chains entrapped inside fillers voids that cannot be extracted by a good solvent. Occluded rubber is not deformable and behaves more similarly to a filler rather than a polymer and leads to a considerable increase of the effective filler volume.

It is also important to underline the change that occurs in the fluid rheological behavior due to the presence of the filler phase. Reinforcing fillers force a non-newtonian behavior, favoring a Bingham type one, characterized by a threshold shear stress (τ) in the η/τ plot.[6] The presence of fillers in the elastomer decreases the volume of the deformable phase. The higher the filler fraction volume, the more pronounced is the non-newtonian behavior.

4.4. Reinforcement of elastomers

4.4.1. *Small deformations properties and Payne effect:*

The reinforcement at small deformations of a loaded and crosslinked elastomer, shown in Figure 4.1, is divided in two main contributions based on the dependency or not on the strain amplitude.

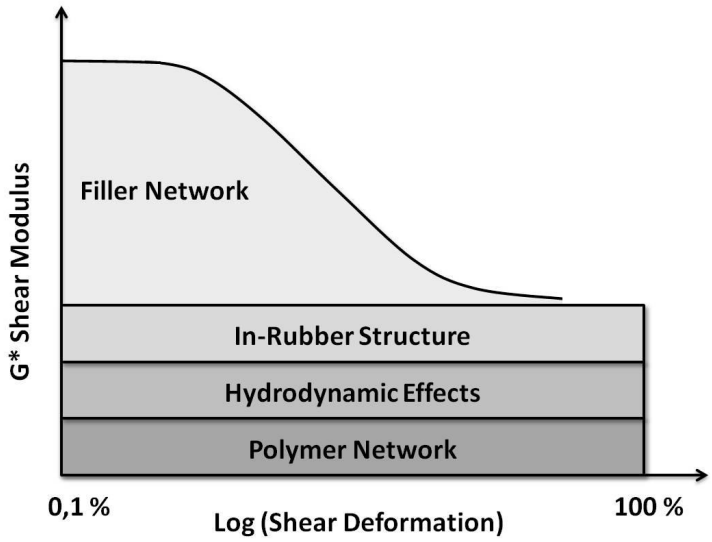

Figure 4.1 Strain amplitude dependence of G*.[7]

Polymer network, hydrodynamic effects and in-rubber structure do not depend on strain amplitude.[1] The polymer network contribution is associated to the presence of entanglements and crosslinks. Hydrodynamic effects are related to the presence of rigid fillers which create a non-deformable phase and so it is dependent on the effective fillers content while in-rubber structure originates from occluded rubber phenomenon and leads to the existence of immobilized polymers chains inside the fillers voids which are no longer deformable.

Young modulus (in shear) can be directly correlated with the viscosity equation. It is independent from strain amplitude contribution and it can be described with the following formula:

$$G^* = G_0^*(1 + 2{,}5\Phi_c + 14{,}1\Phi_C^2)$$

where G_0^* is the shear modulus of the unfilled vulcanized rubber measured at the same shear strain. The small deformation contribution dependent on the strain amplitude is also known as Payne effect. This effect is mainly associated to the filler network and its magnitude is associated to the filler amount, the filler surface area and to the filler dispersion.[5] At 3% of strain amplitude the filler network starts breaking down while at 10% it is mostly destroyed and therefore it is no longer possible to notice the Payne effect. The mechanism responsible for the destruction of the filler network is related to the desorption of the polymeric chains from the filler surface.[3] In the equilibrium condition, polymeric chains are adsorbed on the filler surface but, as an external deformation is being applied, polymer chains extend and, for low shear strain rates, they accommodate the external macroscopic deformation as elastic energy. When the stored elastic energy surpasses the surface adsorption energy, desorption occurs, and the filler network is destroyed. As can be seen in Figure 4.1, G* curve declines slowly because of the gradual desorption of elastomeric chains from the filler surface.

4.4.2. *Large deformations properties:*

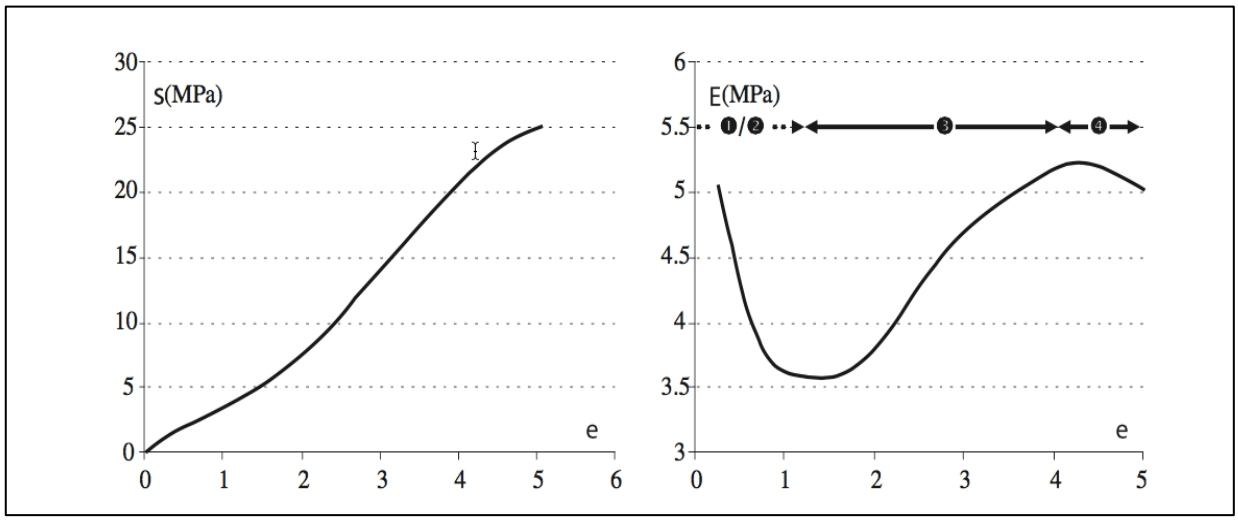

Figure 4.2 Stress and Young's modulus (dS/dε) of a reinforced compound.[3]

In Figure 4.2 Young modulus behavior (curve on the right) can be seen at increasing strain: E decreases for ε<1, reaches a minimum and then raises again. For ε<1 the Young modulus behavior is determined by the aforementioned Payne effect and it is related to the rupture of the filler network.[1] The large deformations behavior is related to the strain amplification effect: rigid fillers are per definition non deformable and, because of this, they induce a higher local stress for a macroscopic deformation. Because of the added stresses, the elongation at break should theoretically decreases. As can be seen in Figure 4.3, this does not occur.

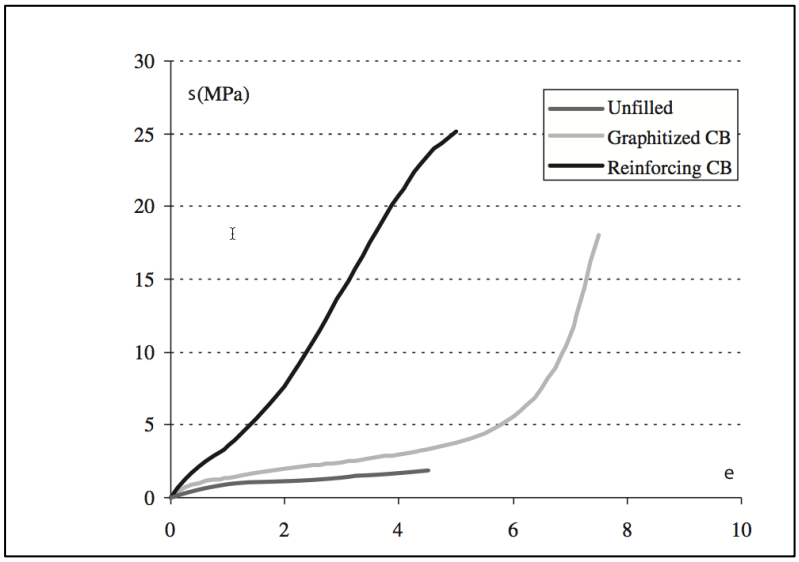

Figure 4.3 Stress-strain curves of: unfilled, graphitized CB and reinforcing CB samples.[3]

The increase of the elongation at break is caused by a homogenization of the polymeric chains between different fillers particles which is made possible by the reversible adsorption mechanism of the polymeric chains on the filler surface. A local distribution of stresses is thus achieved, ensuring a higher fracture strain.

References

[1] S. E. Turri, Course of "Advanced chemistry for materials engineering", Polytechnic University of Milan, 2018.

[2] A Salim, A Hassan, H Ismail, Polymer-Plastics Technology and Engineering, 2018, 57(6), 523-539.

[3] Jean-Baptiste Donnet, Emmanuel Custodero, Chapter 8 - Reinforcement of Elastomers by Particulate Fillers, Editor(s): James E. Mark, Burak Erman, C. Michael Roland, The Science and Technology of Rubber (Fourth Edition), Academic Press, 2013, Pages 383-416.

[4] *C.L. Barrie et al.* Rheology of aqueous carbon black dispersions, *Journal of Colloid and Interface Science 272, 2004. 210–217.*

[5] M. Galimberti, Course of *"Chemistry for elastomer composites"*, Polytechnic University of Milan, 2020.

[6] R. Frassine, Course of "Mechanical behvior and durability of polymers", Polytechnic University of Milan, 2019.

[7]http://www.tainstruments.com/wp-content/uploads/RPA-Bridging-the-Gap-Akron-rubber-workshop.pdf (last access 26/03/2021).

Chapter 5
Vulcanization

5.1. Introduction

Vulcanization is a chemical crosslinking process in which covalent bonds between polymeric chains are generated. This increases elasticity and decreases the plasticity of the material and it is a crucial step for the applicability of elastomers in the real world.

Sulfur and peroxides are the most common vulcanizing agents, and their usage depends on the degree of unsaturation of the polymer. Sulfur is used for unsaturated polymers while peroxides for saturated ones and for specialty elastomers.[1]

Sulfur-based vulcanization is by far the most prevalent process and it is described as follows: elemental sulfur has a cyclic octamer conformation (S_8) which is stable at low temperatures but breaks down and linearize starting from 140 °C. The linear fragments are then reactive against the double bond of an unsaturated polymeric chain. Multiple chains can thus be connected to each-other forming a stable molecular network (Figure 5.1) made possible by C-S_x-C bonds. Longer is the polysulfides chain (higher x) and lower is the thermal stability. Tuning the sulfur quantity and introducing accelerants can limit this detrimental effect.[2]

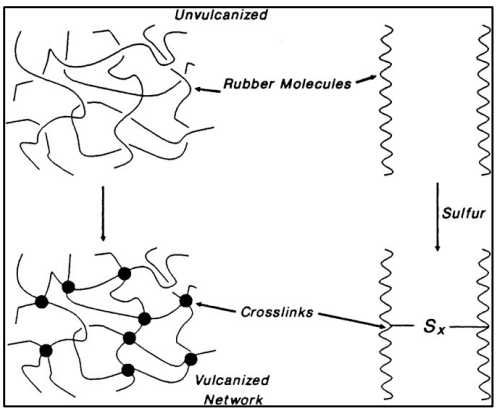

Figure 5.1 Representation of Network formation.[3]

Only sulfur vulcanization per se is a slow, laborious, and economically impracticable process and the final composite presents severe problems such as mechanical instability and degradation. In order to improve the efficiency of the reaction activators and accelerators are adopted. Zinc Oxide (ZnO) is used to improve the sulfur decomposition, stearic acid to improve ZnO solubility in the polymer and organic accelerants to increase the kinetic of the reaction.

5.2. Effects of vulcanization

- Mechanical properties: decrease in plasticity, increase in tensile strength, elasticity, hardness and reduction in elongation and permanent deformation. The listed improvements depend on sulfur amount, presence of additives and curing time.
- Physical properties: because of the reticulation, the density of the polymer increases preventing the motion of small molecules of gas and liquids (decrease in breathability and permeability, respectively).
- Chemical properties: common solvents do not permeate the carbon-sulfur 3D network, making the vulcanized composite chemically stable.

5.3. Monitoring of the vulcanization process

Vulcanization process is carried out by heating the rubber mixed with additives and vulcanizing agents in a mold under pressure [1].

Curing is studied by measuring the torque or the dynamic modulus as time passes. The curve (Figure 5.2) provides information about the kinetic of the process. Higher Torque or dynamic modulus values are associated to higher crosslinking densities.

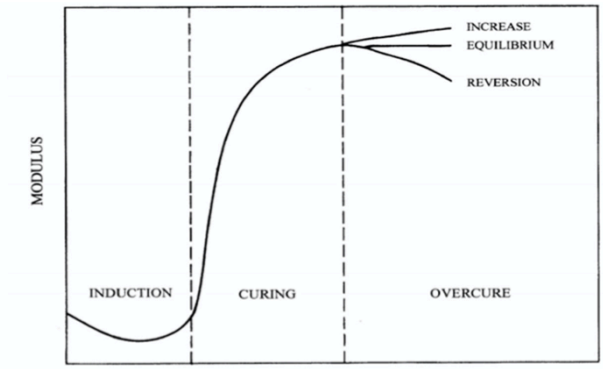

Figure 5.2 Modulus/time plot during vulcanization process.

Curing curve is divided in three main zones:

1. Induction zone: crosslinking has not yet started. The minimum value is generally associated with the viscosity of the composite: the lower the value, the lower is the viscosity.[4] At the end of the induction time the torque start to increase indicating the curing onset
2. Curing zone: the network formation inside the rubber matrix takes place. The slope of the curve is related to the kinetic of the process: higher is the slope and faster is the reaction.

3. Overcure zone: it represents the final step of the vulcanization process. A plateau is usually observed but reversion, associated with polysulfide bonds breakdown, can also take place. Reversion should be avoided as it delivers losses in mechanical performance.

The main parameters which are obtained from this curve are listed as follows:

- Scorch time (ts_1): time required to increase the Torque value by one. It indicates the time available before the onset of the crosslinking process.
- Optimum cure time (t_{90}): time after which the 90 % of the maximum Torque is achieved.
- Minimum Torque value (M_L): lowest achievable Torque. It gives indications about the viscosity of the compound.
- Maximum Torque (M_H): highest achievable Torque. Represents the highest crosslinking level that is reached at a given temperature.
- Delta Torque ($\Delta S = M_H - M_L$): it is the difference between the maximum and the minimum Torque. It gives information about the crosslinking density.[2]

References

[1] L. Nijhof, "*Compounding characteristics for peroxide cure*", Rubber technology course, University of Twente, 2018.

[2] S. E. Turri, Course of "Advanced chemistry for materials engineering", Polytechnic University of Milan, 2018.

[3] A.Y. Coran, Chapter 7 - Vulcanization, Editor(s): James E. Mark, Burak Erman, C. Michael Roland, The Science and Technology of Rubber (Fourth Edition), Academic Press, 2013, Pages 337-381.

[4] M. Galimberti, Course of *"Chemistry for elastomer composites"*, Polytechnic University of Milan, 2020.

Chapter 6
Tires

6.1. Introduction

A tire is a ring-shaped material attached to the rim of the wheel that must provide traction over the ground surface. Good adherence with the ground, good deformability to absorb street irregularities, and an optimized rolling resistance to reduce the fuel consumption are the required characteristics.[1] Rolling resistance, the measure of energy dissipated per unit of distance, is a fundamental parameter that should be considered for the tire design. Small deformations are promoted on the tire surface when it is rolling on the street and are responsible for the resistance to the motion which leads to energy dissipation. In order to minimize this dissipation and reduce fuel consume, rolling resistance requires low hysteresis (low Tan δ) values (wet traction and grip require instead high Tan δ). Low Tan δ values are indicator of a low rolling resistance at 60°C, while high Tan δ at 0°C are an indicator of wet traction. Therefore, based on tire specific uses, tuning of hysteresis values is fundamental.
There are two main types of tires: Tube and Tubeless. The Tube type, as suggested by the name, are characterized by the presence of an inner tube which is not present in the Tubeless type. The difference between the two types of tires relies on the behavior of the tire as it is being punctured. In terms of carcass and rubber composition, Tubeless tires are very compact, preventing air to escape through the pores, while in the Tube type air rapidly exits the tire.

6.2. Tire components

A tire is made up of several different parts (Figure 6.1) to maximize road performances.[2]
Filled rubber is not the only component, otherwise the tire should be too flexible and weak. Each part has specific functions and must satisfy different requirements.

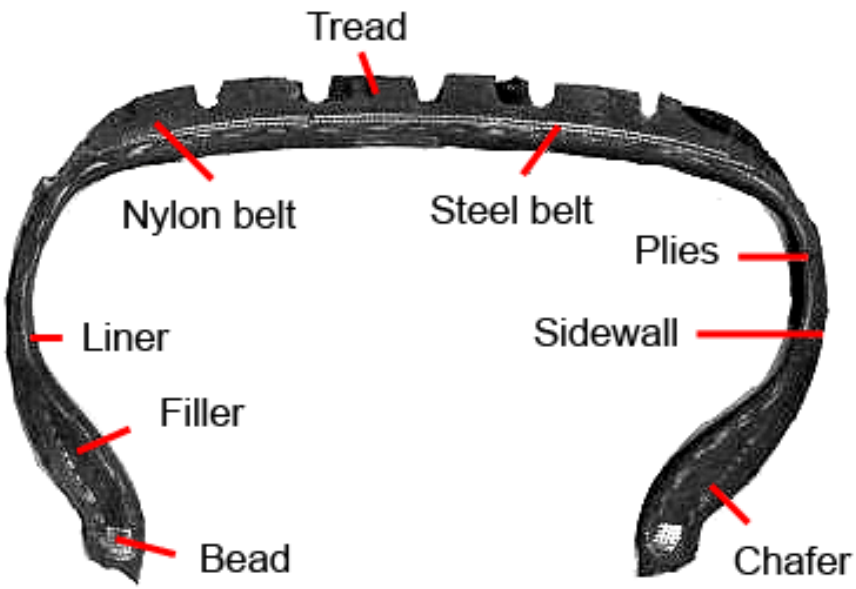

Figure 6.1 Section of a tire.

A tire is generally composed by the following main parts:

- Tread: it is the external part of the tire and it is in direct contact with the ground. It is designed to have great wear resistance, traction, and environmental resistance [3]. The tread pattern is characterized by a system of circumferential grooves and lateral sipes and is designed with the aim to provide a uniform wear, to minimize the noise and to conduct water out of the footprint. Depending on the specific use of the tire, different designs can be employed. NR, SBR and BR are generally used for the tread. [2,4]
- Tread cushion: it is placed between the tread and the steel belt and it has the requisite to show the following performances: low hysteresis, good adhesion, fatigue, tear, and durability [2].
- Steel belt: it is located under the tread and is a layer of rubber coated tire cords made by: steel/brass, aramid fiber, inorganic glass fiber. Their purpose is to improve the flexibility. [4]
- Plies: layers of polyester or Nylon cords which constitute the carcass of the tire. The plies are coated with rubber to bond with the other elastomeric components and are crucial for tire air sealing.
- Carcass: is the primary reinforcing material of the tire casing and guarantees the tensile resistance to inflation pressure along cord direction.
- Sidewalls: protect the carcass and provide lateral stability. NR, BR and SBR are here employed for their high fatigue resistance. [2]

- Liner: it is a thin layer of impermeable rubber, settled under the carcass and it possess different purposes: compressed gases retention, air impermeability and prevention of degradation due to air exposure. Liner is generally formed by butyl-rubber or halogenated derivatives.[2]
- Beads: high tensile strength steel wires encapsulated in a rubber compound which transfer the load from the tire to the rim.
- Chafer: it is a narrow strip of rubberized reinforcing cord necessary to prevent the moisture and dirt penetration inside the tire and to protect the carcass from wearing.
- Belts: they are used to reinforce the area under the tread and to increase the puncture resistance. They are generally made of steel.

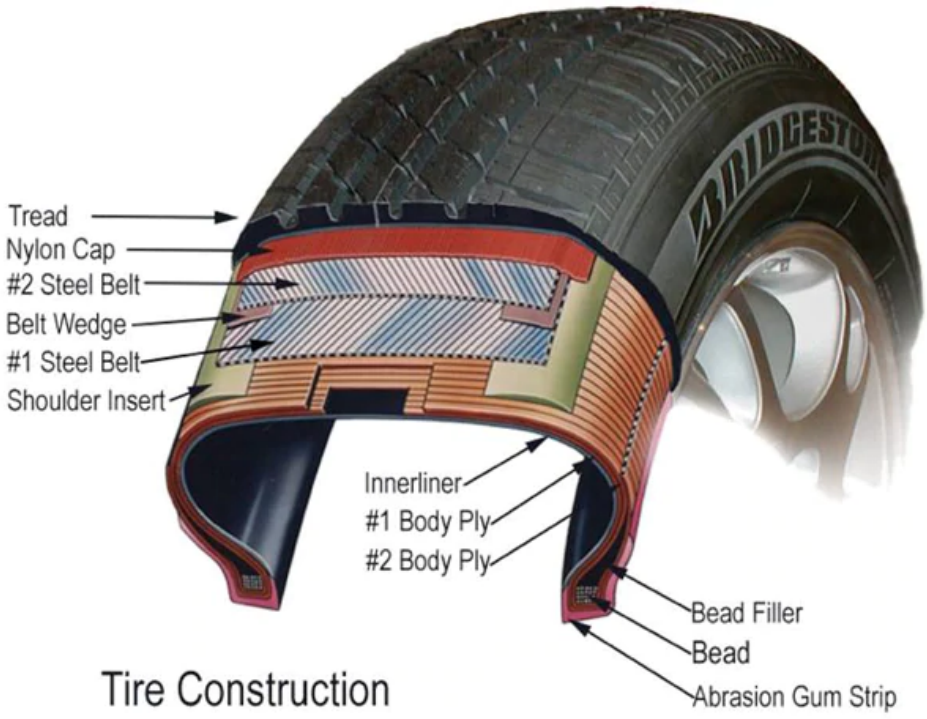

Figure 6.2 Tire construction.

References

[1] G.R. Hamed, *Rubb. Chem. Technol*., 2000, 73, 524.

[2] T. Sabu, *Non-linear viscoelasticity of rubber composite and nanocomposites*, 2014, 281-282.

[3] W. Meyer and J. Walter, eds., *Frictional Interaction of Tire and Pavement*. (West Conshohocken, PA: ASTM International, 1983.

[4] M. Galimberti, Course of *"Chemistry for elastomer composites"*, Polytechnic University of Milan, 2020.

Chapter 7
Functionalization of sp^2 carbon allotropes

7.1. Introduction

Functionalization of sp^2 carbon allotropes, a growing research field, is aimed to improve carbon-based material properties. Carbon allotropes are able to interact with organic molecules through covalent and non-covalent bonds. Non-covalent interactions are hydrogen bonding, π-cation, π-π stacking, π-anion electrostatic forces, hydrophobic interactions and Van-der-Waals forces.[1] These interactions are responsible for some disadvantages of carbon allotropes as the low solubility in many solvents. In the present work a functionalization method involving pyrrole compounds was employed.

7.2. Non-covalent functionalization

Non-covalent functionalization is based on the interactions mentioned above and summarized in Figure 7.1.

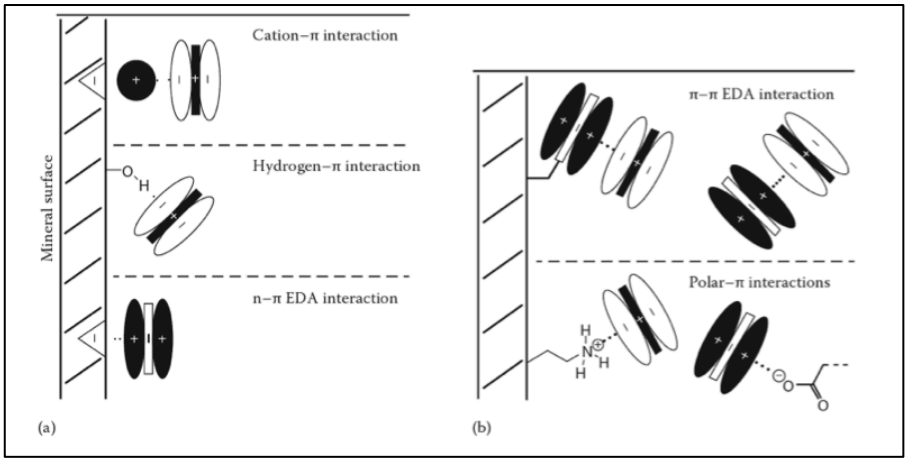

Figure 7.1 Representation of aromatic interactions involving the π-system.[1]

A chemical agent interacts with the surface of a carbon allotrope without altering its properties and electronic configuration. Functional groups are thus introduced in a less invasive way compared to the covalent functionalization.

7.2.1. *Cation-π interaction:*

It is the non-covalent interaction that can arise from the interaction of a cation and a π electron cloud. Cation-π interactions are at the basis of the selective transportation of ions though the membrane. [2]

7.2.2. *π-π interaction:*

π-π interaction takes place between π-acceptor and donor molecules. The p orbitals of the π-conjugated systems overlap, making possible the bond. Aromatic molecules and sp^2 carbon allotropes can develop such weak bonds,[3] which do not affect electronic band structure and crystalline domain of the sp^2 carbon allotropes but can bring to a significant change in the solubility of the carbon material.[4] Thermal and electrical conductivity are weakly influenced by non-covalent functionalization.

7.3. Covalent functionalization

The formation of a covalent bond between an organic molecule and a carbon allotrope is much stronger than a non-covalent type, and generally leads to a perturbation of the system due to the disruption of the hybridization, which can potentially change the physicochemical characteristics of the allotrope.

Covalent functionalization can be achieved involving defects present on carbon atoms[5] because of their intrinsic enhanced chemical reactivity. Carbon allotropes present three types of defects:

- Unsaturated bonds: derived from a lack of bonding between carbon atoms and it is caused by the presence of vacations, dislocations, and atoms in interstitial positions.
- Topological defects: Related to the presence of pentagons in the hexagonal graphitic cell structure and can lead to deformations and changes in the chirality.
- Defects of re-hybridization: presence of different kinds of hybridization within the same carbon allotrope.

Chemical bonds can take place only if certain functional groups are present both on the carbon allotrope and on the chemical. These functional groups are -COOH, -OH and $-NH_2$ [6,7]

The following reactions are involved for the covalent functionalization: free-radical reaction, amidation, carboxylation, fluorination, diazonium and Bingel reactions. Chemical functionalization can be achieved using strong chemical agents such as aryl diazonium salts, benzoyl peroxide, styrene, nitrenes and carbenes.[1]

In this thesis, a functionalization method based on the Diels-Alder reaction was used. This method allows the insertion of functional groups at the edges of the carbon allotrope planes, without altering its bulk structure or its electronic properties.

7.3.1. *Diels-Alder reaction:*

The mechanism of the Diels-Alder (DA) reaction is summarized in Figure 7.2:

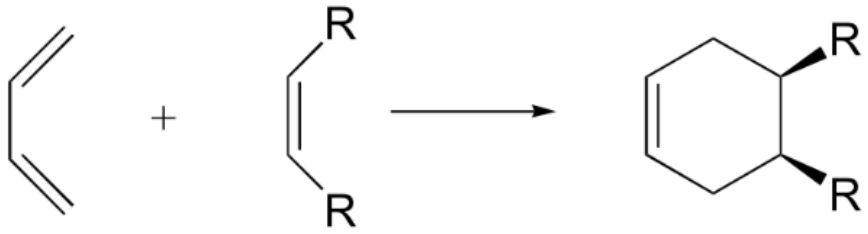

Figure 7.2 Schematic mechanism of the Diels-Alder reaction.

The Diels-Alder reaction is a chemical reaction between a conjugated diene and a substituted alkene, "dienophile", with at least one π-bond. During the reaction, three π-bonds are broken and two σ and one π bonds are formed. Since π-bonds are converted in stronger σ-bonds, the reaction is thermodynamically favored.

The result of this cycloaddition reaction is the formation of a ciclohexene substituted derivative. This reaction is a good example of pericyclic reaction which proceed via concerted mechanisms: breaking and formation of all bonds occurs in a single step with no intermediates generated during the reaction. The Diels-Alder reaction is characterized by a good regio- and stereoselectivity. For these reasons, it is exploited for functionalization purposes: it leads to the insertion of functionalities in peripherical positions without compromise the bulk properties.

7.4 Functionalization of sp^2 carbon allotrope. Prior art Politecnico di Milano.

The research group where this thesis was executed developed a functionalization method to introduce pyrrole compounds decorated by different functional groups on the sp^2 carbon allotrope surface.[4,8,9] This method can be defined as sustainable, as it occurs by simply mixing and providing thermal energy to the reagents, without the use of solvents or catalysts. It is applicable to large-scale productions and it is also characterized by reactions with high yields, and, thus, with high atomic efficiency.

This functionalization method has been named as "pyrrole methodology" and it is shown in Figure 7.3.

The mechanism of the sp^2 carbon allotrope functionalization reaction is thought to be based on two steps (Figure 7.3): the first step is the oxidation of the pyrrole, which leads to oxidized pyrrole derivatives. This reaction is promoted directly by the carbon black surface, which acts as a catalyst.

The second step consists in the Diels-Alder reaction: the oxidized pyrrole derivative would act as the dienophile while the graphitic surface of the carbon black as the diene. [8,9]

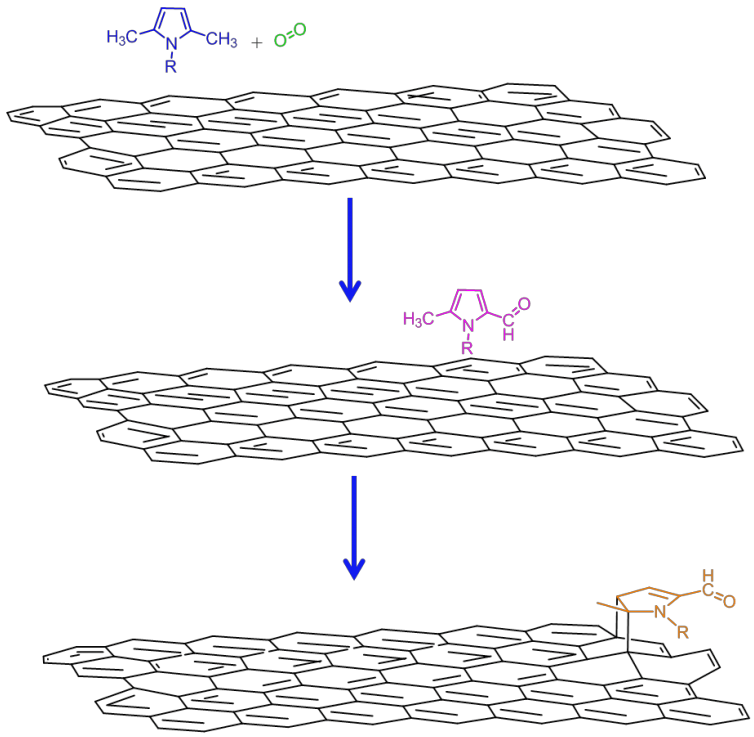

Figure 7.3 Hypothesized mechanism of CB-PyC synthesis.[8]

It can be considered a solid-state reaction, with an air flux considered necessary to oxidize the pyrrole, making the latter suitable for the DA reaction. As suggested by literature, maximum functionalization yields are achieved for temperatures comprised between 150°C and 180°C.[8]

References

[1] V.K Thakur, M.K. Thakur. Chemical Functionalization of Carbon Nanomaterials: Chemistry and Applications (1st ed.). CRC Press, 2015.

[2] J. P. Gallivan, D. A. Dougherty, *Proc. Natl. Acad. Sci. USA*, 1999, 96, 9459-9464.

[3] M. Galimberti, V. Barbera, S. Guerra, et al. Biobased janus molecule for the facile preparation of water solutions of few layer graphene sheets. RSC Advances. 2015;5(99):81142-81152.

[4] M. Galimberti, V. Barbera, S. Guerra, A. Bernardi. Facile functionalization of sp^2 carbon allotropes with a biobased janus molecule. Rubber Chemistry and Technology. 2017;90(2):285-307.

[5] I. Y. Jeon et Al., Edge-carboxylated graphene nanosheets via ball milling PNAS April10, 2012 vol.109 no.15, 5593.

[6] Huang et. Al. Attaching Proteins to Carbon Nanotubes via Diimide-Activated Amidation, Nano Letters, 2002, 311-314.

[7] Vinay Deep Punetha et. Al. Functionalization of carbon nanomaterials for advanced polymer nanocomposites: A comparison study between CNT and graphene. Progress in Polymer Science, 2017, 67, 1-47.

[8] Barbera, V., Brambilla, L., Milani, A., Palazzolo, A., Castiglioni, C., Vitale, A., ... & Galimberti, M. (2019). Domino Reaction for the Sustainable Functionalization of Few-Layer Graphene. Nanomaterials, 9(1), 44.

[9] V. Barbera, A. Bernardi, A. Palazzolo, A. Rosengart, L. Brambilla, M. Galimberti. Facile and sustainable functionalization of graphene layers with pyrrole compounds. Pure and Applied Chemistry. 2018;90(2):253-270.

Chapter 8

Synthesis of N-substituted pyrrole derivative

8.1. Introduction

Aim of the research commented in this chapter was the synthesis of pyrrole compounds with different functional groups on the nitrogen atom. As reported in the Introduction to the Thesis, the pyrrole compounds were selected in order to add bases onto the surface of carbon black. The role of the bases should be to promote faster vulcanization reactions and better interaction between CB and silica. Hence, the pyrrole compounds were prepared starting from the amine shown in Figure 8.1.a and 8.1.b. A further pyrrole compound was prepared, starting from ethanol amine, shown in Figure 8.1.c. The objective was to compare the behaviors of the adducts containing the bases and of the adduct containing the OH group, which should be able, in principle, at least to establish an interaction with the silanols of silica.

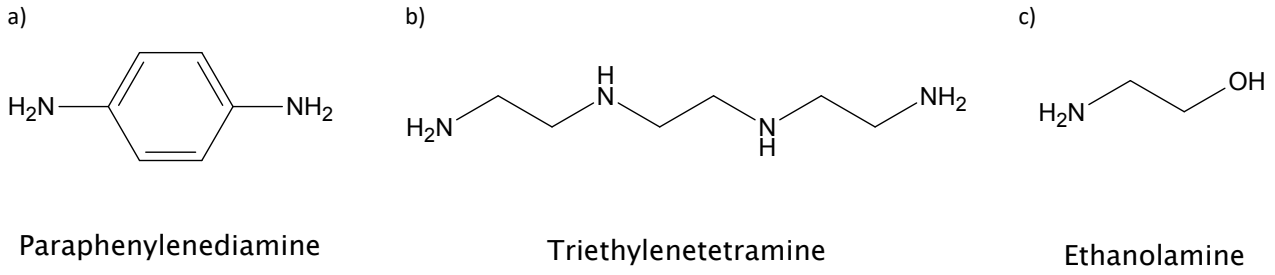

Figure 8.1 a) paraphenylenediamine, b) triethylenetetramine, c) ethanolamine.

The synthesis of pyrrole derivatives is based on the Paal-Knorr reaction. It is a reaction exploited in organic chemistry to obtain substituted pyrroles, furans or thiophenes. The pyrrole synthesis mechanism is summarized in the Figure below:

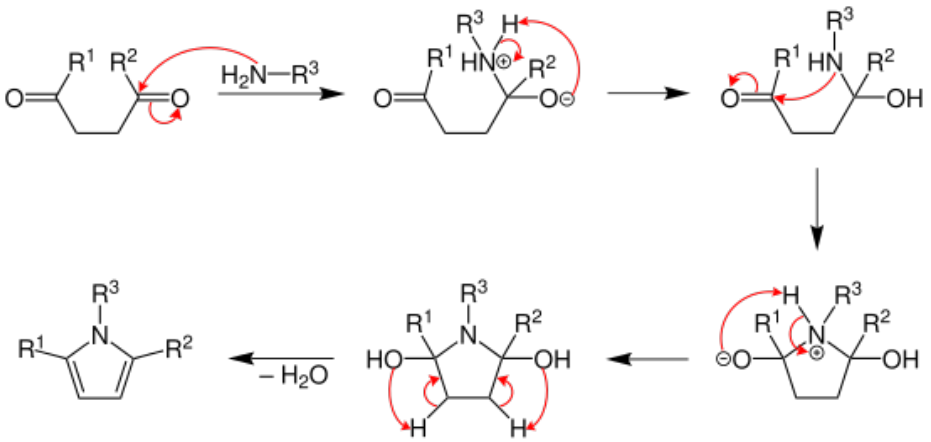

Figure 8.2 Mechanism of the Paal-Knorr pyrrole synthesis.[1]

The Paal-Knorr pyrrole synthesis is a condensation reaction between 1,4 diketones and primary amines.[2] The change in the nitrogen hybridization (from sp^3 to sp^2) can give rise to π-π stacking with aromatic compounds such as carbon allotropes.[3]

The Paal-Knorr reaction was exploited for its versatility, for the high atomic efficiency, for the mild conditions and for the sustainability of the process which did not involve acidic catalysts and produced water as the only byproduct.[4]

All the pyrrole derivatives synthesis were performed in the absence of solvents and catalysts. Reagents commercially available were purchased and used without further purifications with the only exception of p-phenylenediamine, which required a recrystallization.

Pyrrole synthesis reactions were followed by their characterization, by means of nuclear magnetic resonance spectroscopy (NMR) analysis, gas chromatography-mass spectrometry (GC-MS) analysis and pH measurements.

It was found that polyethylene amine pyrrole (TETAP) interacted with the GC column (composed by polysiloxanes) leading to a poor quality of the chromatogram and the presence of peaks not corresponding to nor the reagents or the products.

8.2. Preparation

8.2.1. General procedure

The amine (either ethanolamine, or paraphenylenediamine or triethylenetetramine) was poured in a 250 mL round bottom flask and 2,5-hexanedione was added dropwise. The mixture was heated under stirring for a selected time and then cooled down to room temperature.

A condenser was applied on top of the bottom flask for all the N-substituted pyrroles, with the only exception of mono-ethanolamine pyrrole.

GC-MS and NMR analysis were employed to characterize the resulting products.

The reaction yield was calculated following the equation:

$$Percent\ yield\ = \frac{Actual\ yield}{Theoretical\ yield} \times 100$$

Where Actual yield is the amount of product obtained from the reaction and theoretical yield is the amount of product obtained from the stoichiometry.

8.2.2. Synthesis of Mono-ethanolamine Pyrrole (EAP)

8.2.2.1. *Materials and reactions conditions:*

Table 8.1 Synthesis of EAP at 130°C for 2h.

Chemical	**MW-g/mol**	**Density-g/cm^3**	**Boiling point**	**Mol**	**Temperature**	**Reaction time**	**Stirring**
Ethanolamine	61	1.01	170°C	0.0342	130°C	2h	300 rpm
2,5-hexanedione	114.14	0.973	191°C	0.0342			

8.2.2.2. *Reaction scheme and yield:*

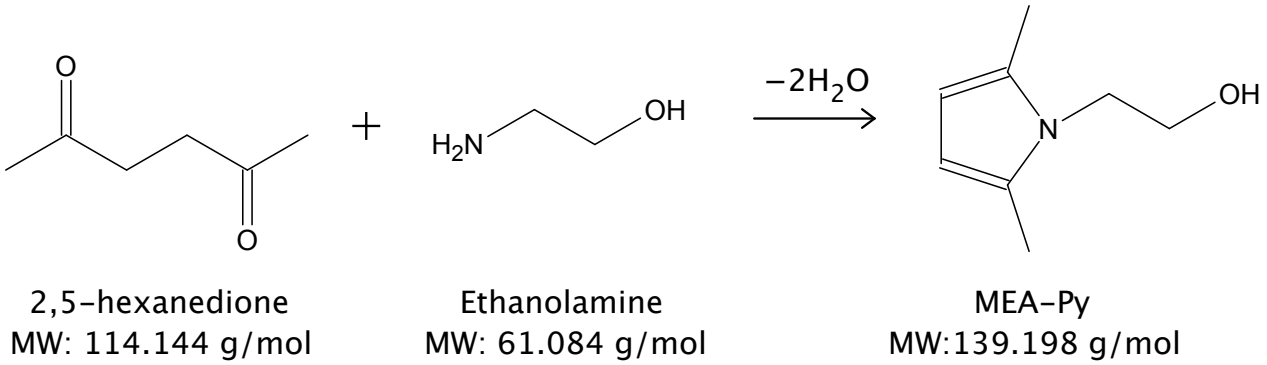

Figure 8.3 EAP synthesis – reaction scheme.

A yield of 84.4 % was estimated for this reaction.

8.2.2.3 Characterization of Mono-ethanolamine Pyrrole (EAP)

EAP was obtained as an amber-viscous liquid at room temperature and atmospheric pressure. GC-MS analysis were performed 30 minutes after the start of the synthesis and are reported in the Figure below.

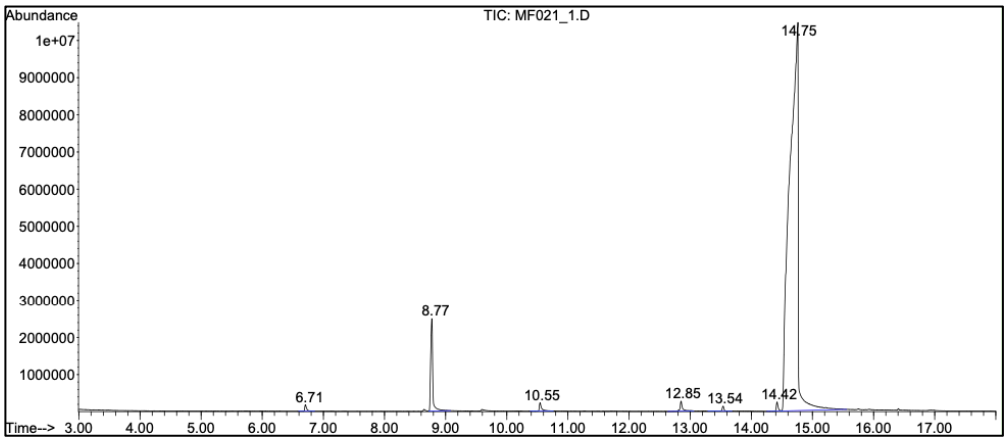

Figure 8.4 Chromatogram of EAP after 30 min at 130°C.

Only two peaks are present, indicating a very good selectivity toward the product. The peak at 8.77 min refers to the unreacted 2,5-hexanedione while the peak at 14.75 min is associated to EAP (MW: 139 g/mol). After 1h 30 min the 2,5-hexanedione peak was not present, confirming the presence of the only product (not represented). Following the stoichiometry of the reaction, a yield of 84.4% was calculated.

8.2.3. Synthesis of p-Phenylenediamine Pyrrole (p-PDAP)

8.2.3.1. *Materials and reactions conditions:*

Table 8.2 Synthesis of p-PDAP at 150°C for 2h.

Chemical	**MW-g/mol**	**Density -g/cm^3**	**Boiling point**	**Mol**	**Temperature**	**Reaction time**	**Stirring**
p-Phenylenediamine	108.1	1.135	267°C	0.035	150°C	1h 30min 30 min (no condenser)	300 rpm
2,5-hexanedione	114.1	0.973	191°C	0.035			

8.2.3.2. *Reaction scheme and yield:*

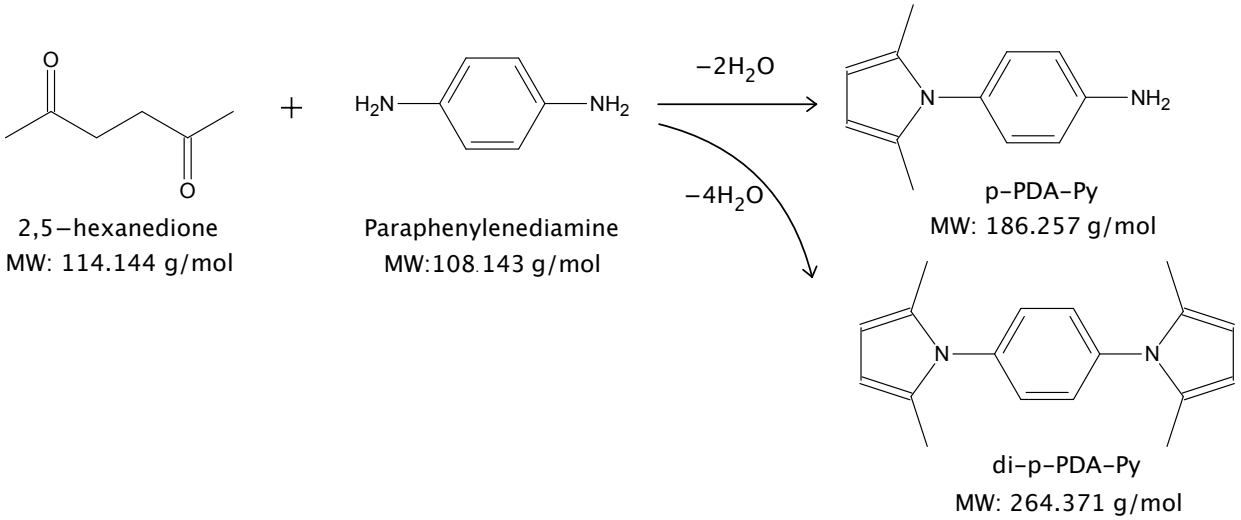

Figure 8.5 p-PDAP synthesis – reaction scheme.

This reaction was characterized by a yield of 93%.

8.2.3.3 Characterization of p-Phenylenediamine Pyrrole (p-PDAP)

In Figure 8.6 is reported the chromatogram obtained after 2h:

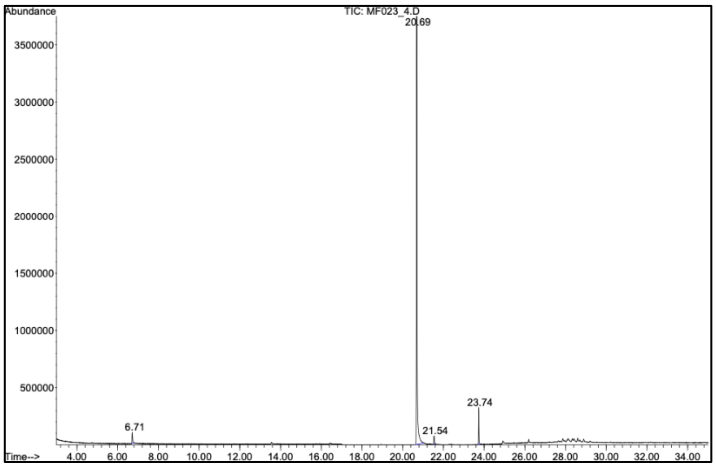

Figure 8.6 Chromatogram of the p-PDAP after 2h at 150°C.

P-phenylenediamine pyrrole was obtained as a brown/red solid at room temperature and atmospheric pressure.

Good reaction selectivity toward the products is visible from the absence of satellite peaks. The peak at 20.69 min is related to mono-p-PDAP while peak at 23.74 min refers to di-p-PDAP.

The yield was calculated assuming a complete selectivity to the main product, mono-p-PDAP. This approximation was made on the basis that the area of the mono-p-PDAP peak was greater than 92% (Figure 8.6). The value of the yield is equal to 93%. It is important to consider that this value was overestimated.

8.2.4. Synthesis of Triethylenetetramine Pyrrole (TETAP)

8.2.4.1. *Materials and reactions conditions:*

Table 8.3 Synthesis of TETAP at 150°C for 2h.

Chemical	MW-g/mol	Density -g/cm^3	Boiling point	Mol	Temperature	Reaction time	Stirring
Triethylenetetramine	146.23	0.98	266.6°C	0.02	150°C	1h 30 min 30 min (no condenser)	300 rpm
2,5-hexanedione	114.14	0.973	191°C	0.02			

8.2.4.2. *Reaction scheme and yield:*

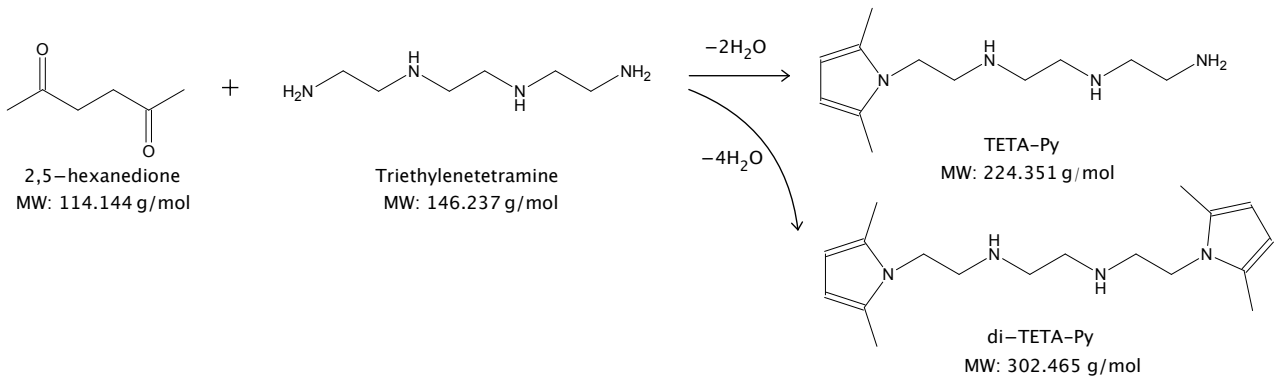

Figure 8.7 TETAP synthesis – reaction scheme.

A yield of 80% was found for this reaction.

8.2.4.3 Characterization of triethylenetetramine Pyrrole (TETAP)

^{13}C NMR spectrum and peaks assignation of TETAP in deuterated chloroform ($CDCl_3$) are shown in Figure 8.8 and in Table 8.4.

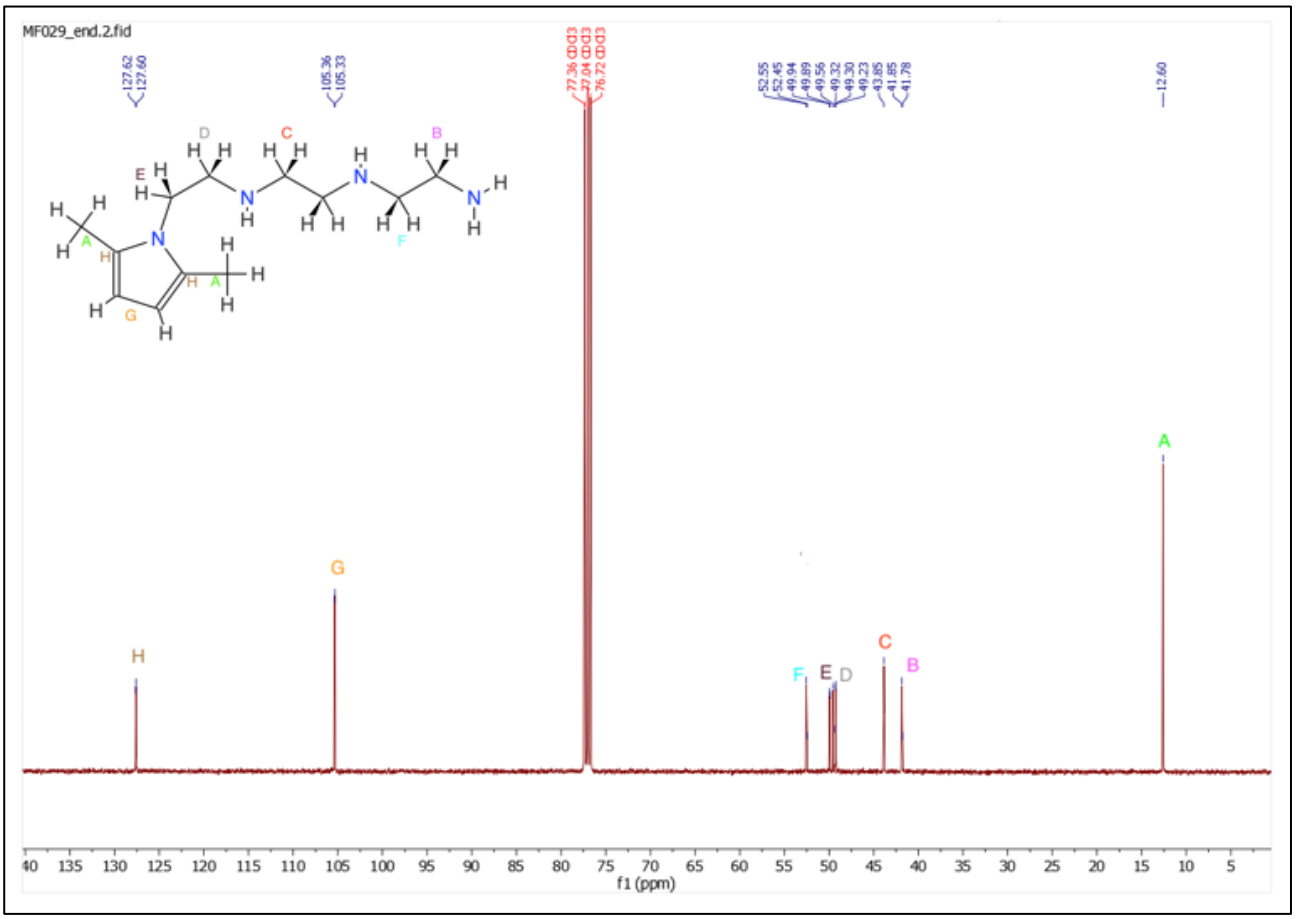

Figure 8.8 C NMR spectrum in $CDCl_3$ of TETAP.

TETAP appeared as an amber viscous liquid at room temperature and atmospheric pressure.

Table 8.4 Peaks assignation of TETAP C NMR spectrum.

Peak	**δ-ppm**	**Assignment**
A	12.6	-CH_3 attached to the pyrrole ring
B-F	41.8-51.6	Alkylamino moiety
G	105.3	β carbon of the pyrrole ring
H	127.6	α carbon of the pyrrole ring

As can be seen in Table 8.4 and in Figure 8.8, C NMR analysis confirmed the presence of the desired product. G and H peaks are found to be doubled, attesting the presence of both mono and di-pyrrole. From H-NMR peaks integration (not represented) a ratio of mono/di-pyrrole of 4:1 was obtained. A yield of 80% was calculated. It is worth to notice that in this case the yield was estimated considering the mono-pyrrole as the primary product.

8.3 pH of amines and pyrrole derivatives

pH was determined following the procedure explained in the Experimental section.

Table 8.5 pH values of primary amines and pyrrole derivatives.

	pH
Ethanolamine	11.5
Ethanolamine pyrrole (EAP)	5.9
P-phenylenediamine	8.5
P-phenylenediamine pyrrole (p-PDAP)	n.d.[a]
Triethylenetetramine	11.5
Triethylenetetramine pyrrole (TETAP)	11.1

a) insoluble in water.

An alkaline behavior was shown by primary amines and by triethylenetetramine pyrrole, while, for ethanolamine pyrrole, a pH of 5.9 was detected.

8.4. Conclusions

The synthesis of the pyrrole compounds was successfully performed. TETA, EAP and p-PDAP were prepared with high yield: 80%, 84.4% and 93%, respectively. EAP and p-PDAP were characterized by a high selectivity, while TETAP was present in a mixture of mono/di-pyrrole (80% and 20%, respectively). All the pyrrole's derivatives synthesis were performed using a green chemistry approach, without solvents and catalysts.

References

[1] https://it.wikipedia.org/wiki/Sintesi_di_Paal-Knorr (last access 29/03/2021).

[2] Avula Balakrishna et. Al.Paal–Knorr synthesis of pyrroles: from conventional to green synthesis. *Catalysis Reviews*, 2018, 84-110.

[3] *Barbera et al.* Polyether from a biobased Janus molecule as surfactant for carbon nanotubes. *eXPRESS Polymer Letters Vol.10, No.7 (2016) 548–558.*

[4] Galimberti M, Barbera V, Citterio A, et al. Supramolecular interactions of carbon nanotubes with biosourced polyurethanes from 2-(2, 5-dimethyl-1H-pyrrol-1-yl)-1, 3-propanediol. Polymer. 2015;63: 62-70.

Chapter 9
Synthesis of CB-PyC adducts

9.1. Introduction

The Objective of the research activity summarized in this Chapter was the preparation of adducts of CB with the pyrrole compounds prepared as described in the previous Chapter.

Carbon black grade was N326, provided by BIRLA Carbon S.p.a. and it was used as supplied without further purifications.

The adducts were prepared by using the functionalization method named "pyrrole methodology", commented in the Introduction to the Thesis and described in Chapter 7. According to the mechanism of the functionalization reaction, a Diels-Alder reaction occurs, in which the pyrrole acts as a dienophile and the edges of the graphitic planes as dienes. [1]

Such a pyrrole methodology appears to be a viable, easy and effective method to provide the carbon black surface with different functional groups, based on the substituent on the nitrogen of the pyrrole ring.

The synthesis of CB-PyC adducts was done by applying the method developed in the research Group. It is worthy underlining that solvents or catalysts were not used during the functionalization reaction. After the reaction, the adducts were thoroughly washed and then characterized by means of thermogravimetric and elemental analysis.

9.2. Preparation

9.2.1. Functionalization of CB with Pyrrole derivatives

9.2.2. *General procedure:*

The pyrrole derivative and carbon black N326 were mixed with acetone and the mixture was sonicated for 20 minutes. The solvent was consequently removed with a rotary evaporator and the mixture was left under stirring for two hours at a temperature between 160 and 180 °C. Reaction setup is visible in Figure 9.1.

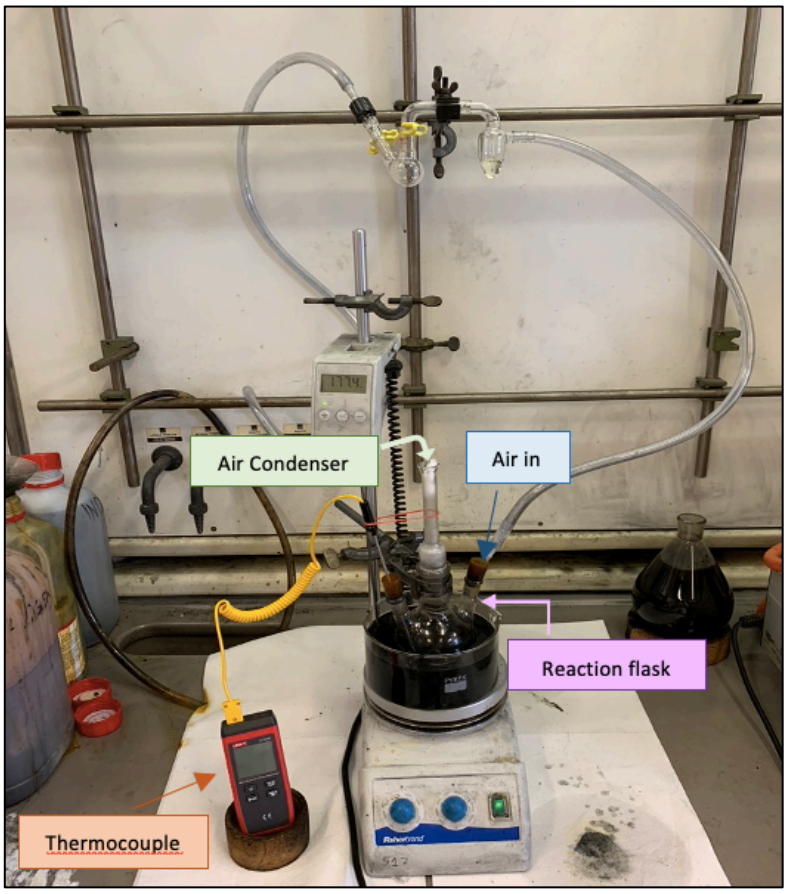

Figure 9.1 CB N326- PyC adducts preparation setup.

Unreacted pyrrole was extracted with acetone using a Soxhlet apparatus overnight. The powder was then dried in an oven at 70 °C, weighed and characterized.

A scheme of CB-PyC adducts preparation is reported in Figure 9.2.

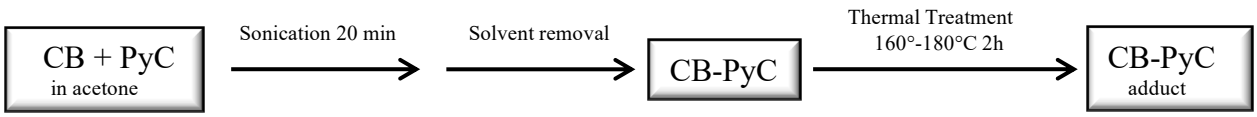

Figure 9.2 Procedure for the functionalization of CB with pyrrole derivatives.

More details about the synthesis of CB-PyC adducts are reported in the Experimental section. Information about each synthesis is summarized in Table 9.1.

9.2.3. *Extraction of the unreacted pyrrole*

All the synthesized CB-PyC adducts were washed with acetone using a Soxhlet apparatus (Figure 9.3). This apparatus was preferred because it uses lower solvent quantities in comparison to normal liquid extraction.

Figure 9.3 Soxhlet apparatus.

Acetone was found to be a suitable solvent for all pyrrole compounds: it has a low boiling point, and it is less toxic than other common solvents. Washing was stopped when the liquid surrounding the cotton thimble was consistently clear, indicating a good extraction of the pyrroles from the carbon allotrope.

9.2.4 *Materials and reactions conditions:*

Adducts list and reaction conditions are listed in Table 9.1.

Table 9.1 Reagents and reactions conditions for the synthesis of CB N326-PyC adducts.

Adducts		Reagents	Weight/g	Temperature[a]	Reaction time	Stirring
1°	**CB/EAP**	CB N326	10.56	180°C	2h	300 rpm
		EAP	1.50			
	CB/p-PDAP	CB N326	10.20			
		p-PDAP	1.502			
	CB/TETAP	CB N326	19.99	160°C		
		TETAP	2.99			
2°	**CB/EAP**	CB N326	30.00			
		EAP	2.60			
	CB/p-PDAP	CB N326	30.00			
		p-PDAP	2.60			
	CB/TETAP	CB N326	30.00			
		TETAP	2.60			

a) Temperature of the oil bath.

9.3. Characterization

9.3.1. *Thermogravimetric Analysis (TGA)*

Thermogravimetric analysis were performed on dried powders. Details of the heating ramp and instrumentation are found in the Experimental section.

Degree of functionalization (η) and p.h.c. (parts per hundred carbon black) were calculated for samples analyzed by TGA using respectively equation 1 and 2:

$$\eta = \frac{wt.\%\ loss\ {}^{CB-PyC\ washed}_{150\rightarrow 900°C} - wt.\%\ loss\ {}^{CB\ Pristine}_{150\rightarrow 900°C}}{wt.\%\ loss\ {}^{CB}_{900\ °C}} \cdot \frac{m_{CB}}{m^{i}_{pyrrole}} \cdot 100, (1)$$

$$phc = \frac{wt.\%\ loss^{CB-PyC\ washed}_{150\rightarrow 900°C} - wt.\%\ loss^{CB\ Pristine}_{150\rightarrow 900°C}}{wt.\%\ loss^{CB}_{900\ °C}} \cdot 100, (2)$$

Where m_{CB} and m^i are the carbon black and the initial pyrrole mass, while wt. % loss is the mass loss of the sample from TGA. The 150-900°C interval was chosen because it is related to the decomposition of pyrrole compounds and exclude water and organic impurities desorption which usually occurs around 100-120°C. [3]

In Figure 9.4 is reported a thermogram with the weight losses in percentages. These are also reported in Table 9.2:

Table 9.2 Mass losses of CB N326 according to thermogravimetric analysis.

	Mass loss (%) for **T<150°C**	**Mass loss (%)** for **150 <T<900°C**	**Mass loss (%)** for **T> 900°C**
CB N326	0.1	3.3	96.6

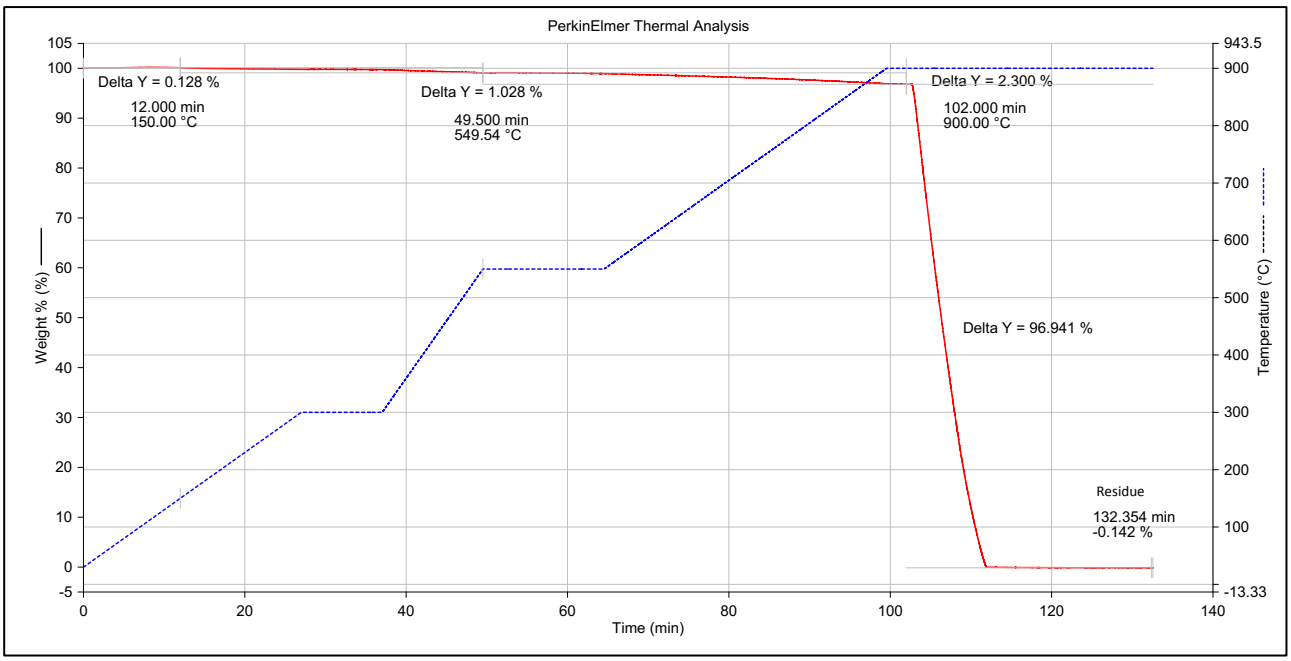

Figure 9.4 Thermograph of CB N326.

The TGA curve, which represents the percentage weight loss as a function of time, is shown in red, while the blue curve shows the temperature ramp.

Mass loss in the temperature range between 150°C and 900°C could be attributed to the decomposition of alkenyl groups, present as defects on the carbon black, and to impurities, coming from the production process and from the packaging.[2] Combustion with oxygen occurs at T>900°C.[2]

9.3.2. *Elemental analysis*

Elemental analysis were performed on dried powders. Details of the instrumentation are found in the experimental section. The amount of pyrrole derivative on the adduct was calculated on the basis of the nitrogen content. Degree of functionalization and p.h.c. were calculated by applying equation (3) and (4), respectively.

$$Degree\ of\ functionalization = \frac{wt.\%_N^{CB-PyC} - wt.\%_N^{CB}}{wt.\%_{N,theoretical}^{CB-PyC}} \times 100, (3)$$

$$phc = \frac{m_{pyrrole}^{i}}{m_{CB}} \times \frac{wt.\%_N^{CB-PyC} - wt.\%_N^{CB}}{wt.\%_{N,theoretical}^{CB-PyC}} \times 100\ , (4)$$

Where m_{CB} and m^i are the carbon black and the initial pyrrole mass while wt. $\%_N$ is the nitrogen's weight percentage. In the Table below are reported data of CB elemental analysis.

Table 9.3 Elemental analysis of carbon black N326.

	N		**C**		**H**	
CB	Wt. %	Dev %	Wt. %	Dev %	Wt. %	Dev %
	3.40	± 0.20	91.51	± 1.50	0.08	± 0.02

9.3.3 *Soxhlet extraction*

The degree of functionalization (equation 5) and phc (equation 6) were also calculated by the analysis of the residual after Soxhlet extraction.

$$\eta_S = \frac{m_{Py,i} - m_{Py,unr}}{m_{Py,i}} \times 100\ , (5)$$

$$phc = \frac{m_{pyrrole}^{i}}{m_{CB}} \times \frac{m_{Py,i} - m_{Py,unr}}{m_{Py,i}} \times 100\ , (6)$$

Where $m_{Py,i}$ is the initial mass of the pyrrole derivative and $m_{Py,unr}$ is the mass of the unreacted pyrrole derivative.

9.4. Synthesis of CB-PyC adducts

Thermogravimetric analysis allowed to determine mass losses of a substance as a function of temperature and time. CB-PyC adducts were analyzed in order to obtain an estimation of the amount of pyrrole derivative present on the carbon black surface by comparing data of pristine and functionalized CB.

The thermogram can be divided into three sections:

- T<150°C: the weight loss below 150°C can be reasonably attributed to the release of water and adsorbed volatiles.
- 150< T<900°C: this range is related to the decomposition of alkenylic groups, defects of CB, and also to the desorption of organic molecules present in the adducts (e.g., PyC in this specific case).[1]
- T >900°C: combustion with oxygen.

In the Figure below are shown the thermographs of the CB-PyC adducts. Mass losses in percentages are summarized in Table 9.4:

Table 9.4 Mass losses of CB/EAP according to thermogravimetric analysis.

	Mass loss (%) for **T<150°C**	**Mass loss (%)** for **150 <T<900°C**	**Mass loss (%)** for **T> 900°C**
CB/EAP	0.4	4.5	95.1
CB/p-PDAP	0.04	4.4	95.56
CB/TETAP	0.1	7.0	92.9

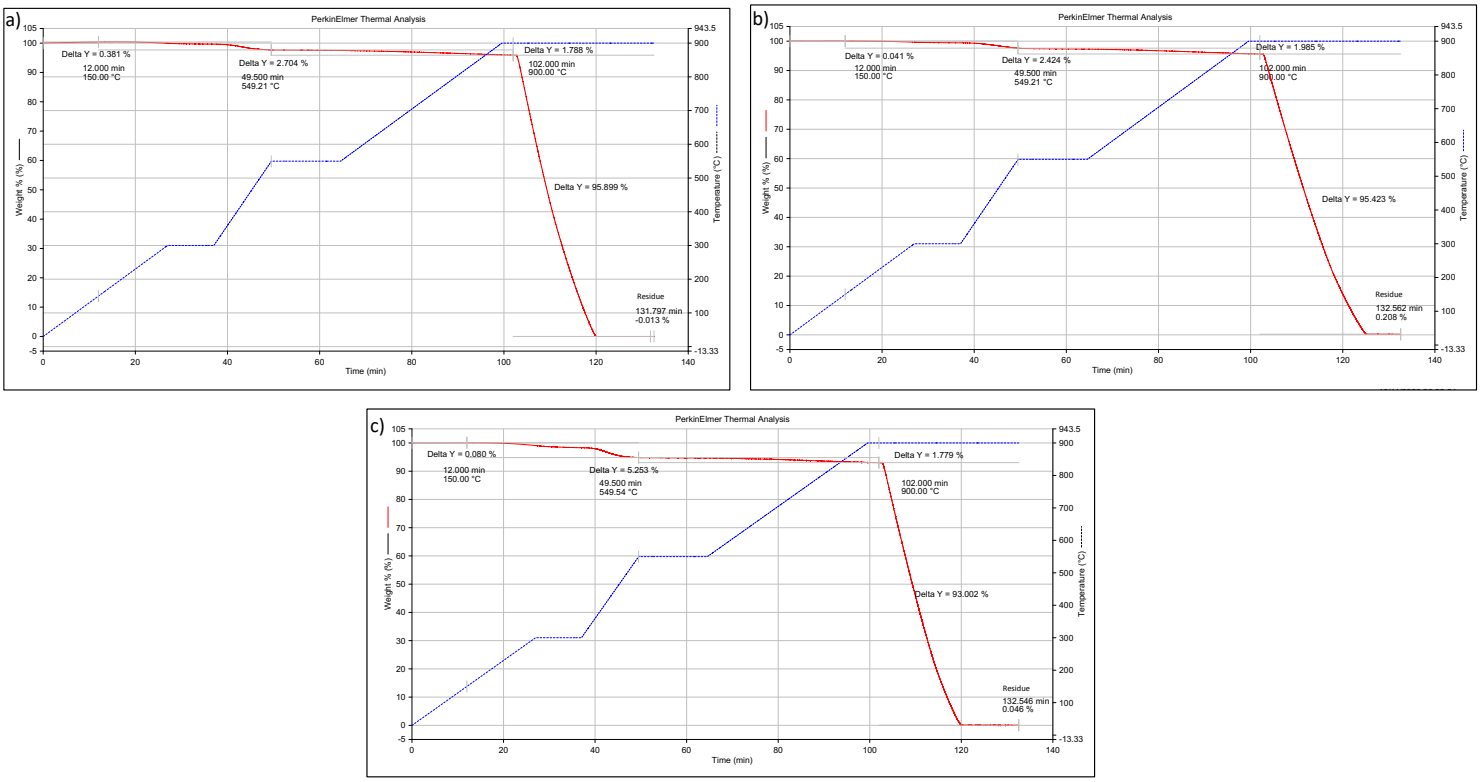

Figure 9.5 Thermograph of: a) CB/EAP, b) CB/p-PDAP, c) CB/TETAP.

In all the adducts the onset temperature of the last step degradation is similar with the one of pristine carbon black, pointing out that the functionalization reaction does not lead to a lower thermal stability of carbon black. An appreciable mass loss is present in the 150-900°C interval for the CB/TETAP (Figure 9.5-c), indicating the formation of a stable adduct.

Elemental analysis of CB/EAP and of CB/p-PDAP adducts are reported in Table 9.5. These were not executed for the CB/TETAP adduct.

Table 9.5 Elemental analysis of CB/EAP and CB/p-PDAP.

	N		**C**		**H**	
CB/EAP	Wt. %	Dev %	Wt. %	Dev %	Wt. %	Dev %
	3.54	± 0.20	91.72	± 1.50	0.20	± 0.02
CB/p-PDAP	Wt. %	Dev %	Wt. %	Dev %	Wt. %	Dev %
	4.02	± 0.20	90.53	± 1.50	0.34	± 0.05

Degree of functionalization and phc were calculated:

- with equations (1) and (2), for TGA.
- with equations (3) and (4), for elemental analysis.
- with equations (5) and (6), for the residual after the Soxhlet extraction.

Due to the absence of elemental analysis, CB/TETAP degree of functionalization and phc were calculated only by TGA and by the residual after Soxhlet extraction. Results are summarized in Table 9.6.

Table 9.6 Degree of functionalization and phc of CB-PyC adducts.

		Degree of functionalization	phc
CB/EAP	a)	14 %	1.2
	b)	17.5 %	1.52
	c)	84%	7.2
CB/p-PDAP	a)	13%	1.1
	b)	52%	4.5
	c)	72%	6.2
CB/TETAP	a)	46 %	4
	c)	84%	7.2

a) from TGA, b) from elemental analysis, c) calculated by the residual after Soxhlet extraction.

For the estimation of the degree of functionalization and phc, elemental analysis were not taken in consideration because the method adopted has to be optimized. It was found that this method overestimates heteroatoms such as nitrogen.

Values from TGA were chosen for the evaluation of the degree of functionalization and phc (equations (1) and (2)). Nevertheless, the alkenylic groups which are supposed to be responsible for the weight loss of pristine carbon black in the 150-900°C interval, could be reactive during the functionalization and so it could be wrong to subtract them in the estimation of the functionalization degree. However, for this thesis, what reported by the authors of functionalization technology[1,2] has been adopted and so the subtraction has been done. The last method is the residual after Soxhlet extraction which, taken in consideration the large molar mass of PyC, should be to a good extent reliable. The high numbers obtained are in line with the previous results of the "pyrrole methodology" as functionalization technology. However, in the present thesis, as already reported, it was decided to use TGA results to estimate phc of the pyrrole compounds and functionalization degree. Nevertheless, the mismatch between values suggest that this aspect has to be further investigated.

9.5. Conclusions

Comparing the pristine and functionalized CB TGA curves (T<900°C), no significant differences can be found. Hence, all the adducts were characterized by a remarkable thermal stability.

Lower functionalization efficiencies were found when preparing higher quantities of adducts (e.g., 20 to 30 grams), possibly indicating a diffusion-limited reaction kinetic.

References

[1] Barbera, V., Brambilla, L., Milani, A., Palazzolo, A., Castiglioni, C., Vitale, A., ... & Galimberti, M. (2019). Domino Reaction for the Sustainable Functionalization of Few-Layer Graphene. Nanomaterials, 9(1), 44.

[2] M. Galimberti , V. Barbera, S. Guerra, et al. Biobased janus molecule for the facile preparation of water solutions of few layer graphene sheets. RSC Advances. 2015;5(99):81142-81152.

Chapter 10

Evaluation of pH and Hansen solubility parameters of CB-PyC adduct

10.1. Introduction

Objective of the activity described in this chapter was the characterization of the adducts of CB with pyrrole compounds.

The following characterization was performed: measurement of the pH of water dispersions and evaluation of the Hansen solubility parameters of adducts of CB with pyrrole compounds. As the CB was modified with pyrrole compound containing bases, a basic pH and the modification of the solubility parameters were expected.

Results of these investigations are presented in this chapter.

Suspensions in water of adducts of CBN326 with pyrrole compounds and of pristine CBN326 (which experienced the same treatment as the adduct, hereinafter CBN326*) were prepared, their stability and pH were investigated.

To evaluate the Hansen solubility parameters, eight solvents, characterized by different polarity and proticity, were selected: xylene, tetrahydrofuran (THF), 2-propanol, methanol, distilled water, acetone, hexane and ethyl acetate.

Numerical methods in MATLAB environment, based on the Nelder-Mead algorithm, were applied to detect the Hansen solubility parameters and the interaction radius of each carbon material. Computational details are described in the next paragraphs.

Details of the applied procedures are in the Experimental part.

10.2. Preparation of carbon black dispersions

10.2.1. *Stability of aqueous suspensions*

Aqueous suspensions were prepared by inserting a desired amount of pristine or functionalized carbon black powder into test tubes containing distilled water. The dispersion was then sonicated and observed for 72 hours.

10.2.2 *Stability of dispersions in solvents:*

Dispersions of carbon black and CB-PyC adducts were prepared in solvents with different polarities. Dispersions' stability was investigated immediately after the sonication step and one week later.

Details of dispersion experiments are present in the Experimental section.

10.3. Hansen Solubility Parameters (HSP) and Hansen Solubility Sphere calculation

To determine Hansen solubility parameters from both CB and CB-PyC dispersions, a program developed by Farhad Gharagheizi, based on polymers' solubility, was implemented and it was adapted to the applied experimental conditions.[1] The three codes HSP.m, Solvent_Database.m and QF.m on which results were obtained are shown in the Appendix section.

HSP.m is the main function and it works as illustrated in the Figure below:

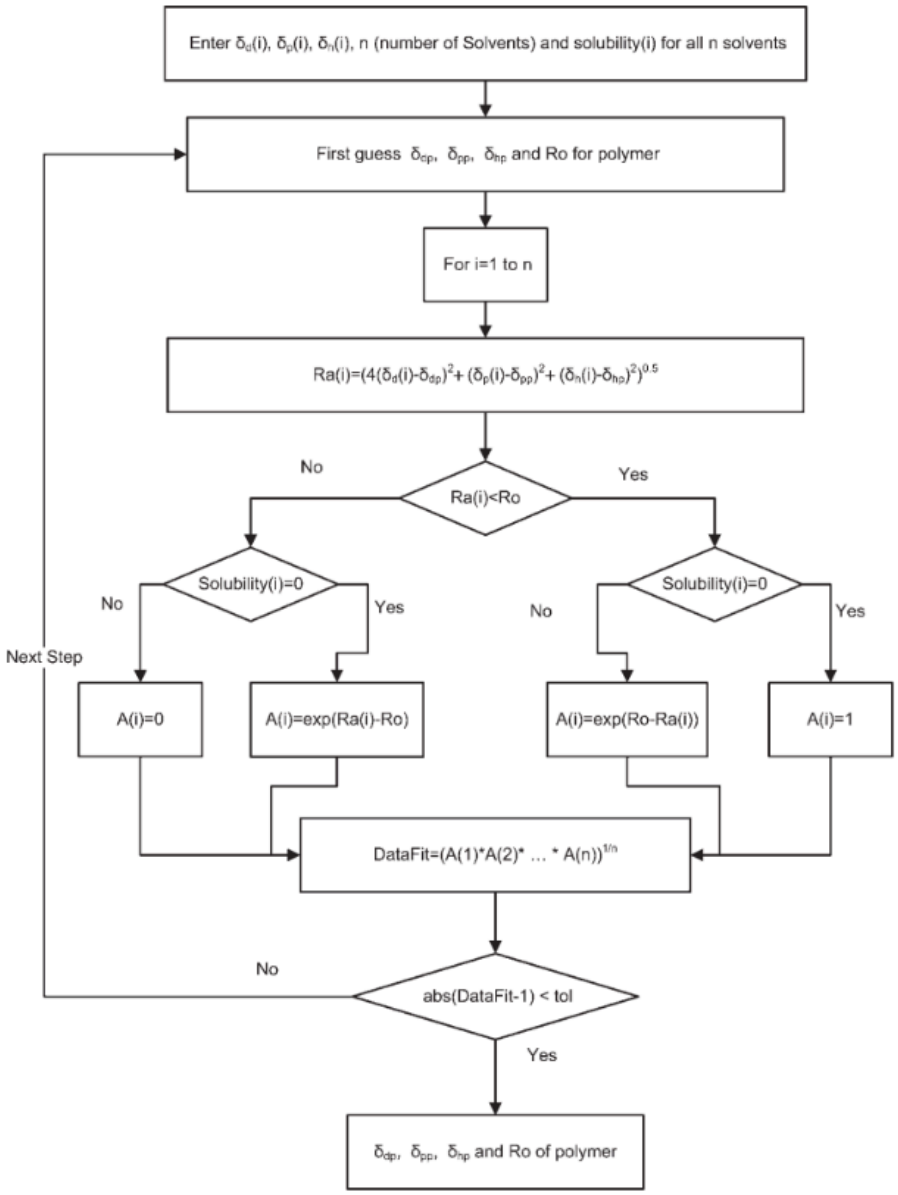

Figure 10.1 Algorithm at the basis of the Hansen solubility parameters and Solubility sphere radius.[1]

Solvent_Database.m function contains the solvents solubility parameters and stability factors for the adduct: a stable interaction and thus a "good" solvent was labelled as "1" while "0" was used for a

"bad" solvent. This function is called by HSP.m in order to find the first guess of target parameters: δ_{DP}, δ_{PP}, δ_{HP} and R_0. δ_D, δ_P and δ_H are the polymers' Hansen solubility parameters and R_0 is the interaction radius.

QF.m contains the DataFit function and it is called by the fminsearch function by MATLAB. This function works with the Nelder-Mead algorithm to minimize the objective function, described as follow:

$$ObjectiveFunction = |DataFit - 1|$$

Where DataFit function is expressed as:

$$DataFit = (A_1 \times A_2 \times \ldots \times A_n)^{\frac{1}{n}}$$

where n is the number of tested solvents. DataFit in the equation above approaches 1 as the fit improves during an optimization and reaches 1 when all "good" solvents are within the sphere while "bad" solvents are outside.

$$A_i = e^{(Error\ Distance)}$$

A_i is equal to one for a given "good" solvent within the sphere and for a given "bad" solvent outside the sphere. [2] After the minimization, results are shown in the MATLAB workspace.

Once detected the solubility parameters and the interaction radius, it was possible to calculate the Hansen solubility sphere.

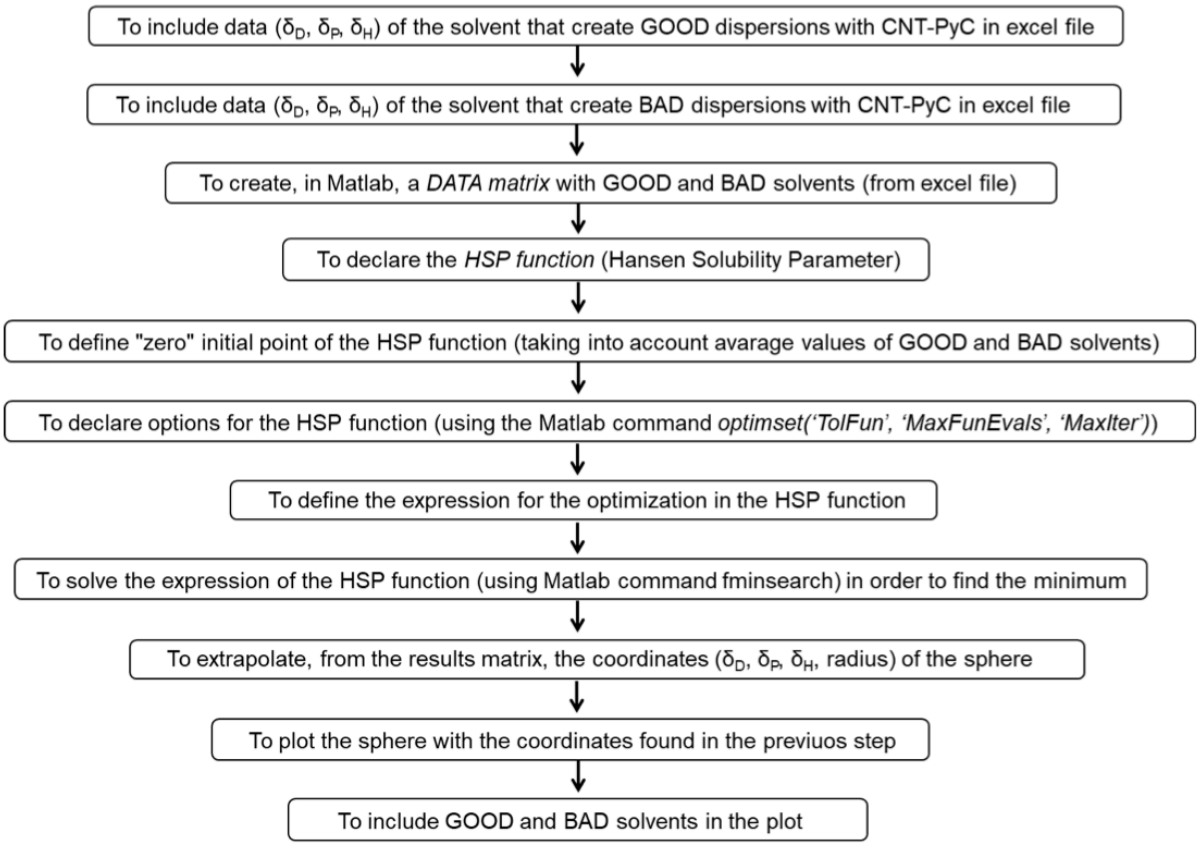

Figure 10.2 Hansen Solubility Sphere's MATLAB algorithm.[3]

The algorithm was used in MATLAB in order to evaluate the coordinates of the spheres[3] and it can be seen in Figure 10.2.

10.4. Results

10.4.1. Stability of aqueous suspensions

A stable suspension is obtained when the attractive forces between particles are lower than the ones between the particles and the solvent. The dynamic equilibrium, shifted towards one force or another, depends on different factors. First, the presence of functional groups on the particle surface strongly affects dispersibility. Concerning carbon black particles there are also two others main factors involved: the surface area and the "structure".

The surface area is directly related to the size of carbon black particles: smaller are the particles, higher is the surface area which defines how much area is available for interaction. [4]

"Structure" refers to size and bulkiness of aggregates and agglomerates. High-structure carbon black refers to large, non-spherical aggregates while low-structure consists of small, spherically shaped aggregates.[5] High structure carbon black is easier to disperse than low structure carbon black because of the augmented difficulty in close packing (Figure 10.3).

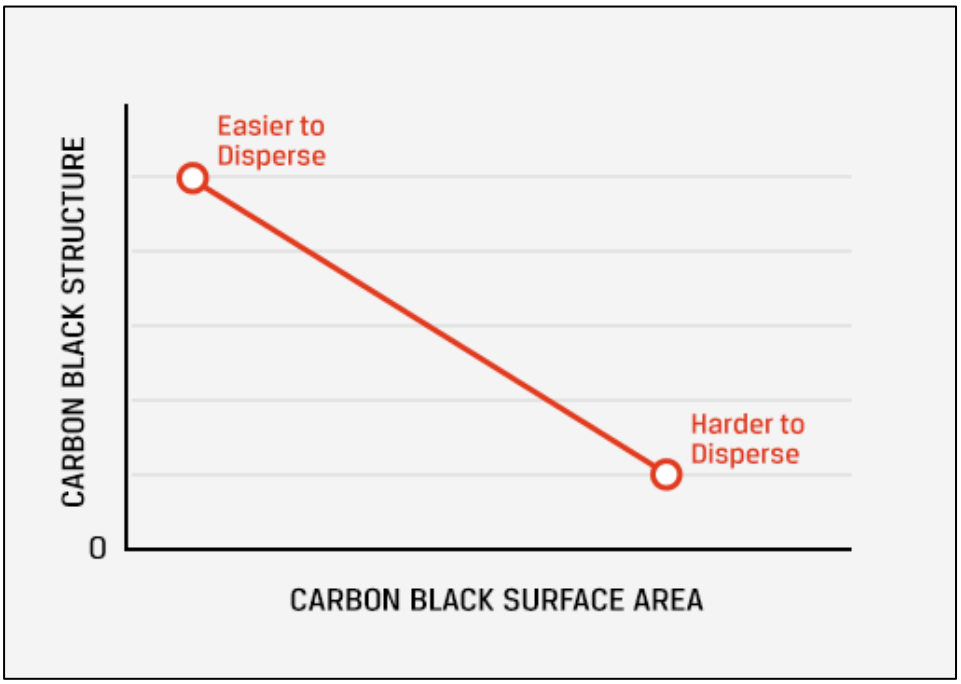

Figure 10.3 Carbon black dispersibility as function of surface area and structure.[6]

10.4.2. Aqueous dispersions of Carbon black and CB adducts

Suspensions pictures were taken after the sonication and after 72 hours.

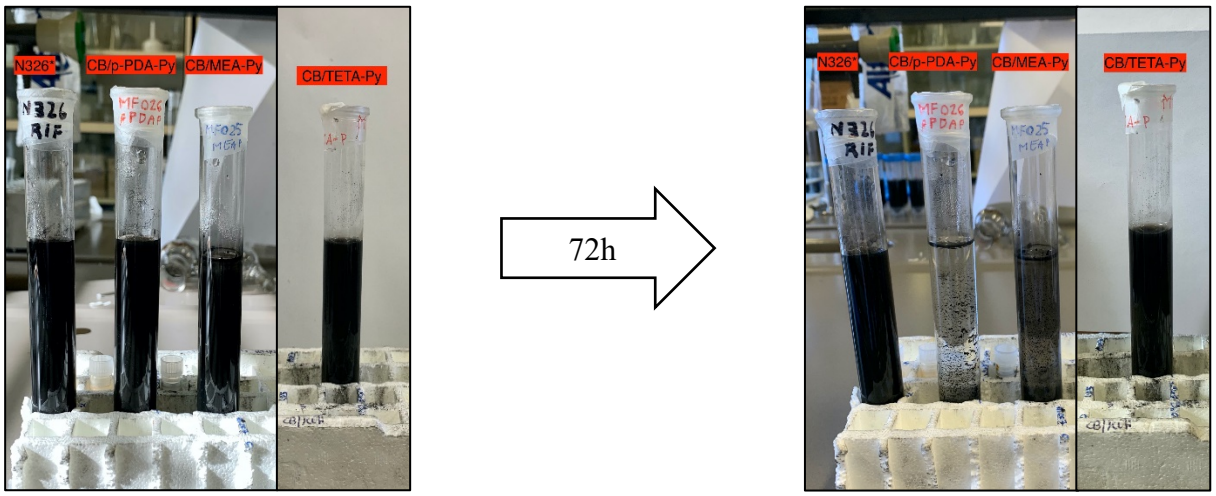

Figure 10.4 Aqueous dispersions of N326*, CB/p-PDAP, CB/EAP and CB/TETAP.

N326* and CB/TETAP adduct formed stable dispersion while CB/p-PDAP and CB/EAP did not. Unstable suspensions were detected for CB/p-PDAP and CB/EAP adducts. It is hypothesized to be related to the aggregates and agglomerates dimensions and to the hydrophobicity promoted by the presence of graphene rings. [4]

10.4.3. pH of aqueous dispersions

The results of the pH measurements are reported in the following histogram:

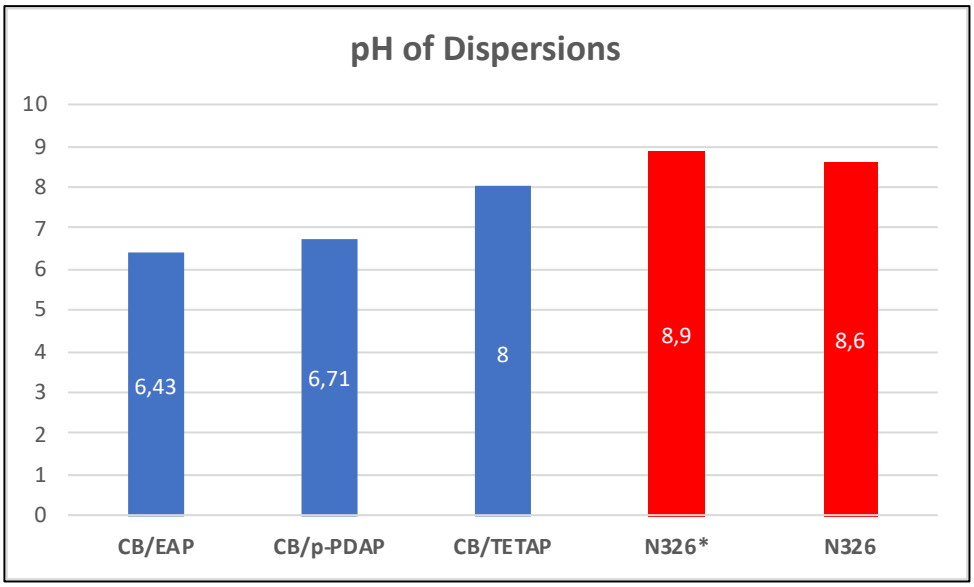

Figure 10.5 pH of aqueous dispersions.

For CB N326, N326* and CB/TETAP adduct, a slightly basic pH value of respectively 8.6, 8.9 and 8 was reported while CB/EAP and CB/p-PDAP adducts showed values of 6.4 and 6.7, respectively. Comparisons between pH values of N326* and pure carbon black were made, pointing out that the procedure, described in the experimental section, to which N326* sample was subjected, did not lead to a significant change in the pH value. [7]

Although pyrrole derivatives were synthesized starting by basic primary ammines, neutral pH values were detected for CB/EAP and CB/p-PDAP adducts.

The more acidic behavior displayed by CB-PyC adducts compared to pristine carbon black is probably related to the presence of acidic species, such as carboxylic and phenolic groups, on the carbon black surface.[4] As reported in Chapter 7, the Diels-Alder reaction is hypothesized to take place after the pyrrole derivative oxidation (Figure 10.6). This could lead to a balance between carboxylic groups due to oxidation and the amino groups of the pyrrole.

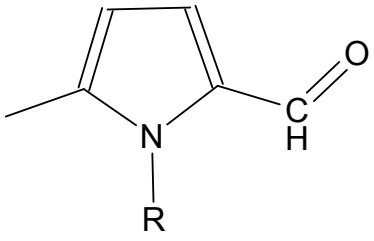

Figure 10.6 Oxidized pyrrole derivative.

10.4.4. Evaluation of dispersions stability of N326, N326* and CB-PyC

Dispersions of N326 and N326* are shown in the following pictures:

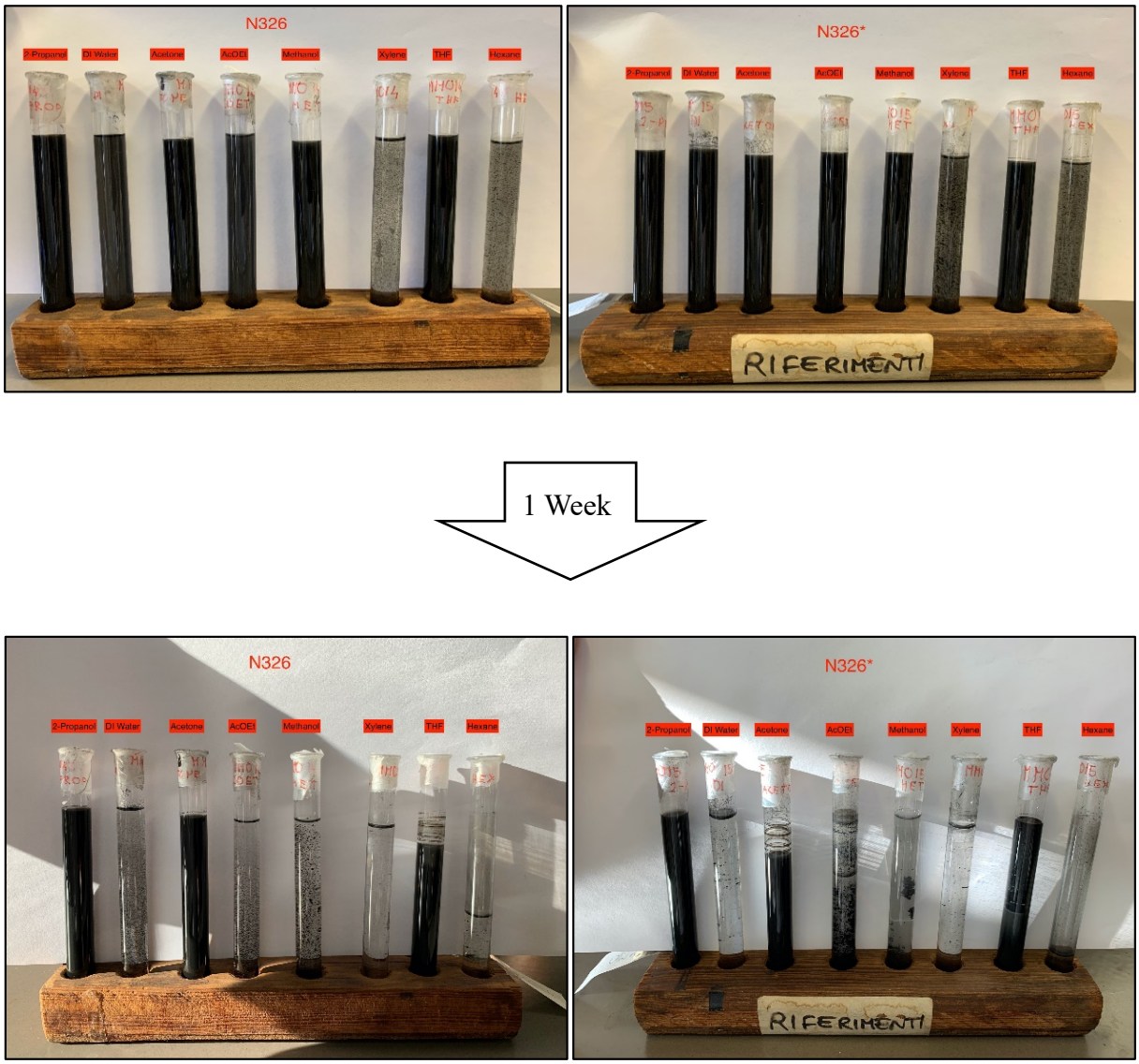

Figure 10.7 Dispersions of N326 and N326* (1 mg/mL).

In the images below are shown dispersions of CB-PyC adducts:

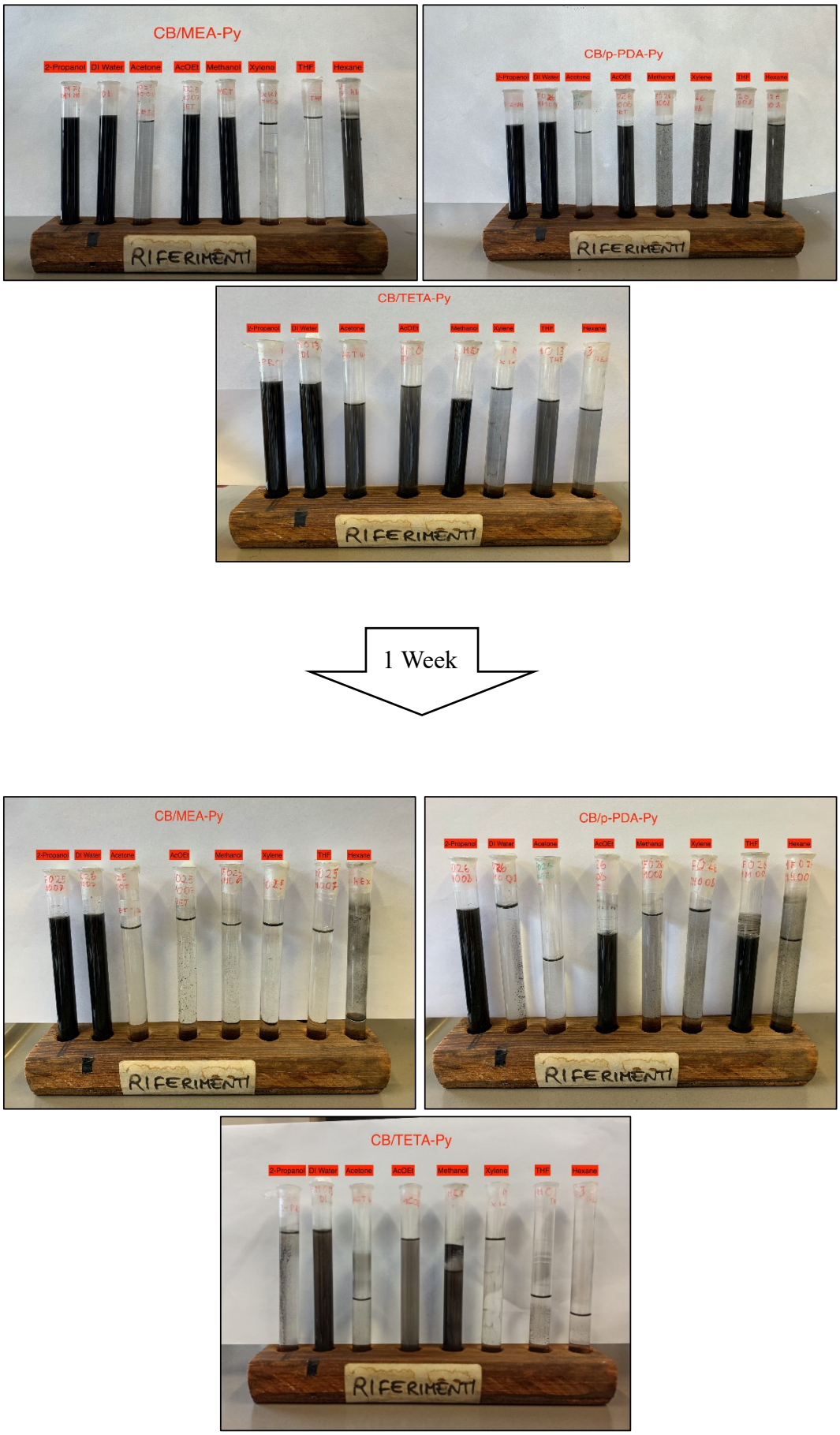

Figure 10.8 Dispersions of CB/EAP, CB/p-PDAP and CB/TETAP (1 mg/mL).

In the following Table are summarized the obtained results:

Table 10.1 Dispersions of N326, N326* and CB-PyC (1 mg/mL) in several solvents after the sonication.

Solvents	N326	N326*	CB/EAP	CB/p-PDAP	CB/TETAP
2-Propanol	GOOD	GOOD	GOOD	GOOD	BAD
DI Water	BAD	BAD	GOOD	BAD	BAD
Acetone	GOOD	GOOD	BAD	BAD	BAD
Ethyl acetate	BAD	BAD	BAD	GOOD	BAD
Methanol	BAD	BAD	BAD	BAD	BAD
Xylene	BAD	BAD	BAD	BAD	BAD
THF	GOOD	GOOD	BAD	GOOD	BAD
Hexane	BAD	BAD	BAD	BAD	BAD

CB N326 proved to be stable in the following solvents: 2-propanol, acetone and tetrahydrofuran. It was unstable in distilled water, ethyl acetate, methanol, xylene and hexane.

N326* showed the same behavior as CB N326, pointing out that the general procedure to which N326* was subjected did not modify significantly the chemistry of the carbon black surface (see experimental details). This was still confirmed by the pH measurements, which reported similar results between aqueous dispersions of N326 and N326*.

CB/EAP adduct was stable in 2-propanol and distilled water. “Bad” interactions were registered for all the other solvents.

Good interactions were established by the CB/p-PDAP adduct toward 2-propanol, ethyl acetate and THF while CB/TETAP was unstable in all the selected solvents.

As a consequence of the functionalization reaction, all the CB-PyC adducts showed different solute-solvent interactions with respect to pristine carbon black and to N326*. This can be exploited in order to increase the carbon black dispersibility toward specific media.

10.5. Hansen Solubility Parameters and Hansen Solubility Sphere

In polymers technology and science, the preparation of stable solutions is a crucial step in order to obtain a good processability of advanced materials. The right selection of a set of solvents able to solubilize the solute is fundamental to achieve a thermodynamically stable solution. The computational tools used in this section aim to detect the unknown Hansen solubility parameters and to make the choice of solvents easier.

For any solution to occur spontaneously, the Gibbs mixing free energy (ΔG_M) should be zero or negative:[1]

$$\Delta G_M = \Delta H_M - T\Delta S_M$$

Where ΔH_M is the mixing Enthalpy, T is the absolute temperature, and ΔS_M is the mixing entropy. The enthalpy of mixing was described by Scott and Hildebrand in the following way:[8]

$$\Delta H_M = \varphi_1 \varphi_2 V_M (\delta_1 - \delta_2)^2$$

Where subscripts 1 and 2 refer respectively to solute and solvent. φ refers to the volume fraction, V_M is the volume of the mixture and δ is the solubility parameter. Analyzing this expression, it is possible to notice that the difference between the solvent and solute solubility parameters is crucial in the determination of the enthalpy of mixing. In particular, closer to zero is the difference of the solubility parameters and lower is the energy of mixing, leading to the formation of a spontaneous solution. Hence, solutes dissolve in solvents whose solubility parameters are not too different from their own. Solubility parameters derive from the energy required to convert a liquid to the gas state. The Hildebrand solubility parameter is defined as the square root of the total cohesive energy density:[9]

$$\delta = \sqrt{\frac{E}{V}}$$

Where V is the molar volume of the pure solvent and E is the cohesive energy. Nevertheless, Hildebrand solubility parameters are applicable only to nonpolar solvents.[9] Hansen overcomes this problem introducing a new approach in which the cohesive energy E is made by three contributions:

$$E = E_D + E_P + E_H$$

Where E_D, E_P and E_H are the contributions due to dispersion (D), polar-polar (P), and hydrogen bonding (H) forces. Dividing the total cohesive energy equation by the molar volume, the following equation is obtained:

$$\frac{E}{V} = \frac{E_D}{V} + \frac{E_P}{V} + \frac{E_H}{V}$$

This equation represents the square of the total (or Hildebrand) solubility parameter that is equal to the sum of the square of the Hansen D, P, H components:

$$\delta_T^2 = \delta_D^2 + \delta_P^2 + \delta_H^2$$

Where δ_T is the Hildebrand solubility parameter and δ_D, δ_P and δ_H are the dispersion, polar-polar and hydrogen-bonds components of the Hansen solubility parameters.

The solute and the solvent are therefore identified by three coordinates ($x=\delta_D$; $y=\delta_P$; $z=\delta_H$) in the Hansen parameters space.[10] The solute, differently from the solvent, is represented also by an interaction radius (R_0). The distance between two points in the Hansen space is related to their difference in cohesive energy density. The cohesive energy density is associated to the mixing enthalpy: closer to zero is the mixing enthalpy, closer to each other are two points in the Hansen space, which correspond to miscible compounds.

For a given solute, it is possible to identify the Hansen solubility sphere, with radius R_0 and centered in the solute HSPs coordinates (Hansen Solubility Parameters). The Hansen solubility sphere should encompass all solvents classified as "good" while "bad" solvents should lie outside the sphere.[9] The distance between the solute and the solvent is R_a, expressed by the following equation:

$$R_a = \sqrt{4(\delta_D - \delta_{DC})^2 + (\delta_P - \delta_{PC})^2 + (\delta_H - \delta_{HC})^2}$$

Where δ_D, δ_P, δ_H are the HSPs of the solvent and δ_{DC}, δ_{PC}, δ_{HC} are the HSPs of the compound. RED (Relative Energy Difference) is used to quantify R_a respect to the interaction radius, R_0:

$$RED = \frac{R_a}{R_0}$$

Three scenarios are possible:

1. RED<1: high solute-solvent affinity.
2. RED>1: low solute-solvent affinity.
3. RED=1: boundary condition.

"Good" solvents and "bad" solvents were distinguished exploiting the dispersions tests reported in the previous section. The qualitative "good" or "bad" classification was used for the detection of the Hansen solubility parameters of N326, N326* and CB-PyC adducts. Once calculated their HSPs, the Hansen solubility sphere was calculated using the fitting sphere algorithm. Distilled water was not taken into consideration for the calculation of the Hansen solubility parameters and spheres. Due to

its very high δ_H value (42.3 $MPa^{\frac{1}{2}}$)[11] with respect to the other solvents, the calculation of the Hansen solubility parameters turned out to be wrong. For those adducts which resulted to be miscible in distilled water, negative HSPs were registered. These results were clearly meaningless since the Hansen solubility parameters are defined as higher than zero. The calculation of the Hansen solubility parameters and the Hansen solubility sphere of CB/TETAP adduct was not possible due to the absence of "good" interactions toward the selected solvents.

In Table 10.2 are listed the solvents used in the dispersion tests and their Hansen solubility parameters with the only exception of distilled water:

Table 10.2 Hansen Solubility Parameters of: 2-propanol, acetone, ethyl acetate, methanol, xylene, THF and hexane.[10,12]

Solvents	$\delta_D\ [MPa]^{\frac{1}{2}}$	$\delta_P\ [MPa]^{\frac{1}{2}}$	$\delta_H\ [MPa]^{\frac{1}{2}}$
2-Propanol	15.8	6.1	16.4
Acetone	15.5	10.4	7.0
Ethyl acetate	15.8	5.3	7.2
Methanol	15.1	12.3	22.2
Xylene	17.6	1	3.1
THF	16.8	5.7	8
Hexane	14.9	0	0

10.6. Results

10.6.1. *Hansen Solubility Parameters and Hansen solubility sphere of N326 and N326**

Hansen solubility parameters of CB N326 and of N326* are listed in Table 10.3.

Table 10.3 Hansen solubility parameters of CB N326 and N326*.

	$\delta_D\ [MPa]^{\frac{1}{2}}$	$\delta_P\ [MPa]^{\frac{1}{2}}$	$\delta_H\ [MPa]^{\frac{1}{2}}$	$R_0[MPa]^{\frac{1}{2}}$
N326	15.4	8.0	11.6	5.3
N326*	15.4	8.0	11.6	5.3

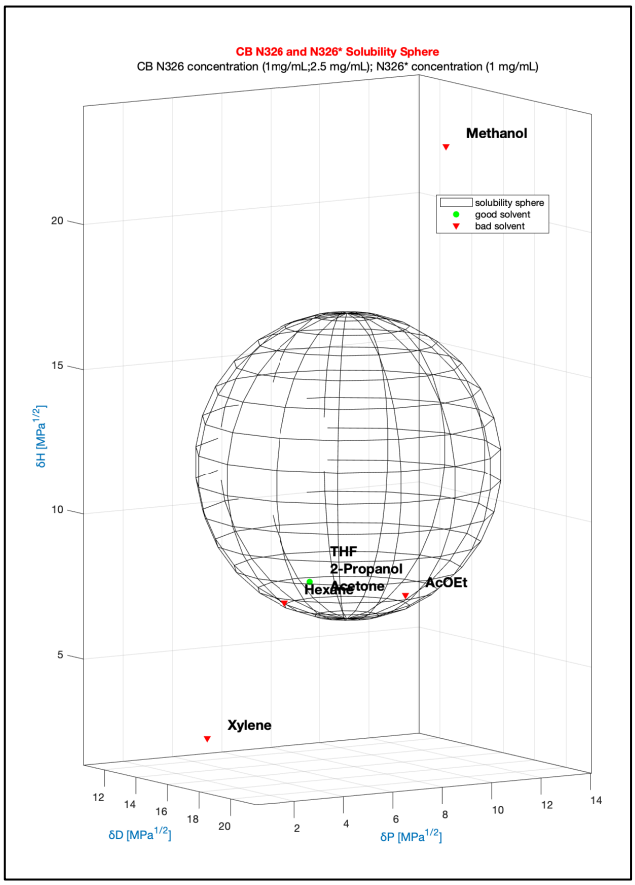

Figure 10.9 Hansen solubility sphere of CB N326 and N326*.

The obtained Hansen solubility parameters of carbon black were quite in agreement with those reported in literature.[13] Differences could be related to a different carbon black type and to a different dispersions' preparation method. The obtained HSPs can also change with the number of selected solvents: higher is the solvents number and more reliable are the results.

Analyzing CB N326 and N326* HSPs, relatively high contributions of polar and hydrogen bond forces suggest a special role of these interactions in the process of dispersion of agglomerates. This is probably related to the presence of impurities and functional groups on the carbon black surface. High δ_D values were also registered. Carbon allotropes showed an important contribution of dispersive forces as a result of strong intermolecular hydrophobic forces.[2]

The fitting sphere algorithm results to be inadequate for CB N326 and N326*. The Hansen sphere, indeed, contained also hexane and ethyl acetate which were classified as "bad" solvents. The objective function (DATAFIT) approaches 1 as the fitting improves during optimization, reaching this end value only when all the "good" solvents are inside the sphere and the "bad" ones outside. It can happen that the DATAFIT does not reach 1, leading to the presence of "bad" solvents inside the sphere or to the opposite situation ("good" solvents outside the sphere).[9]

Although the quality of the regression could always be improved increasing the number of the solvents, these HSP estimates can be used to predict the solvents with a good affinity toward carbon black.

10.6.2. *Hansen solubility parameters and Hansen solubility sphere of CB/EAP adduct:*

Hansen solubility parameters and the interaction radius of CB/EAP adduct are listed in Table 10.4.

Table 10.4 Hansen solubility parameters of CB/EAP adduct.

	$\delta_D\,[MPa]^{\frac{1}{2}}$	$\delta_P\,[MPa]^{\frac{1}{2}}$	$\delta_H\,[MPa]^{\frac{1}{2}}$	$R_0[MPa]^{\frac{1}{2}}$
CB/EAP	16.3	7.3	13.5	5.3

CB/EAP Hansen solubility sphere is illustrated in the Figure below:

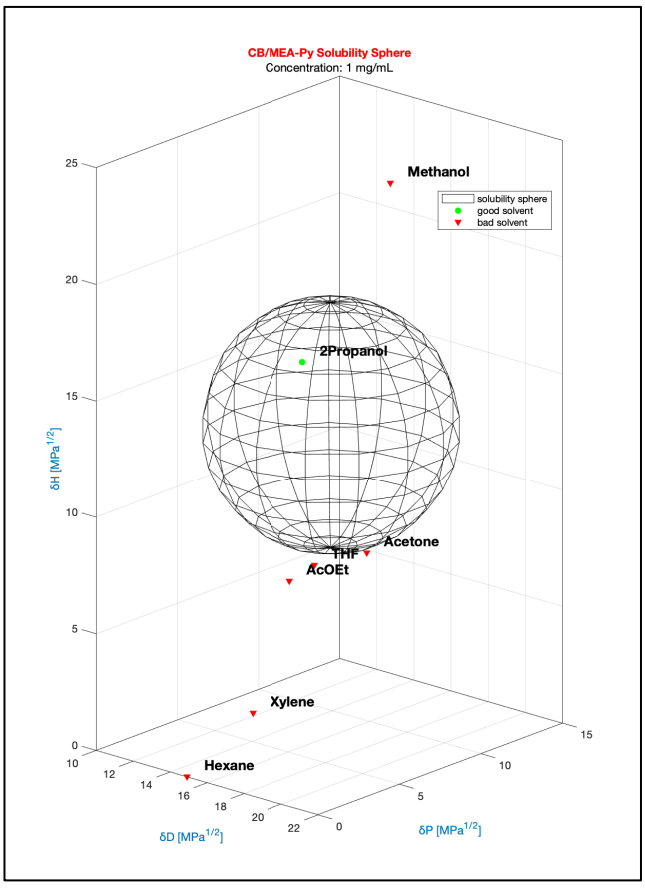

Figure 10.10 Hansen solubility sphere of CB/EAP.

Comparing CB/EAP adduct to pristine carbon black, an increase in the δ_H was registered. This increase in the hydrogen-bond parameter is hypothesized to be related to the introduction of the -OH moieties on the carbon black surface.

The fitting sphere algorithm is accurate in the description of CB/EAP: all the "good" solvents are within the solubility sphere while the "bad" ones are outside.

10.6.3. *Hansen solubility parameters and Hansen solubility sphere of CB/p-PDAP adduct:*

The Hansen solubility parameters of CB/p-PDAP adduct are listed in Table 10.5.

Table 10.5 Hansen solubility parameters of CB/p-PDAP adduct.

	$\delta_D\,[MPa]^{\frac{1}{2}}$	$\delta_P\,[MPa]^{\frac{1}{2}}$	$\delta_H\,[MPa]^{\frac{1}{2}}$	$R_0[MPa]^{\frac{1}{2}}$
CB/p-PDAP	18.6	6.3	10.7	8.0

CB/p-PDAP Hansen solubility sphere is illustrated in Figure 10.11:

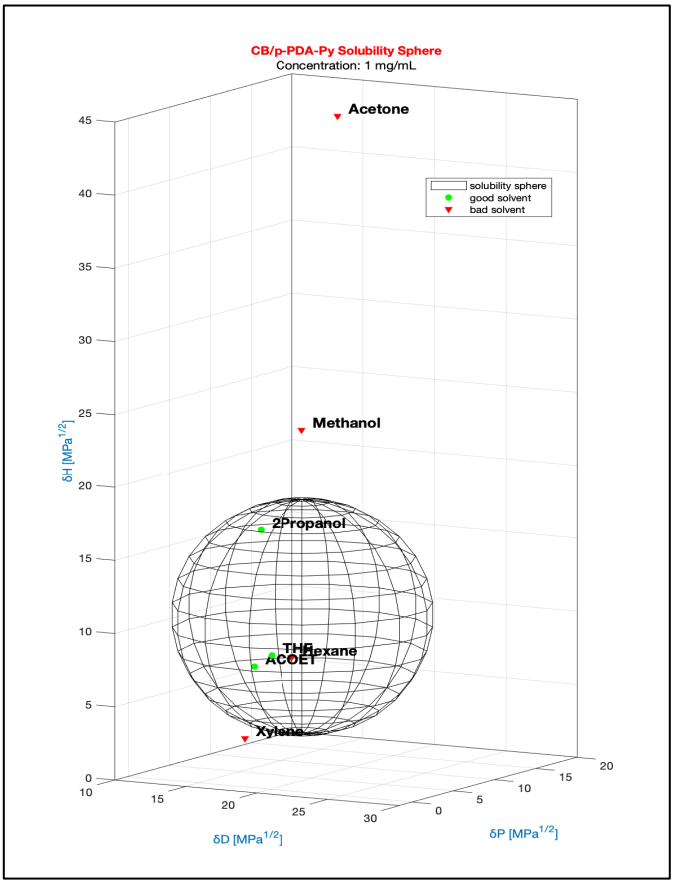

Figure 10.11 Hansen solubility sphere of CB/p-PDAP.

As it can be seen in Table 10.5, δ_D and R_0 parameters of CB/p-PDAP were higher compared to pristine carbon black, while δ_P and δ_H were lower. The high values of δ_D could be related to an increase in the intermolecular hydrophobic forces promoted by the presence of a benzene ring in the p-phenylenediamine pyrrole.

Although CB/p-PDAP was characterized by the same number of "good" interactions with respect to carbon black, it had a higher interaction radius. This is probably related to the inadequacy of the fitting sphere algorithm: due to the presence of "bad" solvents inside the sphere, for both CB/p-PDAP and carbon black the fitting sphere algorithm results not accurate

10.7. Conclusions

CB-PyC adducts properties were investigated through dispersions tests and pH measurements. From the analysis of suspension stability in water, it was not possible to attribute the changes of the registered properties with certainty to the presence of pyrrole derivatives on carbon black surface. Suspension stability of CB-PyC adducts in water was mainly attributed to the aggregates and agglomerates dimensions rather than to the pyrrole derivatives presence. pH measurements showed values comprised between 6.4 and 8.9. Analyzing these results, it can be hypothesized that the oxidation of pyrrole compounds during carbon black functionalization can promote the presence of acidic species, such as carboxylic groups, on the carbon black surface.

If the role of functional groups on the carbon black surface does not emerge unambiguously from suspensions tests in water, it emerges clearly by the analysis of dispersions experiments. All the CB-PyC adducts showed different solute-solvent interactions with respect to pristine carbon black. Hence, the affinity toward a specific media and the dispersibility can be changed by the simple introduction of specific functional groups on the carbon black surface.

Dispersions tests were exploited for the calculation of the Hansen solubility parameters and spheres of pristine carbon black and CB-PyC adducts. All the adducts report different HSPs with respect to the pristine carbon black. The knowledge of the Hansen solubility parameters is needed to assess the compatibility between the adduct and solvents or polymeric matrices. Although the quality of the regression could be always improved by using more solvents, these results can be used for the prediction of CB-PyC behavior in other solvents or their interactions with other materials with known HSPs.

The fitting sphere algorithm results to be accurate only for CB/EAP while it is inadequate in all the other cases. A better implementation of the fitting sphere algorithm should be performed. As suggested by Guilherme et al., [9] the DataFit objective function could be multiplied by a size factor function, defined in the equation below:

$$Size\ Factor = (R_0)^{-\frac{1}{m}}$$

Where m is an empirical degree of the m^{th} root. In this way, the output is for the least radius allowing the maximum DataFit.

References

[1] F. Gharagheizi. New Procedure To Calculate the Hansen Solubility Parameters of Polymers. Journal of Applied Polymer Science, Vol. 103, 31–36 (2007).

[2] J.C. Zuaznabar-Gardona, A. Fragoso. Determination of the Hansen solubility parameters of carbon nano- onions and prediction of their dispersibility in organic solvents. Journal of Molecular Liquids 294, 2019.

[3] D. Locatelli; V. Barbera; L. Brambilla; C. Castiglioni; A. Sironi; M. Galimberti. Tuning the Solubility Parameters of Carbon Nanotubes by Means of Their Adducts with *Janus* Pyrrole Compounds. *Nanomaterials* **2020**, *10*, 1176.

[4] Yoko Hanada et. Al. Analysis of dispersion and aggregation behavior of carbon black particles in aqueous suspension by colloid probe AFM method. Advanced Powder Technology 24 (2013) 844–851.

[5] *C.L. Barrie et al.* Rheology of aqueous carbon black dispersions, *Journal of Colloid and Interface Science 272, 2004. 210–217.*

[6]. https://www.cabotcorp.com/solutions/applications/industrial-rubber-products/dispersion (last access 2/04/2021).

[7] Ciobanu, Marius & Lepadatu, Ana-Maria & Asaftei, Simona. Chemical and Electrochemical Studies of Carbon Black Surface by Treatment with Ozone and Nitrogen Oxide. Materials Today: Proceedings. 3, Supplement 2. S252-S257, 2016.

[8] J.H. Hildebrand, R.L. Scott, The Solubility of Nonelectrolytes, 3rd ed. Reinhold, New York, 1950.

[9] Cañete Vebber, Guilherme & Pranke, Patricia & Pereira, Cláudio. Calculating Hansen Solubility Parameters of Polymers with Genetic Algorithms. Journal of Applied Polymer Science. 131, 2014.

[10] V. Barbera, A. Bernardi, A. Palazzolo, A. Rosengart, L. Brambilla, M. Galimberti. Facile and sustainable functionalization of graphene layers with pyrrole compounds. Pure and Applied Chemistry. 2018;90(2):253-270.

[11] Date, Abhijit & Srivastava, Deepika & Nagarsenker, Mangal & Mulherkar, Rita & Panicker, Lata & Aswal, Vinod & Hassan, Puthusserickal & Steiniger, Frank & Thamm, Jana & Fahr, Alfred. (2011). Lecithin-based novel cationic nanocarriers (LeciPlex) I: Fabrication, characterization and evaluation. Nanomedicine (London, England). 6. 1309-25.

[12] Large, Matthew & Ogilvie, Sean & King, Alice & Dalton, Alan. (2017). Understanding Solvent Spreading for Langmuir Deposition of Nanomaterial Films: A Hansen Solubility Parameter Approach. Langmuir.

[13] S. Süß et al. Determination of Hansen parameters for particles: A standardized routine based on analytical centrifugation. Advanced Powder Technology 29 (2018) 1550–1561.

Chapter 11

Rubber compounds with functionalized carbon black as the only filler

11.1. Introduction

In this chapter, elastomeric composites based on a blend of natural rubber (NR) and butadiene rubber (BR) and filled with carbon black as the only filler are described. NR is poly(1,4-cis-isoprene) and BR is poly(1,4-cis-butadiene). CB was either pristine or functionalized with triethylenetetramine pyrrole (TETAP). The chemical structure of the pyrrole compound is in Figure 11.1.

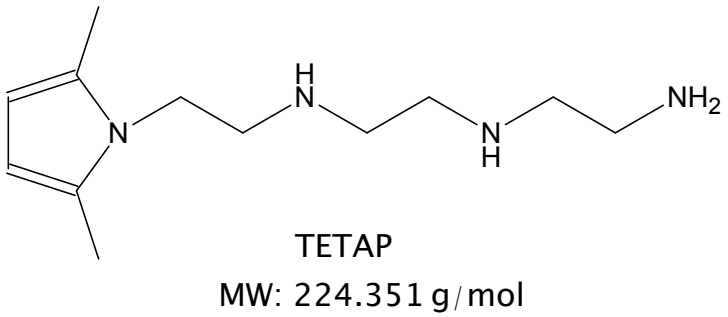

Figure 11.1 Chemical structure of triethylenetetramine pyrrole (TETAP).

This type of compounds, based on the blend of NR and BR, are used in tyres, for example for tyre sidewall. NR is used for its exceptional properties, such as the tack in the uncured state and, upon crosslinking, very high elasticity, tensile strength and crack growth resistance, in static and in fatigue loading conditions. BR is as well characterized by the tack in the uncured state and by high elasticity and crack initiation resistance, in the cured state. In a tyre sidewall, that means a part of a tyre which experiences important fatigue conditions, the combination of NR and BR allows long lasting integrity.

However, the study reported in this chapter has a more general validity, as it allows to understand the behavior of the functionalized CB in rubber compounds based on diene rubbers with only internal double bonds. It is worth commenting that compounds based on this type of rubbers are used in many parts of a tyre, such as undertread, belt, carcass, bead.

Carbon black grade was CB N326 and it was provided by BIRLA Carbon.

The objective of this study was to investigate the effects on the compound properties of the carbon black functionalized with a base such as triethylenetetramine pyrrole. In particular, the objective was to study the kinetics of vulcanization, that means of the crosslinking reaction promoted by a sulphur-based system. The base was expected to lead to a more efficient vulcanization, with shorter induction time, higher vulcanization rate and higher modulus M_H. However, the base was bound to the carbon

black particles and this immobilization could in principle reduce its reactivity. To investigate the effect of the immobilization, a rubber compound was also prepared with the pyrrole compound fed as such. A low amount of pyrrole compound was used: it was about 4% by mass in the adduct and about 0.6 phr in the compound.

Two different kinds of composites' recipes were used:

(i) with high sulphur content: sulphur-accelerator ratio equal to 2.9. This vulcanization system was named conventional as a high amount of Sulphur is conventionally used in internal tyre compounds with NR/BR as the rubber system.

(ii) with a standard sulphur content: sulphur-accelerator ratio equal to 1.1. This vulcanization system was named semi-efficient, because of the lower Sulphur/accelerator ratio.

The preparation of rubber compounds was done by melt blending, using a brabender® type internal mixer.

The elastomeric composites were vulcanized for 10 minutes at 170°C (with RPA 2000 instrument). Characterization was done by means of dynamic-mechanical and tensile properties. Dynamic-mechanical properties were assessed by applying sinusoidal stresses, in the shear and in the axial mode, allowing the determination of G', G'', E', E'' respectively, as well of the ratios between the loss and the storage moduli, Tan Delta. Tensile properties were determined on cured samples, calculating the stresses at different elongations on a universal tensile testing machine (Zwick/Roll 2010) at a strain rate of 1 mm/min.

11.2. BR/NR-based composites filled with only CB - Conventional Vulcanization system

Compounds based on NR and BR, with carbon black as the only filler, were prepared with a conventional vulcanization system, with a sulphur-accelerator ratio equal to 2.9. [1]

Composites were prepared maintaining the same amount of carbon black. Hence, 60 phr (per hundred rubber) of carbon black were replaced by 31.1 and 15.6 phr of CB/TETAP, considering TETAP as an extra ingredient. A further compound was prepared, with TETAP added as such, during the last mixing step.

Recipes of the elastomeric compounds are expressed in phr and are reported in Table 11.1.

Table 11.1 Recipes of NR/BR-based compounds with CB or CB/TETAP as the filler.

Recipes in phr	CB [phr]	CB/TETAP 25% [phr]	CB/TETAP 50% [phr]	CB + TETAP [phr]
BR	60	60	60	60
NR (SIR 20)	40	40	40	40
CB N326	60	45	30	60
CB/TETAP	0	15.6	31.1	
CB		15	30	
TETAP		0.6	1.1	0.6
Sulphur	4.1	4.1	4.1	4.1

Other ingredients used for each composite: Stearic acid 2, ZnO 3.3, 6PPD 2, TBBS 1.4

The procedure for the preparation of the rubber composites is summarized in Figure 11.2 and it is explained in detail in the Experimental section.

A brabender® type internal mixer with a 50-cc chamber and a fill factor of 0.85 (85%) was used.

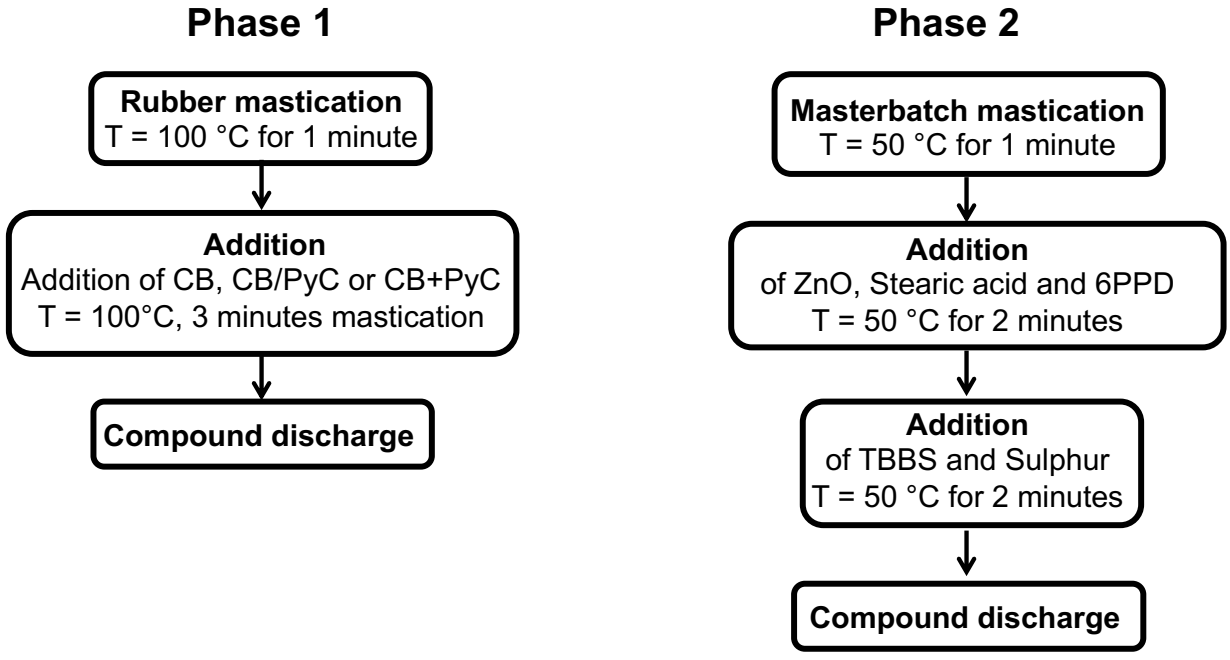

Figure 11.2 Procedure for the composite preparation.

11.2.1. *Vulcanization*

Crosslinking was performed with a sulphur-based system. Rheometric curves were taken at 170°C for 10 minutes and are shown in Figure 11.3. The vulcanization data are summarized in Table 11.2.

Table 11.2 Torque values, induction times (T_{s1}) and times to achieve the optimum level of vulcanization (T_{90}) obtained for rubber composites.

	CB	CB/TETAP 25%	CB/TETAP 50%	CB + TETAP
M_L [dNm]	3.84	4.44	5.17	3.62
M_H [dNm]	25.66	27.39	28.35	24.02
$M_H - M_L$ [dNm]	21.82	22.95	23.18	20.40
T_{90} [min]	4.10	3.43	3.18	3.24
T_{S1} [min]	2.35	2.04	1.81	1.76

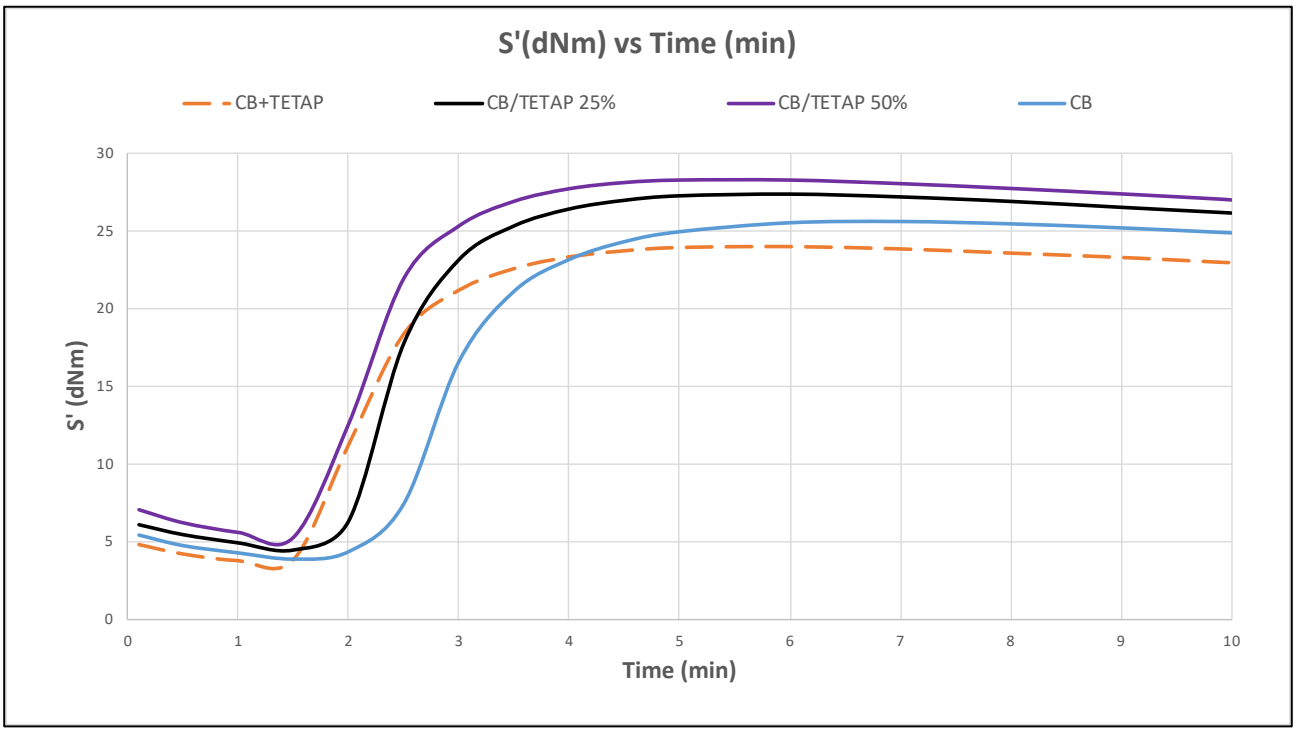

Figure 11.3 Rheometric curves of CB/TETAP compounds: torque versus time.

An increase in both M_H and M_L values was registered for CB/TETAP compared to pristine CB. TETAP functionalization also promoted faster vulcanization kinetics, associated to lower T_{S1} and T_{90} values. These trends were more pronounced for CB/TETAP 50% with respect to CB/TETAP 25%, pointing out that there is a correlation between these behaviors and the amount of functionalized carbon black used in the compound.

CB + TETAP compound also showed faster vulcanization with respect to CB. Nevertheless, torque values were different: both M_L and M_H were lower (3.62 and 24.02, respectively) compared to those of the pristine carbon black composite (3.84 and 25.66, respectively). Considering that M_L is related to the composite viscosity, it could be said that TETAP, added during the mixing, had a plasticizing behavior, lowering the viscosity of the compound.

A clear improvement in vulcanization kinetics was associated to the presence of TETAP. This behavior was hypothesized to be related to the alkalinity of the pyrrole derivative: bases are known to promote more efficient vulcanizations.[2]

11.2.2. *Dynamic-mechanical properties from strain sweep experiments*

In order to investigate dynamic-mechanical properties, strain-sweep experiments were performed at 50°C on crosslinked samples. The detailed procedure is reported in the Experimental section. In Figure 11.4 are respectively reported: A) the dependence of G' vs strain, B) the G plot (G'' vs G'), C) the dependence of G'' vs strain, D) the dependence of Tan Delta vs strain. Tan Delta is the ratio between G'' and G', and ΔG' is the difference between the highest and the lowest G' values in the elongations interval, measured at 0.1% and 25% strain respectively (see experimental details). The obtained results are also summarized in Table 11.3.

Table 11.3 Dynamic-mechanical properties obtained through strain-sweep experiments.

Parameter	**CB**	**CB/TETAP 25%**	**CB/TETAP 50%**	**CB + TETAP**
G' $_{\gamma min}$ (MPa)	3.45	3.26	3.35	3.05
G' $_{\gamma max}$ (MPa)	1.57	1.65	1.71	1.49
ΔG' (MPa)	1.88	1.61	1.64	1.56
ΔG'/G' $_{\gamma min}$	0.54	0.49	0.49	0.51
G'' $_{max}$ (MPa)	0.26	0.23	0.22	0.23
Tan Delta $_{max}$	0.13	0.11	0.10	0.12

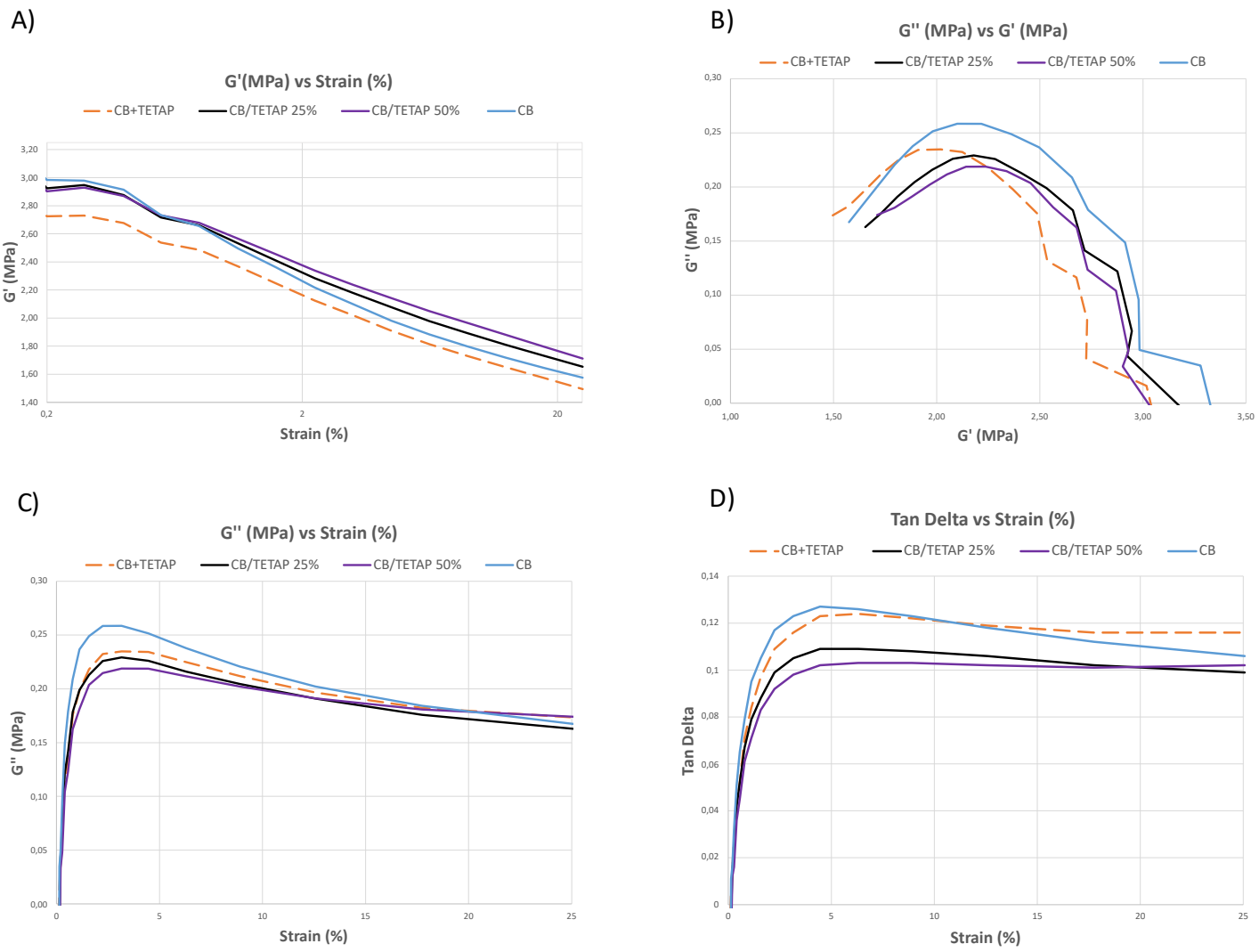

Figure 11.4 A) G' vs strain B) G plot (G" vs G') C) G" vs strain D) Tan Delta vs strain.

The decrease of the modulus with the strain amplitude is known as Payne effect and it is usually indicated by ΔG' and by $\Delta G'/G'_{\gamma min}$ ratio. It is an indication of the filler network, which is due to the interaction of filler particles, either directly or mediated by rubber chains. Hysteresis (Tan δ) is a parameter related to the dissipation of energy: higher hysteresis means higher energy dissipation. Hence, the reduction of the hysteresis is fundamental to lower the dissipation of energy of a tyre compound and thus of fuel consumption and CO_2 emissions. More details are reported in Chapter 6. Analyzing Figure 11.4-A and ΔG' data in Table 11.3, it is possible to notice that CB/TETAP 50% and CB/TETAP 25% promote a reduction of the Payne effect with respect to the CB compound. It is important also to underline the presence of a crossover between CB/TETAP and CB curves. These experimental findings suggested that CB/TETAP was able not only to reduce the filler-network, but also to promote a better interaction between the filler and the polymer-chains. In support of this hypothesis, there was also the reduction of Tan Delta values, shown in Figure 11.4-D: CB/TETAP

curves were always lower than the CB one. Another indication of the reduction of the filler network emerged from the G plot (Figure 11.4-B): for a given level of dynamic stiffness (G'), CB/TETAP compounds showed lower loss modulus (G'') with respect to CB compound. All these behaviors were more pronounced in CB/TETAP 50% with respect to CB/TETAP 25%, pointing out a dependence of the properties on the amount of functionalized carbon black.

Regarding CB + TETAP compound: a reduction of the Payne effect was registered also in this case, however in presence of higher values of Tan Delta with respect to CB/TETAP compounds. A crossover between CB + TETAP and CB curves (Figure 11.4-D) was also present.

11.2.3. *Dynamic-mechanical properties from axial compression tests*

Axial-dynamic mechanical properties were measured in compression. More details are given in the Experimental section. The obtained results are shown in Table 11.4. In Figure 11.5 are shown respectively: A) the dependence of the dynamic storage modulus with the temperature, B) the dependence of Tan δ with the temperature.

Table 11.4 Axial dynamic-mechanical properties of compounds described in Table 11.1.

	CB	**CB/TETAP 25%**	**CB/TETAP 50%**	**CB + TETAP**
E' (10°C)	9.61	10.91	11.59	9.18
E'' (10°C)	1.58	1.69	1.71	1.52
Tan Delta (10°C)	0.16	0.16	0.15	0.17
E' (23°C)	9.11	10.25	10.93	8.74
E'' (23°C)	1.30	1.39	1.41	1.26
Tan Delta (23°C)	0.14	0.14	0.13	0.14
E' (70°C)	8.47	9.52	10.11	8.13
E'' (70°C)	0.94	1.01	1.02	0.93
Tan Delta (70°C)	0.11	0.11	0.10	0.11
ΔE' (E' 10°C –E' 70°C)	1.14	1.39	1.48	1.05

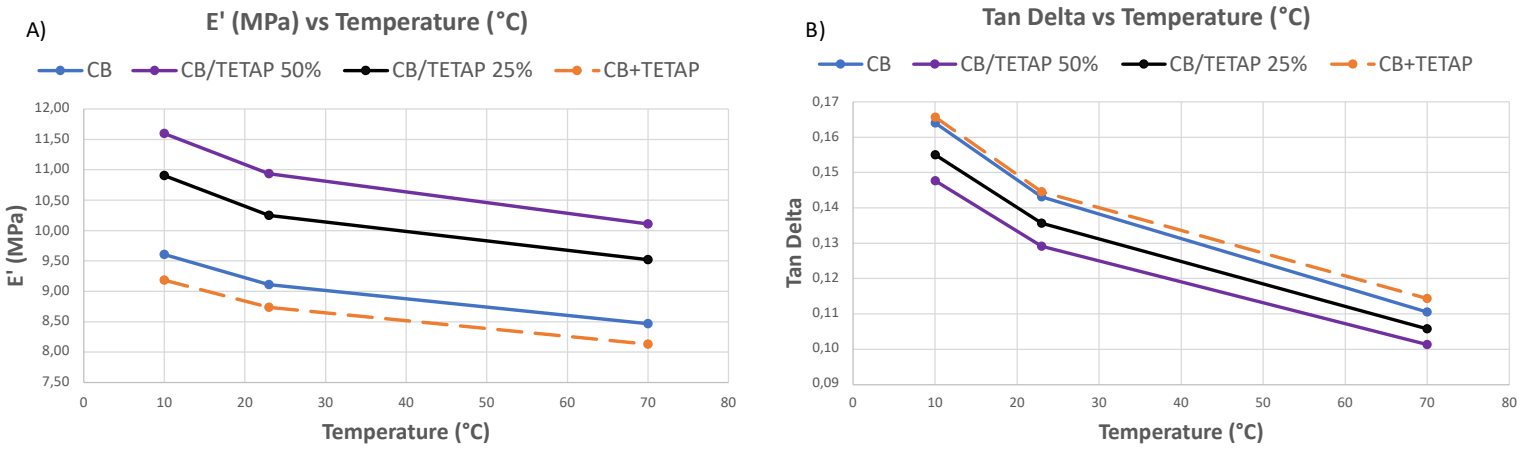

Figure 11.5 A) E' vs T B) Tan Delta vs T.

CB/TETAP compounds were characterized by higher values of E' and lower values of Tan δ for all the three temperatures compared to the CB composite. As reported in the previous paragraph, higher filler loadings corresponded to enhanced behaviors. Axial compression tests were in line with strain-sweep experiments, with composites exhibiting higher stiffness and lower dissipation of energy. Completely different behavior was shown by CB + TETAP compared to CB/TETAP composites: the lowest dynamic storage modulus (E') and the highest loss factors (Tan δ) were registered for all the temperatures. Low E' values suggested that TETAP could act as a plasticizer when added during the mixing step.

11.2.4. *Tensile properties*

Stress-strain properties were measured through quasi-static measurements on vulcanized samples. For each compound, three samples were tested with a strain rate of 1 mm/min. Details are reported in the Experimental section. In Figure 11.6 are reported rheometric curves while stresses at 100 and 200% of elongation (σ_1 and σ_2), stresses at break (σ_B), elongations at break (ε_B) and the fracture energy are reported in Table 11.5:

Table 11.5 Tensile properties of compounds described in Table 11.1.

Parameters	**CB**	**CB/TETAP 25%**	**CB/TETAP 50%**	**CB + TETAP**
σ_1 (MPa)	4.6	4.6	4.9	4.2
σ_2 (MPa)	11.9	11.1		10.8
σ_B (MPa)	14.2	11.1	9.4	16.4
ε_B (%)	226.2	204.9	176.9	265.3
Energy (J/cm^3)	13.8	10.4	8.2	18.2

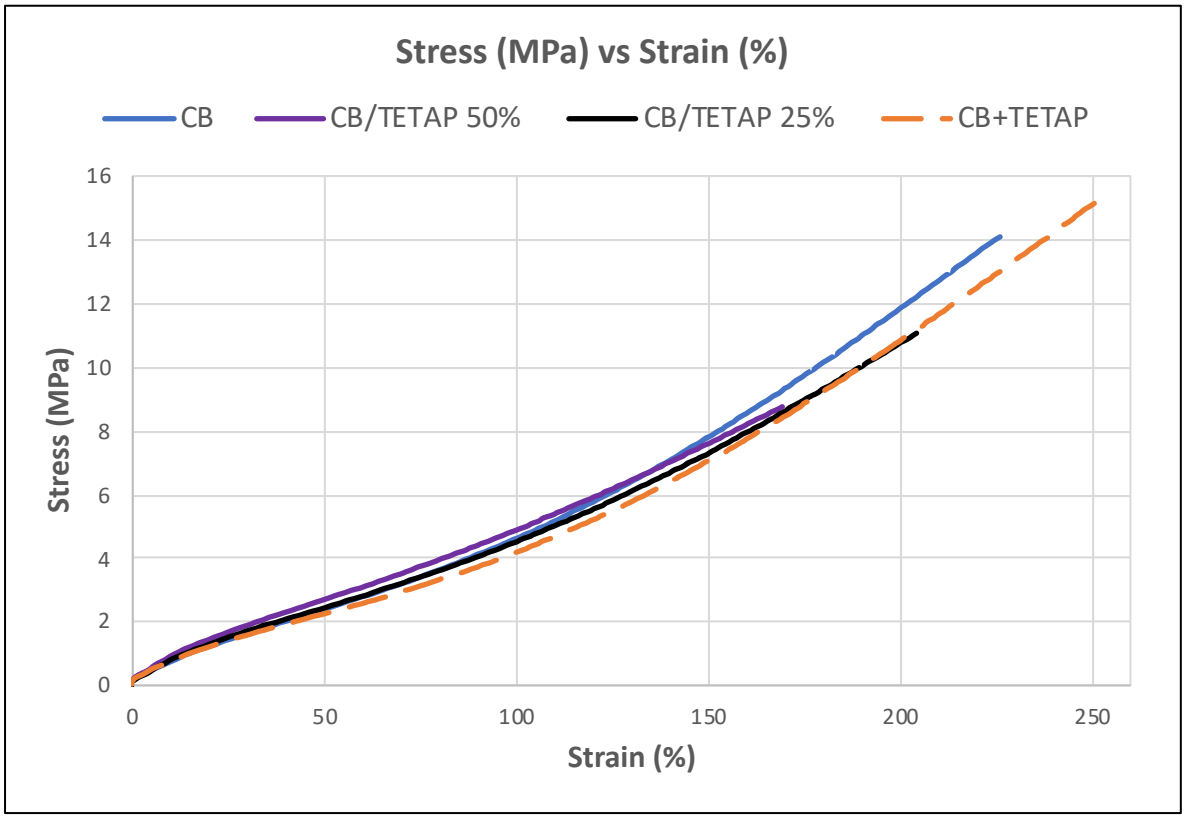

Figure 11.6 Tensile properties of composites in Table 11.1.

Each stress-strain curve represented in Figure 11.6 is an average of the output of three equivalent tensile tests on three equivalent samples. For this reason, standard deviations are represented in Figure 11.7.

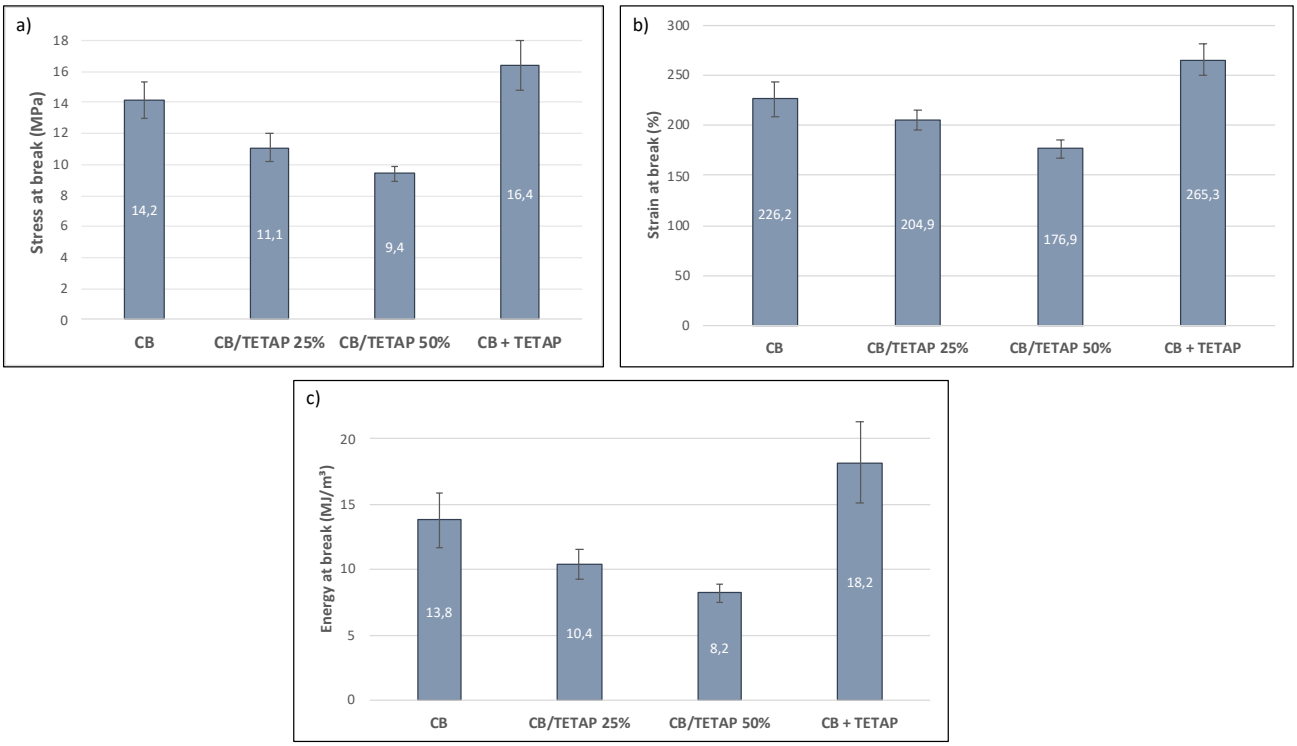

Figure 11.7 a) stress at break, b) strain at break, c) energy at break.

Compared to the pristine carbon black compound, CB/TETAP composites were characterized by lower stresses, elongations and energy at break. These behaviors were, also in this case, more pronounced in the composite with a higher amount of functionalized carbon black.

CB + TETAP showed lower stresses for all the tested strains but, at the same time, the highest elongation and stress at break, confirming the plasticizing behavior emerged by the previous tests.

11.3. BR/NR-based composites filled with only CB - Semi Efficient Vulcanization

This study is focused on natural rubber (NR) and butadiene rubber (BR) based compounds, filled with only carbon black. The behavior of the functionalized carbon black on NR/BR based compounds was investigated through composites characterization by means of dynamic-mechanical and tensile properties.

These composites were characterized by a semi-efficient vulcanization (SEV) curing system, with a sulphur-accelerator ratio equal to 1.1.[1]

The same recipes of the previous study were applied: the only difference relies on the curing system. Recipes of the elastomeric compounds are reported in Table 11.6:

Table 11.6 NR/BR-based compounds filled with only carbon black.

Recipes in phr	CB [phr]	CB/TETAP 25% [phr]	CB/TETAP 50% [phr]	CB + TETAP [phr]
BR	60	60	60	60
NR (SIR 20)	40	40	40	40
CB N326	60	45	30	60
CB/TETAP	0	15.6	31.1	
CB		15	30	
TETAP		0.6	1.1	0.6
Sulphur	2	2	2	2

Other ingredients used for each composite: Stearic acid 2, ZnO 4, 6PPD 2, TBBS 1.8

As in the study done with the "conventional vulcanization system", a CB + TETAP composite was prepared with the aim of highlighting the behavior of the pyrrole compound, fed as such in the compound or covalently bound to the CB surface.

The procedure for the composites' preparation was the same adopted in the previous study and it is shown in Figure 11.2. A brabender® type internal mixer was used, with a 50-cc chamber and a fill factor of 0.85 (85%).

11.3.1. *Vulcanization*

Vulcanization was performed with a sulphur-based system at 170°C for 10 minutes.

Vulcanization's data are listed in Table 11.7 and rheometric curves are shown in Figure 11.8:

Table 11.7 Torque values, induction times (T_{S1}) and times to achieve the optimum level of vulcanization (T_{90}) obtained for rubber composites.

	CB	CB/TETAP 25%	CB/TETAP 50%	CB + TETAP
M_L [dNm]	3.75	4.63	5.19	3.80
M_H [dNm]	22.50	23.56	24.15	20.89
$M_H - M_L$ [dNm]	18.75	18.93	18.96	17.09
T_{90} [min]	4.18	3.50	3.04	2.95
T_{S1} [min]	2.39	2.16	1.96	1.86

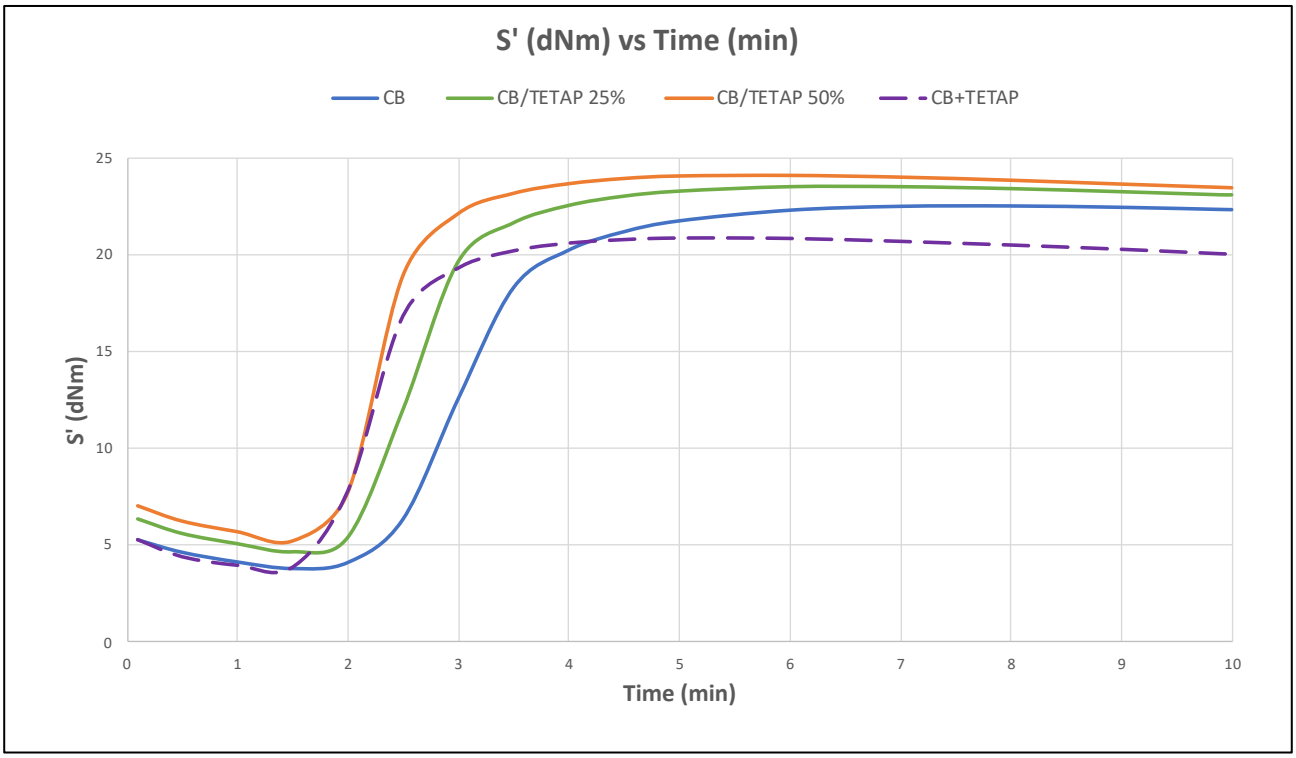

Figure 11.8 Curing curves for CB/TETAP compounds: torque vs time.

Lower values of T_{S1} and T_{90} for the CB/TETAP compounds compared to CB were registered, indicating the accelerating behavior of the TETAP functionalized carbon black. Higher M_H and M_L values were registered for CB/TETAP composites with respect to CB, behaviors more pronounced in the composite with a higher amount of functionalized carbon black.

TETAP accelerating behavior for the vulcanization reaction was still confirmed by the CB + TETAP compound: this composite was indeed characterized by the lowest values of both T_{S1} and T_{90}. Unlike CB/TETAP composites, CB + TETAP showed similar M_L and lower M_H values compared to carbon black.

11.3.2. *Dynamic-mechanical properties from strain sweep experiments*

Dynamic-mechanical properties were investigated by means of strain-sweep experiments (at 50°C) on crosslinked samples. In Figure 11.9 are respectively reported: A) the dependence of G' vs strain B) the G plot (G'' vs G') C) the dependence of G'' vs strain D) the dependence of Tan Delta vs strain. In Table 11.8 are listed the corresponding results:

Table 11.8 Dynamic-mechanical properties obtained through strain-sweep experiments.

Parameters	CB	CB/TETAP 25%	CB/TETAP 50%	CB + TETAP
G' $_{\gamma min}$ (MPa)	3.05	3.01	3.06	2.76
G' $_{\gamma max}$ (MPa)	1.43	1.47	1.51	1.30
ΔG' (MPa)	1.62	1.54	1.55	1.46
ΔG'/G' $_{\gamma min}$	0.53	0.51	0.50	0.53
G'' $_{max}$ (MPa)	0.27	0.25	0.22	0.28
Tan Delta max	0.14	0.13	0.12	0.16

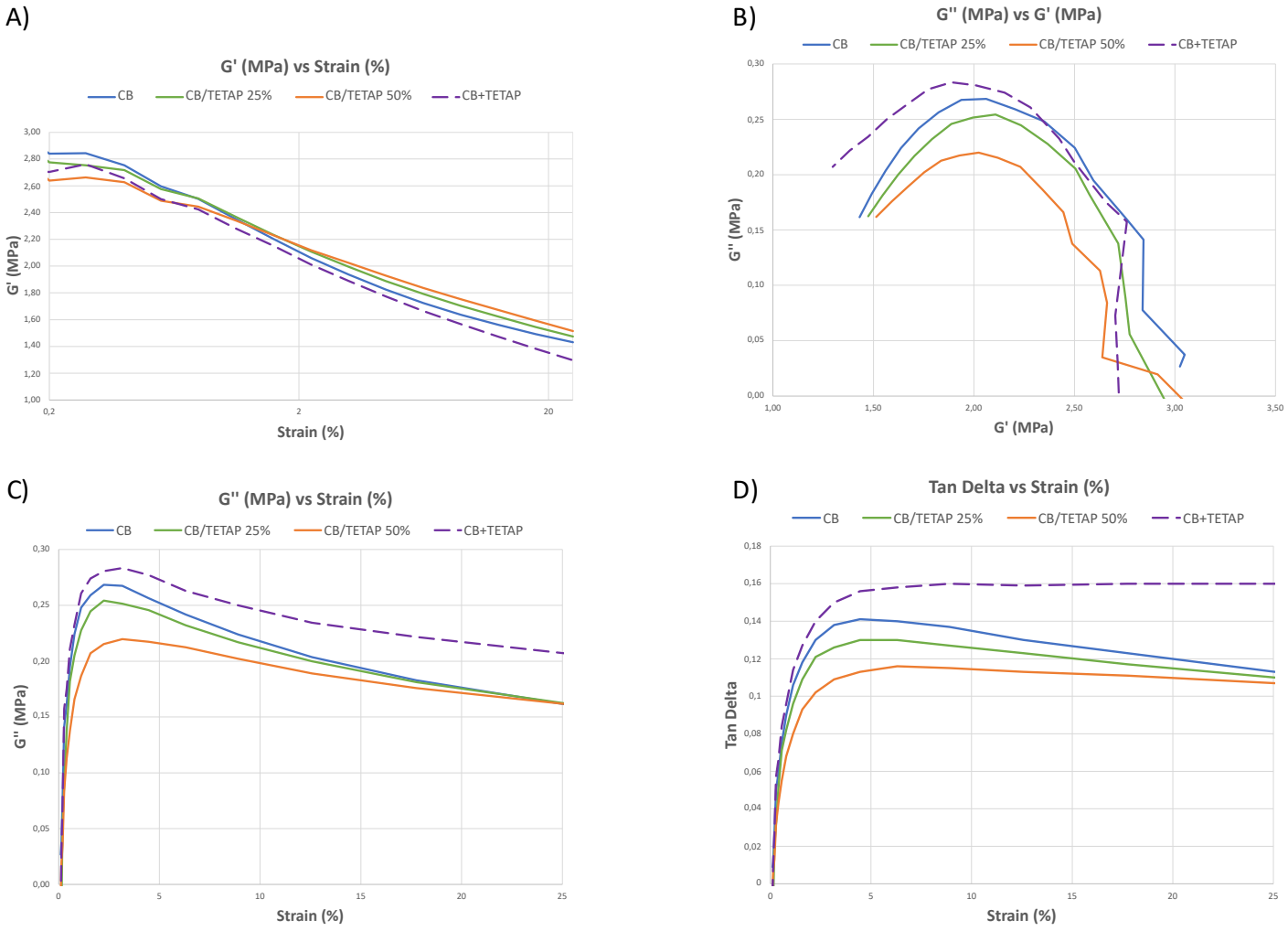

Figure 11.9 A) G' vs strain B) G'' vs G' C) G'' vs strain D) Tan Delta vs strain.

From Figure 11.9A and from ΔG' data in Table 11.8, a reduction of the Payne effect was associated to CB/TETAP compounds. A crossover between CB/TETAP and CB curves was also present. These experimental findings suggested that the filler network was reduced by the TETAP presence and the enhancement of filler-polymer interactions could be assumed. This hypothesis was still supported by the reduction of both Tan δ (Figure 11.9 D) and loss modulus (Figure 11.9 C), which characterize CB/TETAP composites with respect to CB. It is worth reminding that Tan δ is related to the energy dissipation in elastomeric composite. Hence, composites with functionalized carbon black displayed the lowest energy dissipation. All the above-mentioned trends were more marked in CB/TETA 50% than CB/TETAP 25%.

Analyzing CB + TETAP compound, a slight decrease of the Payne effect was still present. Nevertheless, the absence of a crossover with the CB curve in Figure 11.9 A, the higher values of both the loss modulus (Figure 11.9 C) and of the loss factor (Figure 11.9D) compared to carbon black, did not allow to assume an interaction of the filler with the polymer chains.

11.3.3. *Dynamic-mechanical properties from axial compression tests*

Axial-dynamic mechanical properties were measured in compression, as reported in the experimental section. The dependence of the dynamic storage modulus (11.10 A) and of Tan δ (11.10 B) with the temperature is shown in Figure 11.10. E', E'' and Tan δ values at 10°C, 23°C and 70°C are listed in the Table below:

Table 11.9 Axial-dynamic mechanical properties of composites of Table 11.6.

	CB	**CB/TETAP 25%**	**CB/TETAP 50%**	**CB + TETAP**
E' (10°C)	8.92	9.77	10.41	8.57
E'' (10°C)	1.58	1.66	1.65	1.58
Tan Delta (10°C)	0.18	0.17	0.16	0.18
E' (23°C)	8.46	9.21	9.82	8.13
E'' (23°C)	1.33	1.40	1.39	1.35
Tan Delta (23°C)	0.16	0.15	0.14	0.17
E' (70°C)	7.63	8.33	8.94	7.38
E'' (70°C)	0.97	1.05	1.07	1.01
Tan Delta (70°C)	0.13	0.13	0.12	0.14
ΔE' (E' 10°C - E' 70°C)	1.29	1.44	1.47	1.19

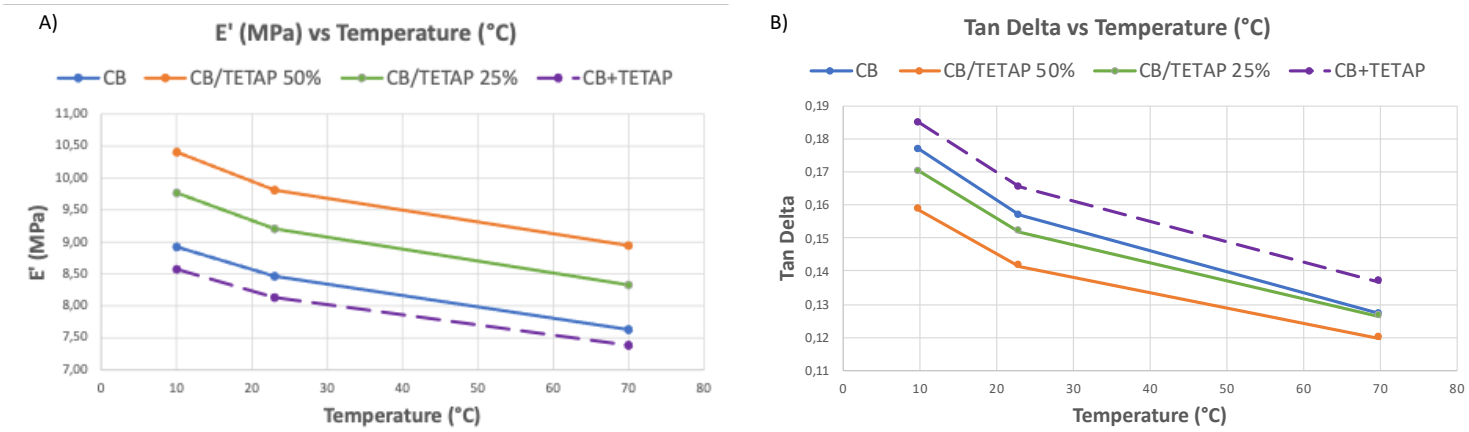

Figure 11.10 A) E' vs T B) Tan Delta vs T of composites of Table 11.6

At a given temperature, higher E' and lower Tan δ values characterized TETAP compounds with respect to CB. These results are in line with strain-sweep experiments. A dependence of the dynamic-mechanical parameters can be observed also in this case.

Opposite trends, with respect to CB/TETAP compounds, were shown by CB + TETAP: highest levels of loss factors and lowest values of dynamic storage modulus were recorded, confirming the behaviors that emerged from the strain-sweep experiments.

11.3.4. *Tensile properties*

Stress-strain curves, obtained through quasi-static measurements on crosslinked samples, are reported in the Figure 11.11, while results are schematized in Table 11.10.

Table 11.10 Tensile properties of composites of Table 11.6.

Parameters	CB	CB/TETAP 25%	CB/TETAP 50%	CB + TETAP
σ_1 (MPa)	4.0	4.2	3.9	3.4
σ_2 (MPa)	10.5	9.7	8.5	8.4
σ_B (MPa)	18.4	14.0	13.2	20.7
ε_B (%)	297.6	259.2	268.8	362.7
Energy (J/cm^3)	22.9	16.1	16.5	31.4

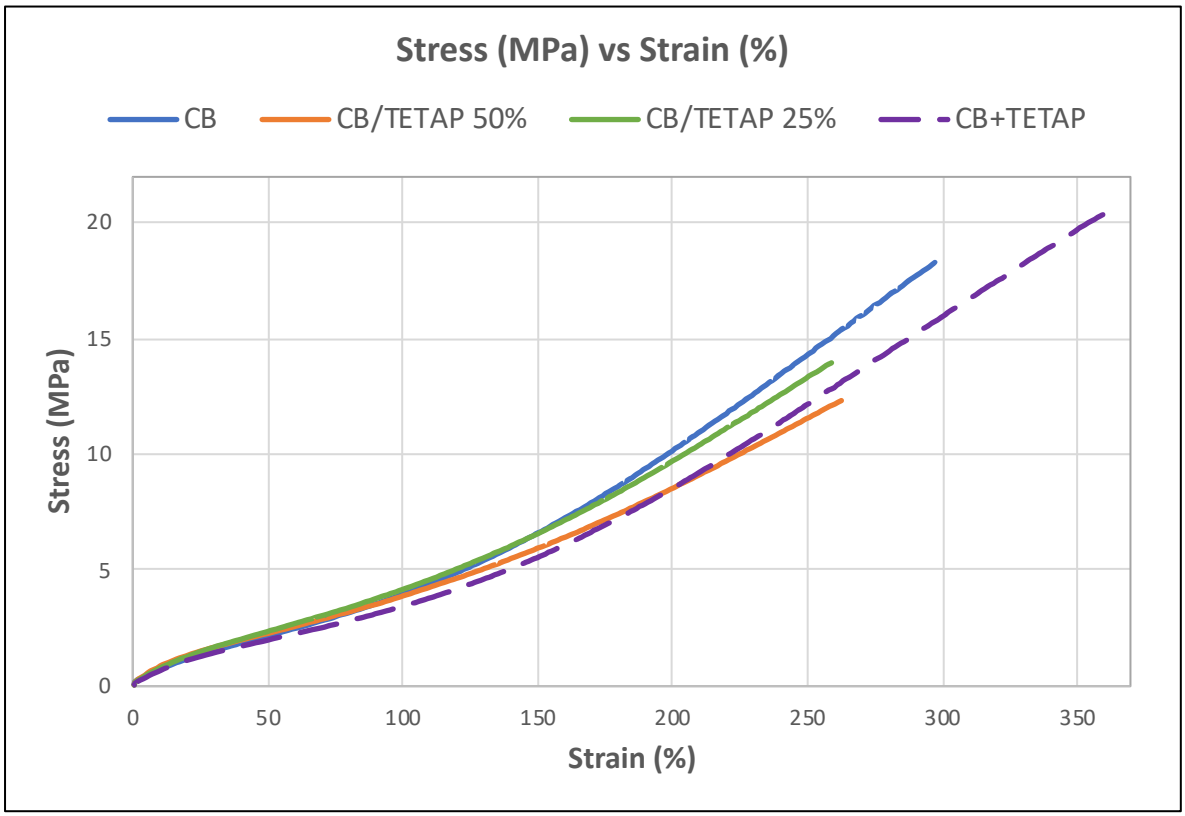

Figure 11.11 Tensile properties of composites of Table 11.6.

Standard deviations are reported in the Figure below:

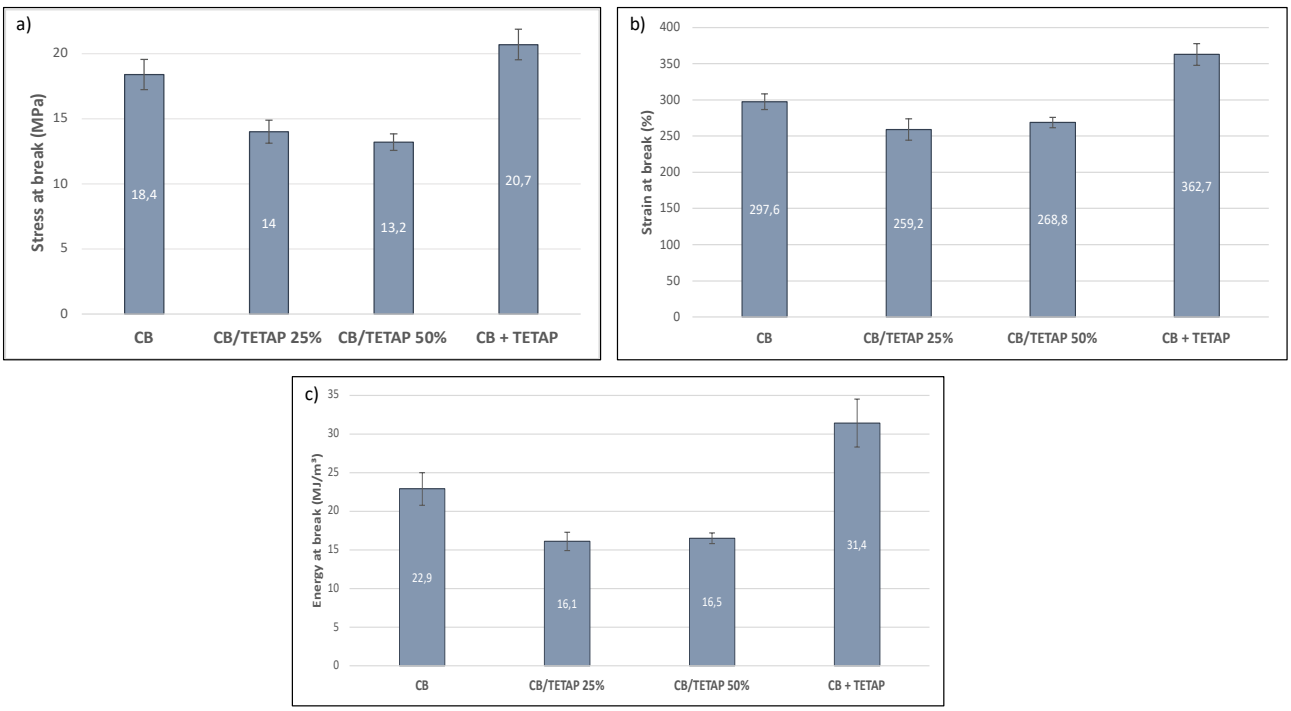

Figure 11.12 a) stress at break, b) strain at break, c) energy at break.

CB/TETAP composites were characterized by lower stresses, elongations and energy at break compared to CB.

As seen for the composites prepared with the conventional vulcanization system, sample CB + TETAP showed larger elongation and energy at break compared to CB.

11.4. Comparison between NR/BR-based composites filled with only CB

In order to understand the effect of the pyrrole compound, fed as such or bound to the CB surface, as a function of the recipe of the vulcanization system, so basically as a function of the sulphur/accelerator ratio, data reported in previous Tables, coming from the rheometric curves and describing dynamic-mechanical and tensile properties, are compared *vis a vis* in the following Tables.

11.4.1. *Curing curves*

Comparison of data from rheometric curves are shown in Table 11.11. Data of the CB compound were taken as the reference (set at 100) and relative values were calculated for the other compounds.

Table 11.11 Torque values, induction times (T_{S1}) and times to achieve the optimum level of vulcanization (T_{90}) obtained for rubber composites.

	Conventional vulcanization system				Semi-efficient vulcanization system			
	CB	**CB/TETAP 25%**	**CB/TETAP 50%**	**CB + TETAP**	**CB**	**CB/TETAP 25%**	**CB/TETAP 50%**	**CB + TETAP**
M_L [dNm]	100	115.6	134.6	94.3	100	123.5	138.4	101.3
M_H [dNm]	100	106.7	110.5	93.6	100	104.7	107.3	92.84
$M_H - M_L$ [dNm]	100	105.2	106.2	93.5	100	101.0	101.0	91.1
T_{90} [min]	100	83.6	77.6	79.0	100	83.7	72.7	70.6
T_{S1} [min]	100	86.8	77.0	75.0	100	90.3	82.0	77.8

It can be seen from Table 11.11 that the accelerating effect was due to the presence of TETAP, as such or in the CB/TETAP adduct. TETAP led to the decrease of induction vulcanization time and of T_{90}. The reduction appears to be slightly more pronounced (T_{S1}) for the conventional vulcanization system and, in particular, for TETAP used as such. Maximum modulus values were, however, higher in presence of CB/TETAP and lower in CB + TETAP compounds compared to the reference CB composite. For M_H, larger effect can be clearly observed for the vulcanization system with higher sulphur content.

Concerning M_L values, it is evident the increase of viscosity in presence of the functionalized CB.[3]

11.4.2. *Dynamic-mechanical properties from strain sweep experiments*

A comparison between Dynamic-mechanical properties from strain sweep experiments is summarized in Table 11.12.

Table 11.12 Dynamic-mechanical properties obtained through strain-sweep experiments.

	Conventional vulcanization system				Semi-efficient vulcanization system			
Parameters	**CB**	**CB/TETAP 25%**	**CB/TETAP 50%**	**CB + TETAP**	**CB**	**CB/TETAP 25%**	**CB/TETAP 50%**	**CB + TETAP**
G' $_{\gamma min}$ (MPa)	100	94.5	97.1	88.4	100	98.7	100.3	90.5
G' $_{\gamma max}$ (MPa)	100	105.1	108.9	94.9	100	102.8	105.6	91.0
ΔG' (MPa)	100	85.6	87.2	82.9	100	95.0	95.7	90.0
ΔG'/G' $_{\gamma min}$	100	90.7	90.7	94.4	100	96.2	94.3	100.0
G'' $_{max}$ (MPa)	100	88.5	84.6	88.5	100	92.6	81.5	103.7
Tan δ max	100	84.6	77.0	92.3	100	92.85	85.7	114.3

TETAP led to a reduction of the Payne effect, G'' and of Tan delta, particularly in compounds with larger sulphur content. The curing system did not influence the overall trend of CB and CB/TETAP compounds. Higher loss factors and loss modulus were, instead, displayed by SEV CB + TETAP compared to CV CB + TETAP.

11.4.3. *Dynamic-mechanical properties from axial compression tests*

The comparison between axial dynamic-mechanical properties is shown in the Table below:

Table 11.13 Axial dynamic-mechanical properties of CV and SEV composites.

	Conventional vulcanization system				Semi-efficient vulcanization system			
	CB	**CB/TETAP 25%**	**CB/TETAP 50%**	**CB + TETAP**	**CB**	**CB/TETAP 25%**	**CB/TETAP 50%**	**CB + TETAP**
E' (10°C)	100	113.5	120.6	95.5	100	109.5	116.7	96.0
E'' (10°C)	100	106.9	108.2	96.2	100	105.1	104.1	100.0
Tan Delta (10°C)	100	100.0	93.8	106.2	100	94.4	88.9	100.0
E' (23°C)	100	112.5	119.9	95.9	100	108.9	116.0	96.0
E'' (23°C)	100	107.0	108.5	97.0	100	105.3	104.5	101.5
Tan Delta (23°C)	100	100.0	92.8	100.0	100	93.75	87.5	106.3
E' (70°C)	100	112.4	119.4	95.9	100	109.2	117.2	96.7
E'' (70°C)	100	107.5	108.5	98.9	100	108.2	110.3	104.1
Tan Delta (70°C)	100	96.4	91.0	100.0	100	100.0	92.3	107.7
ΔE' (E' 10°C - E' 70°C)	100	121.9	129.8	92.1	100	111.6	113.9	92.2

The increase of dynamic storage modulus (E') was not influenced by the temperature and was slightly higher for the CV system, with larger Sulphur content.

It is worth underlining that the CB/TETAP led to the reduction of Tan Delta, whereas TETAP to the increase.

11.4.4. *Tensile properties*

Stresses at 100 and 200% of elongation (σ_1 and σ_2), stresses at break (σ_B), elongations at break (ε_B) and the fracture energy of CV and SEV composites are reported in Table 11.14:

Table 11.14 tensile properties of CV and SEV composites.

	Conventional vulcanization system				Semi-efficient vulcanization system			
Parameters	**CB**	**CB/TETAP 25%**	**CB/TETAP 50%**	**CB + TETAP**	**CB**	**CB/TETAP 25%**	**CB/TETAP 50%**	**CB + TETAP**
σ_1 **(MPa)**	100	99.6	106	90.2	100	103.2	96.3	84.2
σ_2 **(MPa)**	100	93.2		91.1	100	92.8	81.6	80.6
σ_B **(MPa)**	100	78.4	66.5	116.0	100	76.0	71.6	112.3
ε_B **(%)**	100	90.5	78.2	117.3	100	87.1	90.3	121.8
Energy (J/cm^3)	100	75.6	59.3	132.1	100	70.3	72.2	137.2

Tensile properties resulted to be strongly influenced by the curing system. Higher fracture energy, stresses and elongation at break were displayed by SEV compounds with respect to the CV ones: larger Sulphur content leads to lower elongation and worsen the tensile properties.

11.5 Crosslinking density of CV composites

Swelling measurements were performed for the determination of the crosslinking density, by applying the Flory-Rehner equation (1).

$$\nu_e = \frac{-(\ln(1 - V_r) + V_r + \chi_1 V_r^2)}{\frac{V_1\left(V_r^{\frac{1}{3}} - V_r\right)}{2}}, (1)$$

Where ν_e is the effective number of chains in a real network per unit volume, V_1 is the molar volume of the solvent, χ_1 is the Flory solvent-polymer interaction term and V_r is the volume fraction of polymer in a swollen network in equilibrium with pure solvents and it is calculated with equation (2).

$$V_r = \frac{\frac{weight\ of\ dry\ rubber}{density\ of\ dry\ rubber}}{\frac{weight\ of\ dry\ rubber}{density\ of\ dry\ rubber} + \frac{weight\ of\ solvent\ absorbed\ by\ sample}{density\ of\ dry\ rubber}}, (2)$$

Sulphur bridges length was measured with the so-called thiol-ammine chemistry. More details are reported in the experimental section. In Table 11.15 are listed the obtained values.

Table 11.15 Crosslinking density and length of sulfidic bridges for CV composites.

	Total X-link (mol/g·10^{-5})	**Mono and di-sulfide (% mass)**	**Poly sulfide (% mass)**
CB	4.33	52.70	47.30
CB/TETAP 25%	3.28	52.10	47.90
CB/TETAP 50%	3.42	56.40	43.60

CB/TETAP composites were characterized by a lower crosslinking density with respect to the reference CB sample. Analyzing data reported in Table 11.15, it emerged that CB/TETAP promoted the formation of mono and di-sulfide rather than poly sulfidic bridges. However, this behavior was present only in CB/TETAP 50% and not in CB/TETAP 25%, which showed a length of sulfidic bridges very similar to the reference sample.

11.6. Overall discussion of the results and conclusions

In this chapter, NR/BR based elastomeric composites reinforced with only carbon black were presented. Two different studies were discussed: composites based on a conventional vulcanization (CV) curing system and compounds based on a semi-efficient vulcanization (SEV) curing system. To better investigate the effect of binding the pyrrole compound onto the CB surface, TETAP was also added as such to the compound, during the mixing.

Results reported in previous paragraphs appear consistent and can be reasonably summarized.

In presence of the functionalized CB, faster vulcanization reactions were observed, together with an enhancement of the torque values (M_L and M_H). The increase of M_L can be attributed to the interaction between the aggregates of functionalized CB: the chemical groups onto the CB surface favor such interaction. Dynamic-mechanical tests in the shear mode revealed a reduction of the Payne effect and lower Tan δ values associated to composites containing CB/TETAP. Dynamic-mechanical tests in the axial mode revealed higher E' values and lower Tan Delta values. Lower stresses, elongations and energy at break were registered for compounds with CB/TETAP. Overall, the effects appear to be more pronounced in presence of the larger amount of CB/TETAP, that means CB/TETAP 50% with respect to CB/TETAP 25%, pointing out a correlation between properties and amount of functionalized carbon black in compounds.

In the case of CB + TETAP sample, acceleration of the crosslinking reaction was still present, but lower torque values were registered. Reduction of the Payne effect was also visible, but less pronounced than in CB/TETAP composites. Lower values of E' were obtained and tan delta was

higher, both in shear and axial dynamic-mechanical measurements. Larger elongation and energy at break were measured.

From the comparison between CV and SEV composites, it emerged, to a different extent, a more pronounced effect of the CB/TETAP in composites with larger sulphur content.

The above reported results could be explained with a more efficient vulcanization reaction. The presence of a base on CB in composites is expected to promote a more efficient use of sulphur. Indeed, larger effects by CB/TETAP adducts were observed in the case of the compound with the larger amount of sulphur. A more efficient use of Sulphur should mean shorter Sulphur bridges and larger crosslinking density. Such a picture of the crosslinking network could justify the experimental results. However, the results obtained from the x-linking network analysis are not in line with these expectations. Indeed, the total x-linking network density is lower in the presence of functionalized CB. It is also worth observing that the pyrrole compound TETAP, fed as such, led to a faster vulcanization but did not lead to large E' and to the reduction of tan delta.

Therefore, the results discussed in this Chapter need an alternative explanation. It appears that the key role is played by the anchoring of the pyrrole compound on to the CB surface. Two hypotheses can be made:

(i) the effect of the base occurs in the proximity of CB, which is then framed in a dense crosslinking network and this emphasizes its reinforcing effect.

(ii) Sulphur, activated by the presence of the base, is able to react with the surface of carbon black, creating a hybrid crosslinking network which involves the filler and achieving the ultimate goal for a filler, the covalent bond with the rubber chains.

To assess the validity in particular of hypothesis (ii), further experimental activity should be done.

The research group, where this thesis was done, published, as a working hypothesis, a mechanism to justify the formation of covalent bonds between Sulphur and the surface of an sp^2 carbon allotrope. Such mechanism is reported as follows in Figure 11.13.

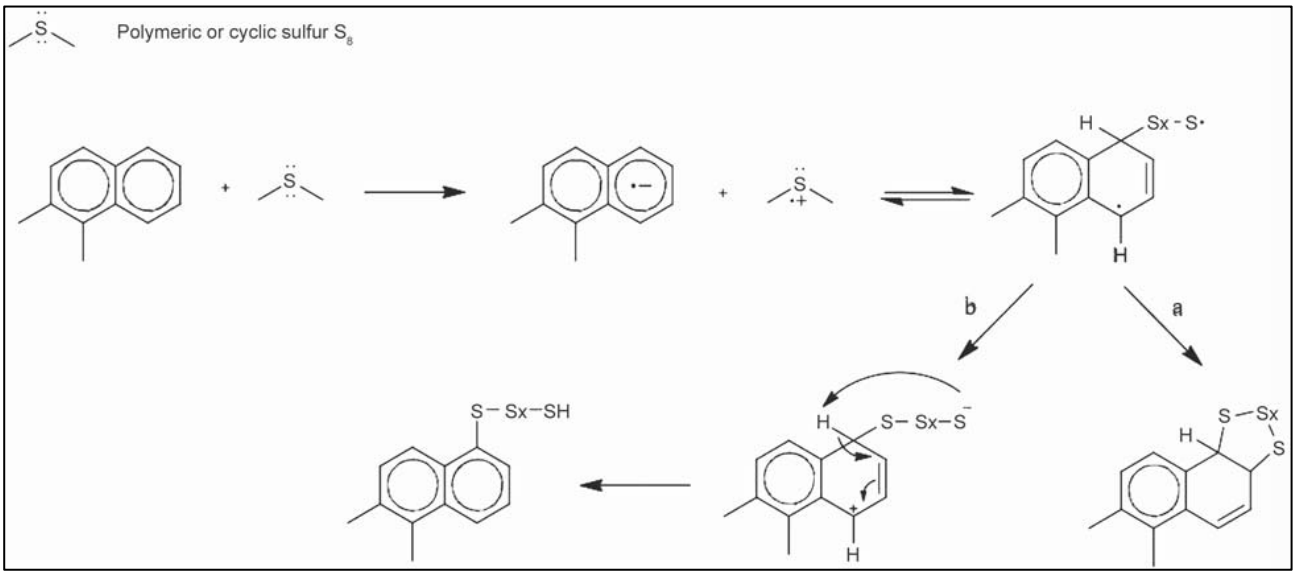

Figure 11.13 Proposed mechanism for the reaction of sulphur with a carbon allotrope.

As it is written in the manuscript, “The carbon allotrope is supposedly able to accept electrons from sulphur, with the subsequent formation of radical cations, favoring the quick start of the vulcanization reaction. Electrons, that could remain on carbon, would then be responsible for the higher activation energy.” A basic environment could favor the formation of anions on the surface of carbon black.

References

[1] Felipe Nunes Linhares at. Al. Effect of different sulphur-based crosslink networks on the nitrile rubber resistance to biodiesel. *Fuel*.Vol.191, 130-139, 2017.

[2]S.J. Park, M.K. Seo,C. Nah. Influence of surface characteristics of carbon blacks on cure and mechanical behaviors of rubber matrix compoundings. J Colloid Interface Sci. 2005.

[3] A. Larpkasemsek, L. Raksaksri, S. Chuayjuljit, P. Chaiwutthinan, and A. Boonmahitthisud, "Effects of sulfur vulcanization system on cure characteristics, physical properties and thermal aging of epoxidized natural rubber", *J. Met. Mater. Miner.*, vol. 29, no. 1, Mar. 2019.

Chapter 12
NR/BR-based composites filled with both CB and Silica

12.1. Introduction

In this Chapter, NR/BR based composites, with the hybrid carbon black / silica filler system, are described.

The objective was to investigate the effect of the CB/PyC adduct on the compound properties. An accelerating effect of the vulcanization was expected, in the light of the results discussed in Chapter 11. Particular objective was to investigate the effect of the CB/PyC adduct on the compounds' properties which have to do with the interaction of the two fillers, silica and carbon black. The base anchored on the surface of CB was expected to have a favorable interaction with silica.

Three different types of functionalized carbon black were used. Functionalization was performed with the following pyrrole compounds: triethylenetetramine pyrrole (TETAP), p-phenylenediamine pyrrole (p-PDAP), and mono-ethanolammine pyrrole (EAP), whose preparation was described in Chapter 9 and whose chemical structure is in Figure 12.1.

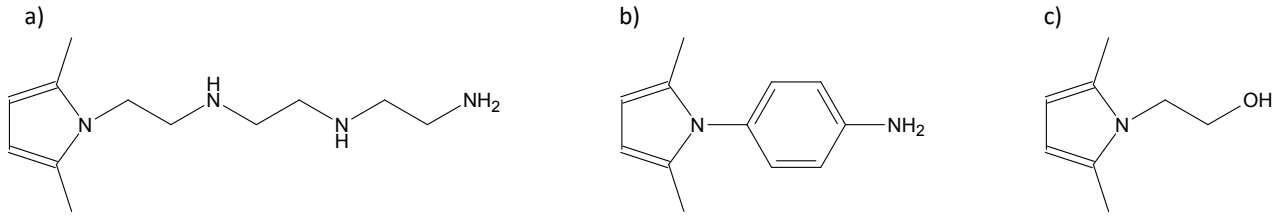

Figure 12.1 a) triethylenetetramine pyrrole (TETAP), b) p-phenylenediamine pyrrole (p-PDAP), c) mono-ethanolammine pyrrole (EAP).

The two first pyrrole compounds contain a larger amount of nitrogen atoms, also a primary amine in the case of TETAP, and are expected to interact with silica through an acid-base interaction. The third pyrrole compound was selected in order to investigate a different type of interaction. The OH group could interact by hydrogen bonds and could also condense with the silanol groups.

Carbon black grade was N326, provided by BIRLA Carbon, while silica was Zeosil 1165, from Solvay. The same recipe was adopted for the composite's preparation. The only difference relied on the pyrrole derivative employed for the functionalization reaction.

Rubber composites were prepared by melt blending. It is worth commenting the experimental procedure adopted for the preparation, which is summarized in Figure 12.2.

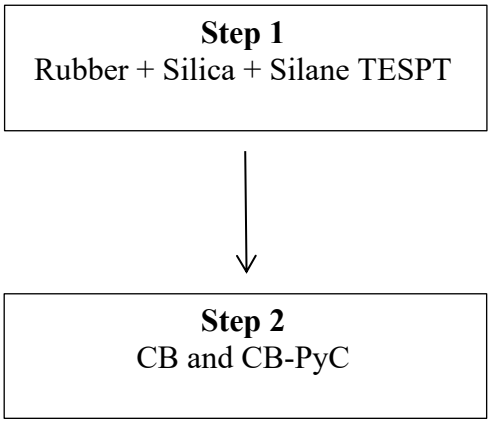

Figure 12.2 Procedure adopted for the preparation of the compound.

In a first step, silica was mixed with the rubber and was silanized with a Sulphur based silane, the traditional rubber-silica coupling agent, whose chemical structure is in Figure 12.3.

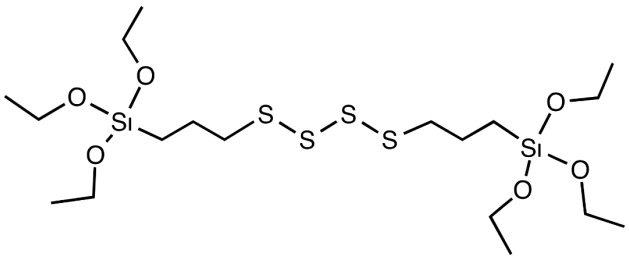

Figure 12.3 Bis(triethoxysilylpropyl)tetrasulfide.

In a following step, CB, either pristine or functionalized, was added to the compound. In this way, the interaction between silica and the functionalized carbon black occurs after the silanization reaction, that means after covering with the silane the most reactive silanols of silica. This could lead to reduce the effect of the base grafted onto CB.

Composites were vulcanized for 10 minutes at 170°C (with RPA 2000 instrument). Characterization was made by means of dynamic-mechanical and tensile measurements. Dynamic-mechanical properties were investigated through shear strain-sweep experiments and in traction compression-mode, allowing the determination of G', G'', E', E'' and Tan Delta. Tensile properties were determined by means of quasi static experiments, measuring the stresses at different elongations on a universal tensile testing machine (Zwick/Roll 2010) at a strain rate of 1 mm/min.

Results are reported in the following, as a function of the CB/PyC adduct.

12.2. NR/BR silica-based composites with CB/TETAP

The first study is on NR/BR silica-based compounds with CB/TETAP. Conventional vulcanization (CV) curing system was applied, with a sulfur-accelerator ratio equal to 2.9, and a carbon black-silica ratio equal to 50/50 in volume was used. Compounds were prepared maintaining the same amount of

carbon black and thus 30 phr of carbon black were replaced by 31.2 and 15.6 phr of CB/TETAP, considering TETAP as an extra ingredient. TETAP amount on CB (4% in wt.) was obtained via thermogravimetric analysis. Recipes of the elastomeric compounds are reported in Table 12.1:

Table 12.1 Recipes of NR/BR-based composites with Silica and CB or CB/TETAP as the filler.

Reciepes in phr	**CB** **[phr]**	**CB-Silica** **[phr]**	**CB/TETAP 50%** **[phr]**	**CB/TETAP 100%** **[phr]**
BR	60	60	60	60
NR (SIR 20)	40	40	40	40
CB N326	60	30	15	0
CB/TETAP	0	0	15.6	31.2
CB			15	30
TETAP			0.6	1.2
Silica	0	35	35	35
TESPT	5.6	5.6	5.6	5.6
Sulphur	4.1	4.1	4.1	4.1

Other ingredients used for each composite: Stearic acid 2, ZnO 3.3, 6PPD 2, TBBS 1.4

Although silica was not used in the first compound (named CB), a sulfur containing silane (TESPT, see Figure 12.3) was used, in order to have the same chemicals in all the compounds and to allow the comparison among them.

The procedure for the composites' preparation is summarized in Figure 12.4 with the details reported in the experimental section. A brabender® type internal mixer was used, with a 50-cc chamber and a fill factor of 0.85 (85%).

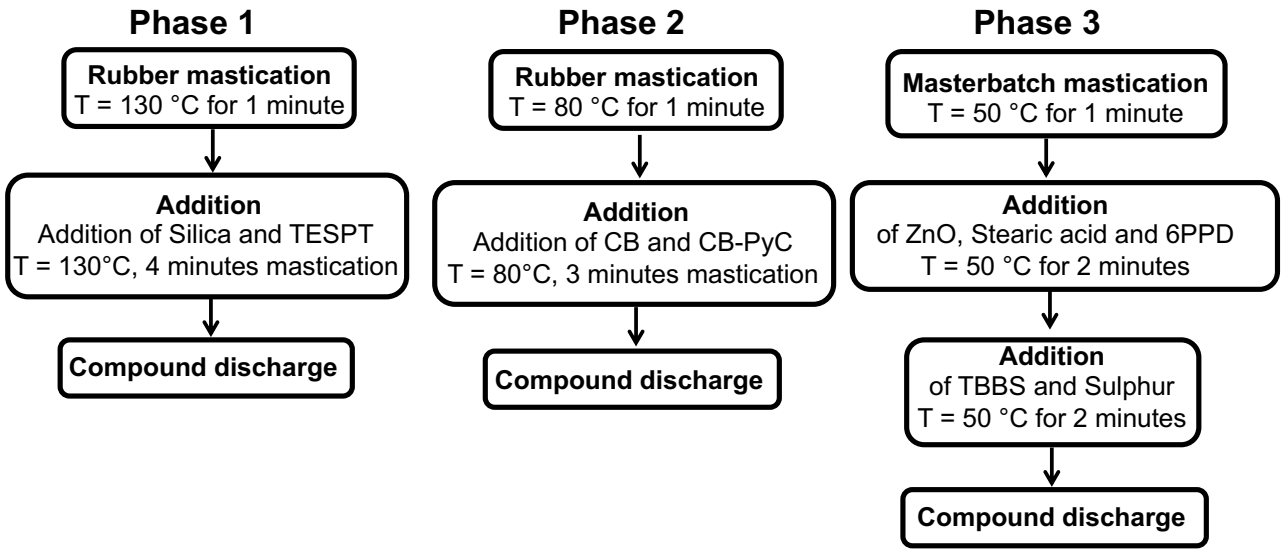

Figure 12.4 Procedure for the composites' preparation.

Results below are organized as follows: data are in the Tables and Figures show the curves of the silica-based compounds.

12.2.1. *Vulcanization*

Rheometric curves, taken at 170°C for 10 minutes, are shown in Figure 12.5 while vulcanization data are summarized in Table 12.2.

Table 12.2 Torque values, induction times (T_{S1}) and times to achieve the optimum level of vulcanization (T_{90}) obtained for rubber composites.

	CB	**CB-Silica**	**CB/TETAP 50%**	**CB/TETAP 100%**
M_L [dNm]	4.06	4.78	5.68	6.21
M_H [dNm]	27.69	23.19	26.21	27.48
$M_H - M_L$ [dNm]	23.63	18.41	20.53	21.27
T_{90} [min]	4.27	6.06	4.66	4.15
T_{S1} [min]	2.46	2.43	2.08	1.88

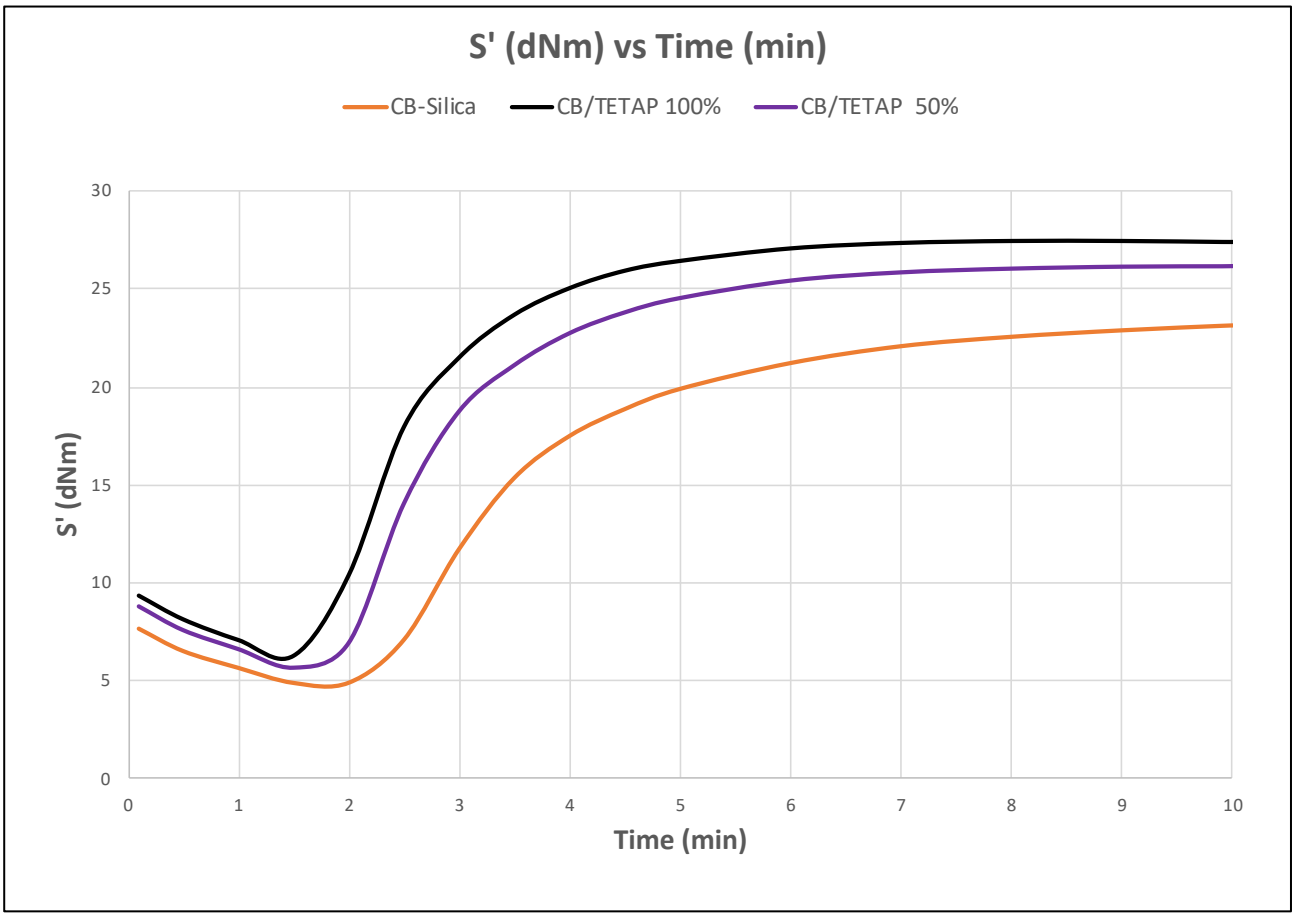

Figure 12.5 Rheometric curves of composites described in Table 12.1.

A significant increment in the vulcanization kinetics occurred in presence of the pyrrole derivative: both T_{S1} and T_{90} values were lower in CB/TETAP composites than in the reference CB-Silica compound. In CB/TETAP 100%, T_{S1} and T_{90} were even lower than those of the CB compound.

The curves in Figure 12.5 reveal a marching modulus for the CB-silica compound, which does not appear for the compounds with CB/TETAP. Marching modulus is a problem, particularly at the industrial scale, as it makes difficult to determine the optimal curing time and affects the reproducibility of the crosslinking and, as a consequence, of the compound properties. Hence, it should be avoided or at least minimized. [1] Secondary accelerators are used to this purpose. Some of them, as for example the diphenyl guanidine, known as DPG, have critical safety data sheet and should be replaced.

In line with what reported and commented in Chapter 11, faster curing reactions could be attributed to the alkalinity of the pyrrole derivative, which is known to promote more efficient vulcanizations.[2] CB/TETAP led to the increase of torque values, in comparison with CB-Silica composite: both M_H and M_L values were higher. As seen in Chapter 11, there is a correlation between the amount of pyrrole derivative in the composite and the change in the mechanical properties.

12.2.2. *Dynamic-mechanical properties from strain sweep experiments*

To investigate dynamic-mechanical properties, strain-sweep tests were performed at 50°C on crosslinked samples. Dynamic-mechanical results are shown in Table 12.3. In Figure 12.6 are respectively reported: A) the dependence of G' vs strain B) the dependence of G'' vs strain C) the dependence of Tan δ vs strain.

Table 12.3 Dynamic-mechanical properties obtained through strain-sweep experiments.

Parameters	**CB**	**CB-Silica**	**CB/TETAP 50%**	**CB/TETAP 100%**
G' $_{\gamma min}$ (MPa)	4.00	4.24	4.75	4.44
G' $_{\gamma max}$ (MPa)	1.87	1.85	2.01	1.91
ΔG' (MPa)	2.13	2.39	2.74	2.53
ΔG'/G' $_{\gamma min}$	0.53	0.56	0.58	0.57
G'' $_{max}$ (MPa)	0.28	0.43	0.41	0.38
Tan Delta max	0.12	0.17	0.16	0.18

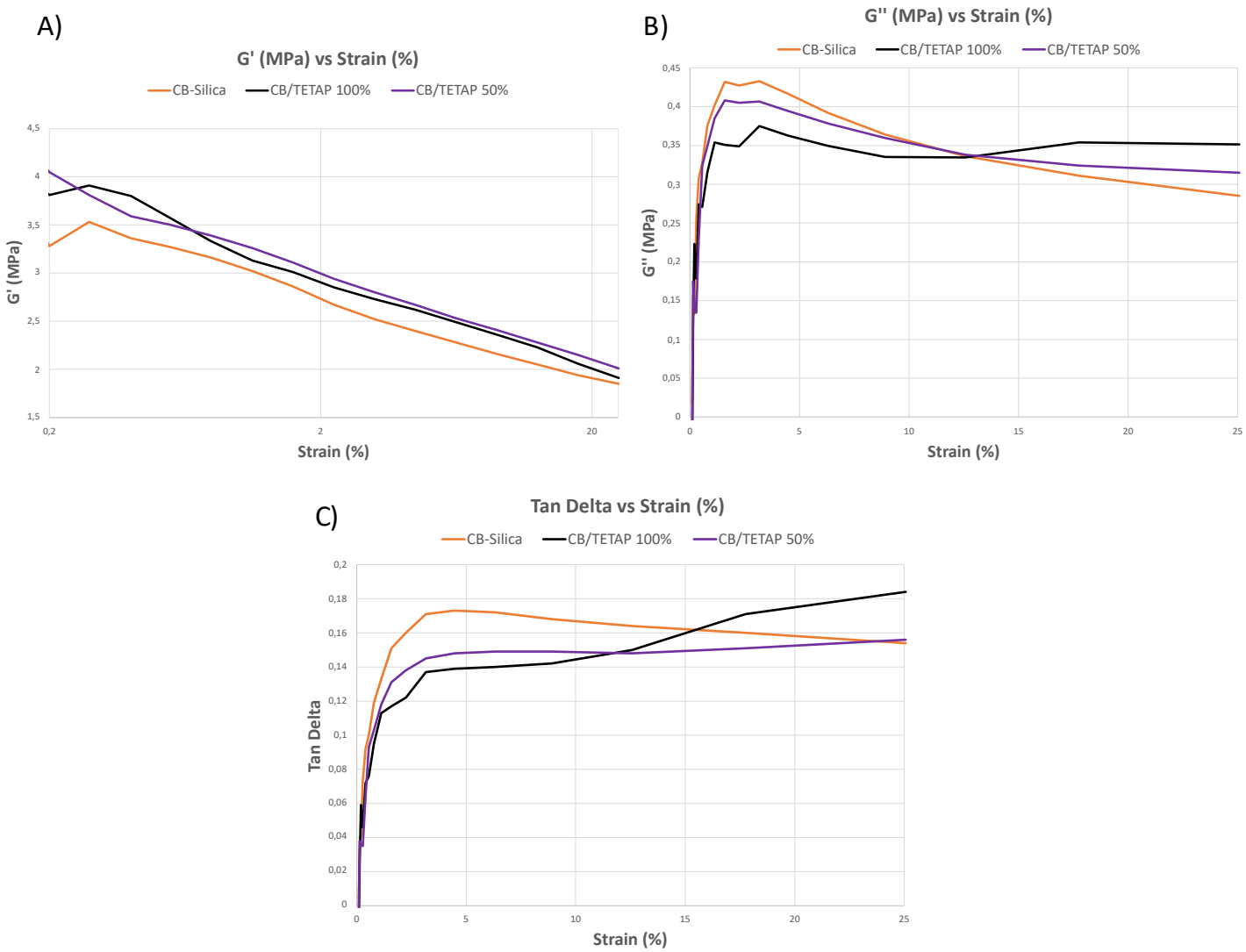

Figure 12.6 A) G' vs strain, B) G" vs strain, C) Tan Delta vs strain.

Analyzing Figure 12.6-A and values reported in Table 12.3, it is worth observing the higher values of G' for composites with CB/TETAP, both at minimum and maximum strain, in particular for the composite with CB/TETAP 50%. A slight increase of the Payne effect is also observed. The highest values of ΔG' and normalized $\Delta G'/G'_{\gamma min}$ values are shown by CB/TETAP 50%.

Figure 12.6-C shows that at low strain values, the CB-silica compound has higher hysteresis and that a crossover of the curves occurs as the strain increases. In particular, at large strain, the tan delta increases particularly for the CB/TETAP 100% composite.

These findings lead to hypothesize the presence of a network formed by silica and the functionalized CB. This network is based on supramolecular acid-base interactions and is responsible for the lower Tan Delta at low strain. When this supramolecular network faints, the crossover of the curves occurs.

To conclude the comments to the data in Table 12.3, it is worth compare the properties of the compounds with only CB and with CB-silica. It is indeed worth observing that the lowest value of

ΔG' (Payne effect index) and Tan δ values were obtained with the CB based compound. Hence, the CB based compound gives lower hysteresis than a silica-based compound. This is an unexpected result and has to do with the unusual high amount of TESPT added to the formulation. The interaction of TESPT with CB should be considered, even though the formation of covalent bonds cannot be reasonably assumed, on the basis of the chemical nature of these substances. Further investigations should be done.

12.2.3. *Dynamic-mechanical properties from axial compression tests*

Axial-dynamic mechanical properties were measured in compression, as reported in the experimental section. E', E'' and Tan Delta values at 10°C, 23°C and 70°C are listed in Table 12.4. In Figure 12.7 are listed: A) the dependence of the dynamic storage modulus with the temperature, B) the dependence of Tan Delta with the temperature.

Table 12.4 Axial dynamic-mechanical properties of composites described in Table 12.1.

	CB	**CB-Silica**	**CB/TETAP 50%**	**CB/TETAP 100%**
E' 10°C	10.56	12.66	13.11	14.33
E'' 10°C	1.81	2.64	2.47	2.58
Tan Delta 10°C	0.17	0.21	0.19	0.18
E' 23°C	9.92	11.73	12.25	13.30
E'' 23°C	1.49	2.32	2.18	2.25
Tan Delta 23°C	0.15	0.20	0.18	0.17
E' 70°C	8.93	10.17	10.60	11.63
E'' 70°C	1.02	1.78	1.67	1.73
Tan Delta 70°C	0.12	0.18	0.16	0.15
ΔE' (E' 10°C-E' 70°C)	1.63	2.49	2.51	2.70

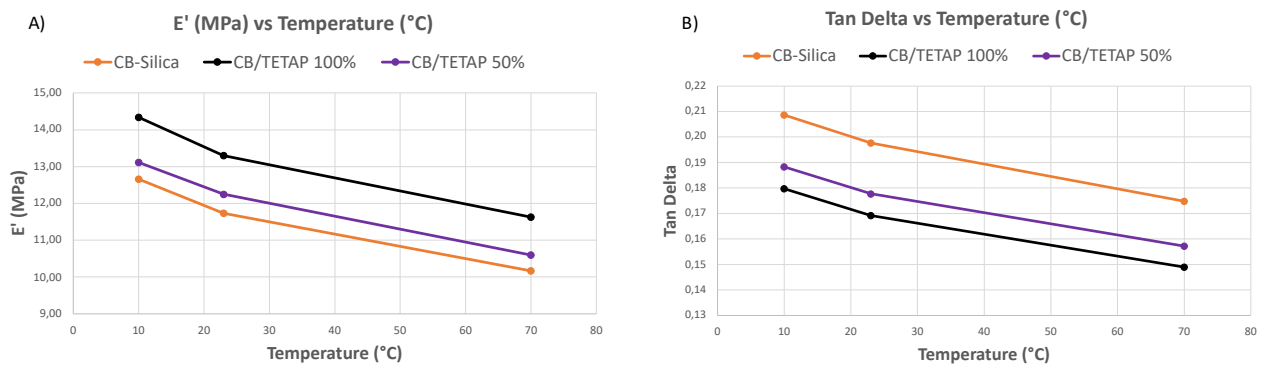

Figure 12.7 A) E' vs T, B) Tan Delta vs T.

TETAP promoted higher E' values at all the temperatures as well as higher values of ΔE'. Remarkably lower Tan δ values are for the CB/TETAP composites, in particular CB/TETAP 100%, as compared to the CB-Silica compound.

12.2.4. *Tensile properties*

Tensile properties were measured through quasi-static measurements. For each compound, three samples were tested with a clamp rate of 1 mm/min. Results are reported in Figure 12.8 and Table 12.5.

Table 12.5 Tensile properties of composites of Table 12.1.

Parameters	**CB**	**CB-Silica**	**CB/TETAP 50%**	**CB/TETAP 100%**
σ_1 (MPa)	4.7	4.6	6.3	6.4
σ_2 (MPa)	12.2	10.3		
σ_B (MPa)	14.4	11.6	10.7	10.2
ε_B (%)	225.2	222.0	166.7	155.1
Energy (J/cm^3)	13.9	12.2	9.0	8.0

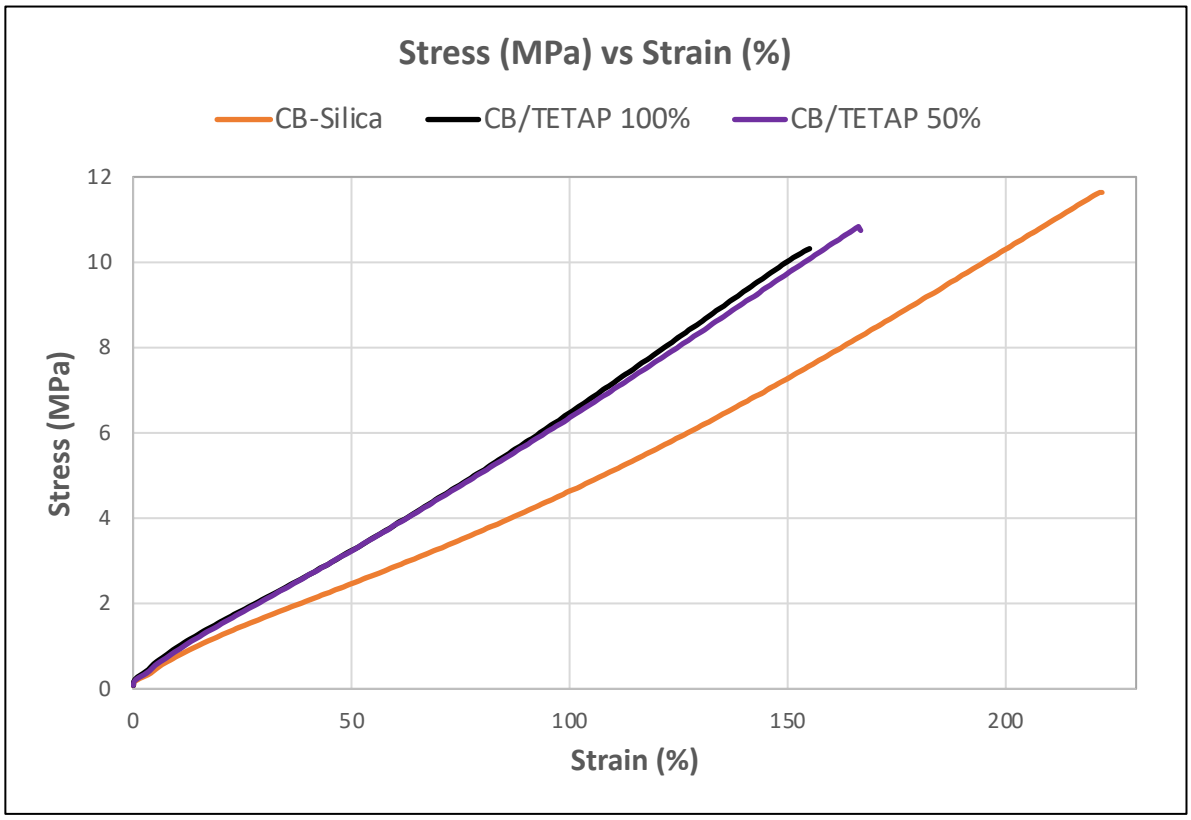

Figure 12.8 Tensile properties of composites described in Table 12.1.

Since each stress-strain curve represented in Figure 12.8 is an average of the output of three equivalent tensile tests on three equivalent samples, standard deviations of stress, strain and energy at break are represented in Figure 12.9:

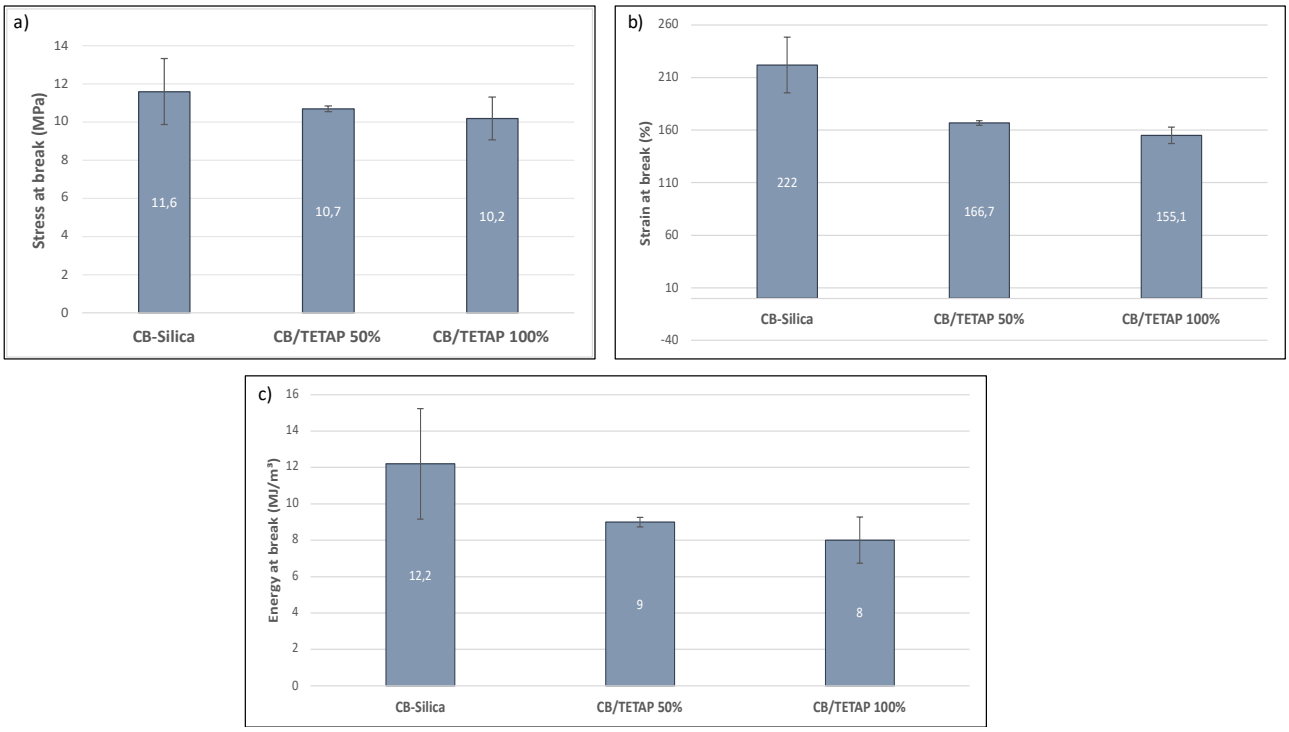

Figure 12.9 a) stress at break, b) strain at break, c) energy at break.

Larger stresses can be observed for the CB/TETAP composites, at all the elongations, up to the break. CB/TETAP compounds show a higher stiffness, in line with the results of dynamic-mechanical tests. These composites achieve lower elongation and thus have lower stresses and energies at break, with respect to the reference CB-Silica. These behaviors are more pronounced in CB/TETAP 100% with respect to CB/TETAP 50%.

12.3. NR/BR-based composites filled with CB/p-PDAP

Compounds with the CB/p-PDAP adduct were prepared by melt blending adopting the scheme shown in Figure 12.2 and the procedure shown in Figure 12.4, described in detail in the experimental section. The adduct contained 4 % by mass of p-PDAP on CB (calculated via TGA).
Recipes of the elastomeric compounds are reported in Table 12.6:

Table 12.6 Recipes of NR/BR based composites filled with silica and CB or CB/p-PDAP as fillers.

Recipes in phr	**CB** **[phr]**	**CB-Silica** **[phr]**	**CB/p-PDAP 50%** **[phr]**	**CB/p-PDAP 100%** **[phr]**
BR	60	60	60	60
NR (SIR 20)	40	40	40	40
CB N326	60	30	15	0
CB/p-PDAP	0	0	15.6	31.2
CB			15	30
p-PDAP			0.6	1.2
Silica	0	35	35	35
TESPT	5.6	5.6	5.6	5.6
Sulphur	4.1	4.1	4.1	4.1

Other ingredients used for each composite: Stearic acid 2, ZnO 3.3, 6PPD 2, TBBS 1.4

A reference CB compound with only carbon black as filler was also prepared. A brabender® type internal mixer was used, with a 50-cc chamber and 0.85 (85%) as fill factor.
Characterization of the compounds was performed by dynamic-mechanical measurements, whereas tensile properties were not determined.

12.3.1. *Vulcanization*

Curing was performed at 170°C. Rheometric data and curves are reported respectively in Table 12.7 and in Figure 12.10.

Table 12.7 Rheometric data of composites described in Table 12.6.

	CB	CB-Silica	CB/p-PDAP 50%	CB/p-PDAP 100%
M_L [dNm]	4.1	4.8	8.4	9.0
M_H [dNm]	27.7	23.2	28.3	29.2
$M_H - M_L$ [dNm]	23.6	18.4	19.9	20.2
T_{90} [min]	4.3	6.1	5.9	5.6
T_{S1} [min]	2.5	2.4	2.1	2.1

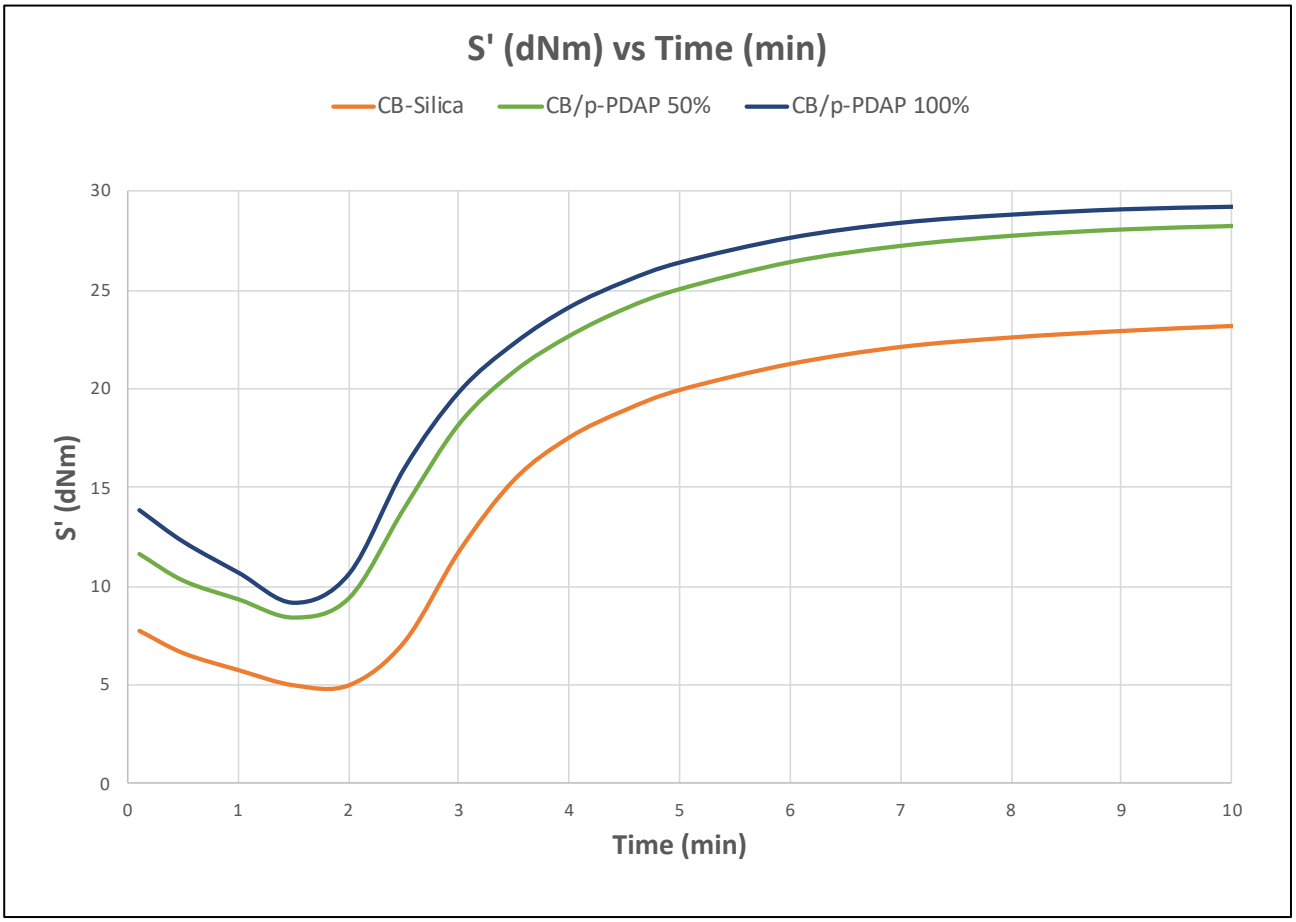

Figure 12.10 Rheometric curves of composites described in Table 12.6.

A slight accelerating effect characterized CB/p-PDAP composites compared to the reference CB-Silica, related presumably to the amino group moiety of the pyrrole on the CB surface.

Analyzing torque values reported in Table 12.7, a clear increase in both M_H and M_L values was associated to CB/p-PDAP compounds. The increase in M_L indicates the increase of viscosity. Larger values of both M_H and M_L were obtained with larger amount of adducts.

12.3.2. *Dynamic-mechanical properties from strain sweep experiments*

Dynamic-mechanical properties were determined through strain-sweep experiments on cured samples. Figure 12.11 shows the dependence of the storage modulus (G'), the loss modulus (G'') and the loss factor (Tan δ) on the strain amplitude. Table 12.8 reports data obtained from strain-sweep experiments.

Table 12.8 Dynamic-mechanical properties obtained through strain-sweep experiments.

Parameters	**CB**	**CB-Silica**	**CB/p-PDAP 50%**	**CB/p-PDAP 100%**
G' $_{\gamma min}$ (MPa)	4.00	4.24	4.41	4.11
G' $_{\gamma max}$ (MPa)	1.87	1.85	1.91	1.94
ΔG' (MPa)	2.13	2.39	2.50	2.17
ΔG'/G' $_{\gamma min}$	0.53	0.56	0.57	0.53
G'' $_{max}$ (MPa)	0.28	0.43	0.38	0.36
Tan Delta max	0.12	0.17	0.16	0.18

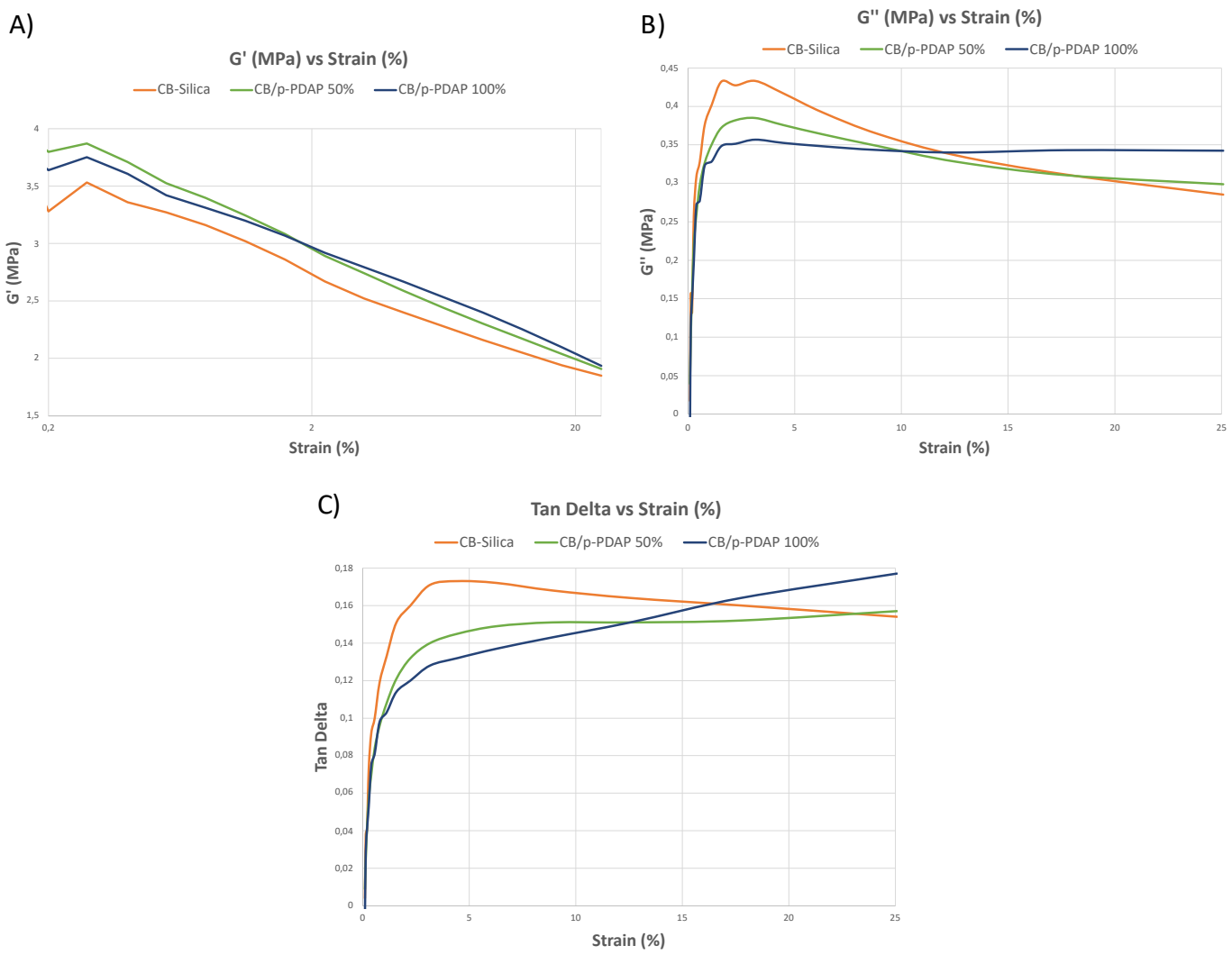

Figure 12.11 A) G' vs strain, B) G" vs strain C) Tan Delta vs strain.

The comparison among all the silica-based compounds reveals small differences. Bearing this in mind, it could be commented that a reduction of the Payne effect (ΔG') was obtained with CB/p-PDAP 100 % compound. As already observed for the compounds with CB/TETAP as the adduct, increase of Tan δ occurs as the strain increases (Figure 12.11 C). The same explanation can be proposed: the filler-network built by the supramolecular interaction of CB adduct and silica faints at higher deformations.

It is worth again underlining that the lowest ΔG' and Tan Delta values were given by the CB compound with an unusual large amount of TESPT in the formulation. However, these results suggest the lower tendency of carbon black to interact with itself in comparison with a hybrid carbon black / silica filler system.

12.3.3. *Dynamic-mechanical properties from axial compression tests*

Axial-dynamic properties were measured in compression and are reported in Figure 12.12 and Table 12.9.

Table 12.9 Axial-dynamic mechanical properties of compounds described in Table 12.6.

	CB	CB-Silica	CB/p-PDAP 50%	CB/p-PDAP 100%
E' 10°C	10.56	12.66	12.98	14.47
E'' 10°C	1.81	2.64	2.34	2.39
Tan Delta 10°C	0.17	0.21	0.18	0.17
E' 23°C	9.92	11.73	12.15	13.54
E'' 23°C	1.49	2.32	2.06	2.13
Tan Delta 23°C	0.15	0.20	0.17	0.16
E' 70°C	8.93	10.17	10.76	11.84
E'' 70°C	1.02	1.78	1.65	1.76
Tan Delta 70°C	0.12	0.18	0.15	0.15
ΔE' (E' 10°C-E' 70°C)	1.63	2.49	2.22	2.63

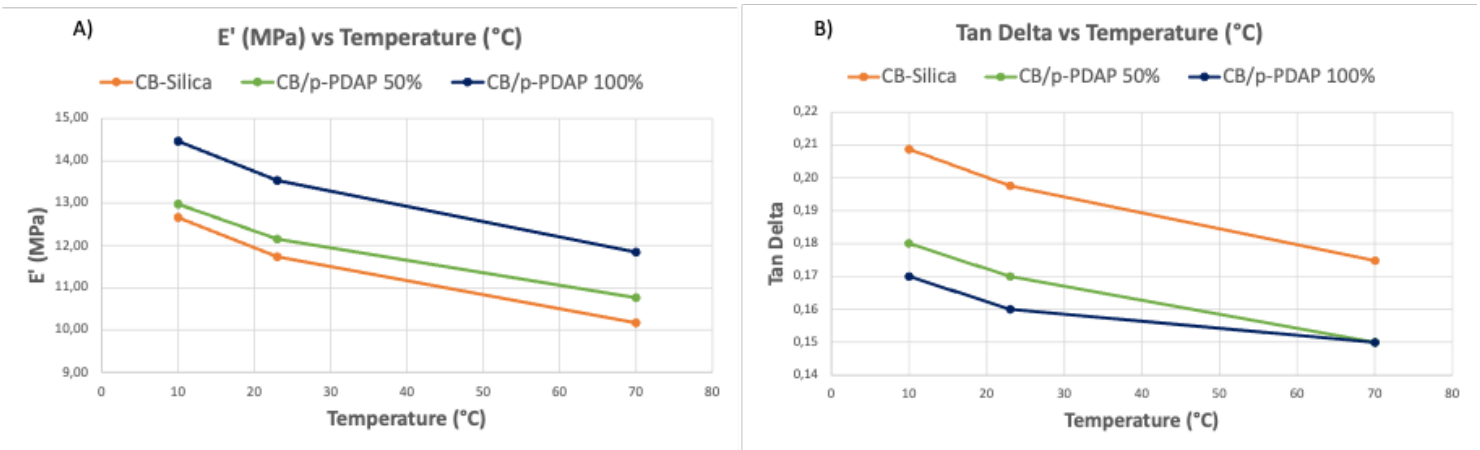

Figure 12.12 A) E' vs T, B) Tan Delta vs T.

Higher E' values for all the tested temperatures were associated to CB/p-PDAP samples compared to the reference CB-Silica. These results were not unexpected: both M_H values from the curing curve and the results from the strain-sweep experiments, suggested that p-PDAP presence in compounds could increase the stiffness. While CB/p-PDAP 50% displayed a lower ΔE' compared to CB-Silica, CB/p-PDAP 100% was characterized by a higher ΔE' value in comparison to the reference CB-Silica.

Lower Tan δ values for all the temperatures were shown by CB/p-PDAP samples compared to CB-Silica. This suggested that the use of CB/p-PDAP adducts in compounds can reduce the dissipation of energy. A correlation appears between the amount of CB/p-PDAP and the effect on the composite properties.

12.4. NR/BR-based composites filled with CB/EAP

As anticipated in the introduction to this Chapter, CB/EAP was also used as the adduct to compare the behavior of different types of adducts and thus of interactions with silica. Compounds were based on Natural rubber (NR) and butadiene rubber (BR) and were filled with carbon black and silica as a hybrid filler system, analogously to what seen in the previous paragraphs. The same recipes of the precedent studies were adopted. The only difference relies on the amount of pyrrole derivative. As reported in chapter 9, the amount of EAP in the adducts was around 1% (in wt.) compared to carbon black.

Recipes of the elastomeric compounds are reported in Table 12.10:

Table 12.10 Recipes of NR/BR based composites filled with silica and CB or CB/EAP as the fillers.

Recipes in phr	**CB** **[phr]**	**CB-Silica** **[phr]**	**CB/EAP 50%** **[phr]**	**CB/EAP 100%** **[phr]**
BR	60	60	60	60
NR (SIR 20)	40	40	40	40
CB N326	60	30	15	0
CB/EAP	0	0	15.2	30.4
CB			15	30
EAP			0.2	0.4
Silica	0	35	35	35
TESPT	5.6	5.6	5.6	5.6
Sulphur	4.1	4.1	4.1	4.1

Other ingredients used for each composite: Stearic acid 2, ZnO 3.3, 6PPD 2, TBBS 1.4

The procedure for the preparation of the composites was the same already reported in Figure 12.1. A brabender® type internal mixer was used, with a 50-cc chamber and a fill factor of 0.85 (85%).

A CB compound without silica was also prepared.

The behavior of the adducts in NR/BR based compounds was investigated through composites characterization by means of dynamic-mechanical properties. Stress-strain experiments were not performed.

12.4.1. *Vulcanization*

Curing was performed at 170°C for 10 minutes and rheometric curves are shown in Figure 12.13. Torque values, induction times and times to achieve the optimum level of vulcanization are reported in Table 12.11.

Table 12.11 Torque values, induction times (T_{S1}) and times to achieve the optimum level of vulcanization (T_{90}) of composites described in Table 12.10.

	CB	**CB-Silica**	**CB/EAP 50%**	**CB/EAP 100%**
M_L [dNm]	4.1	4.8	6.4	6.7
M_H [dNm]	27.7	23.2	25.3	26.0
$M_H - M_L$ [dNm]	23.6	18.4	18.9	19.3
T_{90} [min]	4.3	6.1	6.2	6.1
T_{S1} [min]	2.5	2.4	2.3	2.2

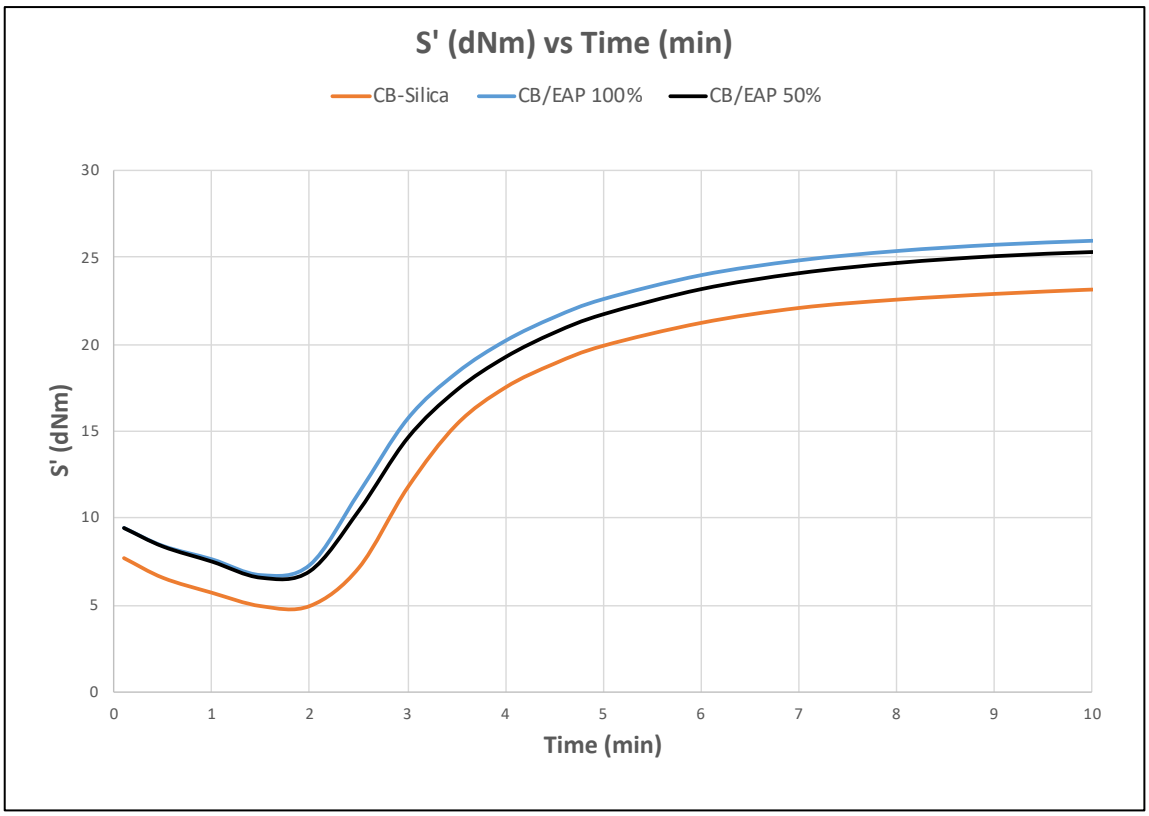

Figure 12.13 Rheometric curves of composites described in Table 12.10.

The use of adducts in place of CB did not have effect on the induction of vulcanization and slightly increased the T_{90} values. This could be also due to the low amount of pyrrole derivative present in CB/EAP adducts, but it is definitely due to the chemical nature of the nitrogen substituent of the pyrrole compound.

Larger values of M_L and M_H were obtained. It can be commented that the adduct promotes the formation of filler agglomerates. The increase in M_H and M_L values was more pronounced in the sample with a higher amount of functionalized carbon black.

12.4.2. *Dynamic-mechanical properties from strain sweep experiments*

Dynamic-mechanical tests in torsional mode were conducted on vulcanized samples. The dependence of G', G'' and Tan δ as a function of the strain amplitudes are shown respectively in Figure 12.14 A, B and C. The obtained results are summarized in the Table below:

Table 12.12 Dynamic-mechanical properties obtained through strain-sweep experiments.

Parameters	**CB**	**CB-Silica**	**CB/EAP 50%**	**CB/EAP 100%**
G' $_{\gamma min}$ (MPa)	4.00	4.24	4.40	4.46
G' $_{\gamma max}$ (MPa)	1.87	1.85	1.84	1.84
ΔG' (MPa)	2.13	2.39	2.56	2.62
ΔG'/G' $_{\gamma min}$	0.53	0.56	0.58	0.59
G'' $_{max}$ (MPa)	0.28	0.43	0.42	0.41
Tan Delta max	0.12	0.17	0.17	0.16

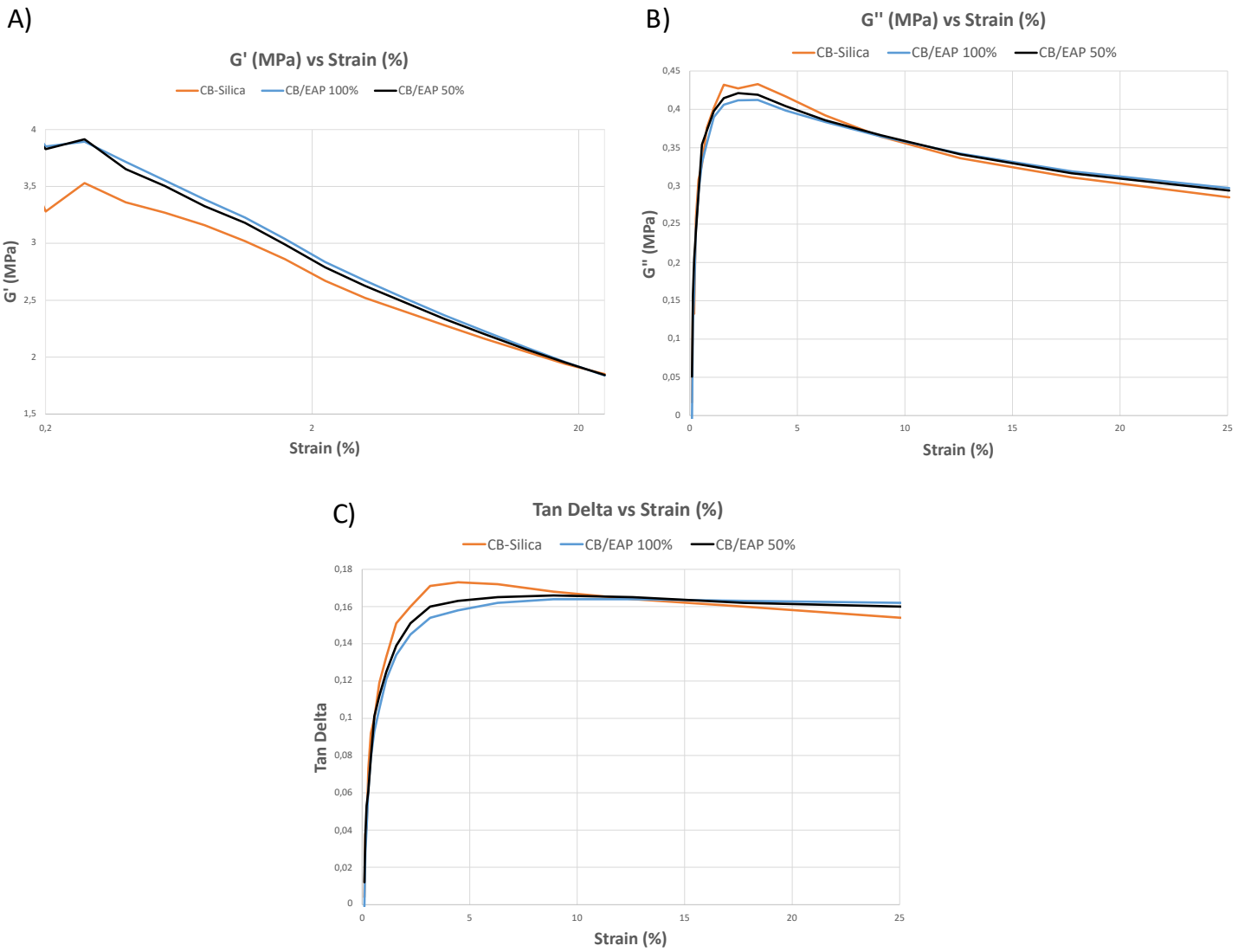

Figure 12.14 A) G' vs strain B) G" vs strain C) Tan Delta vs strain.

A slight increase in Payne effect (ΔG') was observed in CB/EAP composites, in comparison with the reference sample. Both G'' and Tan δ curves (Figure 12.14-B, C) did not present significant changes between CB-Silica composites.

12.4.3. *Dynamic-mechanical properties from axial compression tests*

Axial-dynamic mechanical properties were measured in compression. These are shown in Figure 12.15 and data are collected in Table 12.13.

Table 12.13 Axial-dynamic mechanical properties of compounds described in Table 12.10.

	CB	CB-Silica	CB/EAP 50%	CB/EAP 100%
E' 10°C	10.56	12.66	12.46	12.83
E'' 10°C	1.81	2.64	2.50	2.53
Tan Delta 10°C	0.17	0.21	0.20	0.20
E' 23°C	9.92	11.73	11.6	11.91
E'' 23°C	1.49	2.32	2.20	2.22
Tan Delta 23°C	0.15	0.20	0.19	0.19
E' 70°C	8.93	10.17	9.95	10.21
E'' 70°C	1.02	1.78	1.71	1.73
Tan Delta 70°C	0.12	0.18	0.17	0.17
ΔE' (E' 10°C-E' 70°C)	1.63	2.49	2.51	2.62

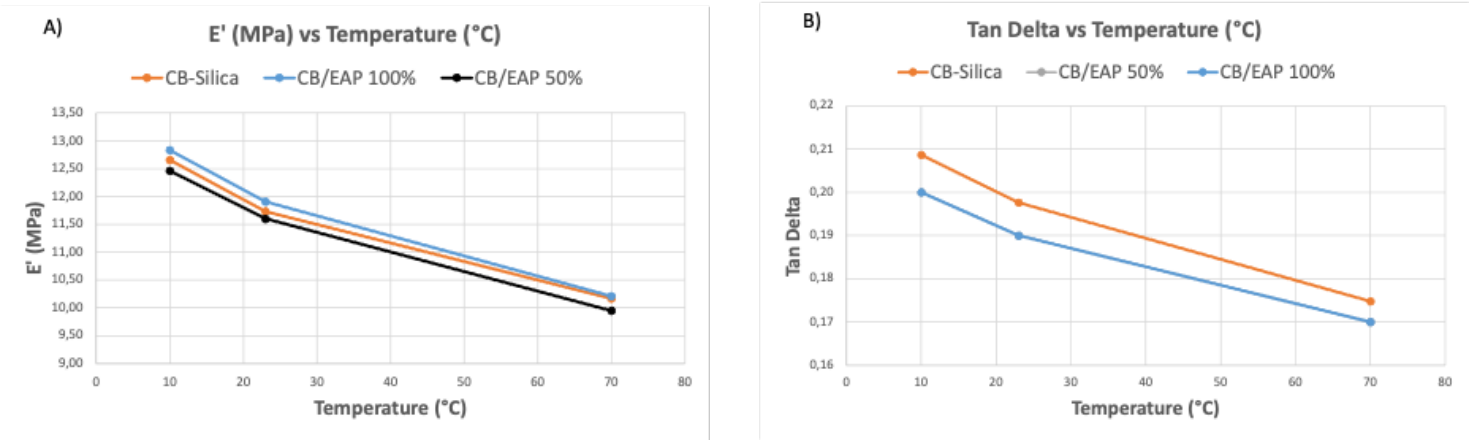

Figure 12.15 A) E' vs T B) Tan Delta vs T.

As it can be seen, no modification emerged from the different curves. E' and Tan δ were very similar, indicating that the amount of pyrrole derivative was too small to promote appreciable changes.

12.5. Conclusions

NR/BR based compounds filled with a hybrid filler system carbon black/silica were studied. Three different adducts of CB were investigated.

The results show that a clear effect on the compound properties was revealed when CB/TETAP was used. In particular: faster vulcanization reaction, larger dynamic-mechanical rigidity, lower hysteresis.

Lower effects were observed when CB-p-PDAP was used and one could say, no effects when CB-EAP was used.

Besides the due considerations on the amount of the pyrrole compound onto the CB surface, a key role is played by the chemical nature of the pyrrole compound. It appears that the acid-base interaction promoted by TETAP leads to the mentioned, remarkable, effects in the compound.

A common feature in all the compounds is the increase of the viscosity and this is an indication of the tendency to agglomerate of the functionalized CB. In the case of the compounds reported in this Chapter, the agglomeration is with silica.

It is worth commenting that the appreciable effect due to TETAP was obtained in spite of the procedure adopted for the preparation of the compound (see in particular Figure 12.2): the adduct got in contact with a silanized silica. It appears that this type of adduct could be interesting as an ingredient for silica-based compounds. The effect on the marching modulus of the silica-based compound appears to be enough to justify further investigations.

References

[1] J. Jin, J.W.M. Noordermeer,W.K. Dierkes, A. Blume. The Effect of Silanization Temperature and Time on the Marching Modulus of Silica-Filled Tire Tread Compounds. Polymers (Basel). 2020.

[2] S.J. Park, M.K. Seo,C. Nah. Influence of surface characteristics of carbon blacks on cure and mechanical behaviors of rubber matrix compoundings. J Colloid Interface Sci. 2005.

Chapter 13

NR/BR-based composites filled with both CB and Silica: SEV

13.1 Introduction

This study was focused on BR/NR-based compounds filled with both silica and carbon black. CB was either pristine or functionalized with triethylenetetramine pyrrole (TETAP). The chemical structure of the pyrrole compound is reported in Figure 13.1.

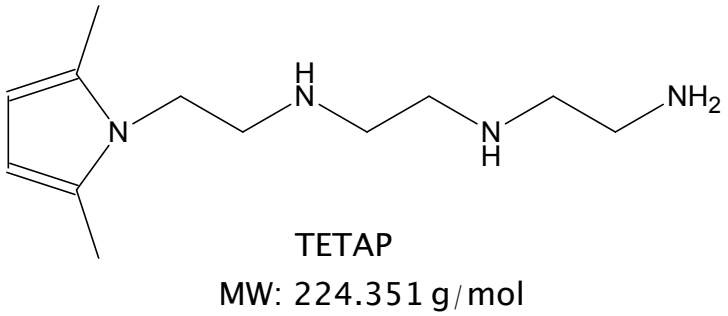

Figure 13.1 Chemical structure of triethylenetetramine pyrrole (TETAP).

The objective was to investigate the effect of CB/TETAP on the compound properties. A semi-effective vulcanization system was preferred instead of the conventional vulcanization system adopted in the precedent activity. In order to further decrease the sulfur content in compounds, a bis(3- triethoxysilylpropyl)disulfide (TESPD) was used (Figure 13.2).

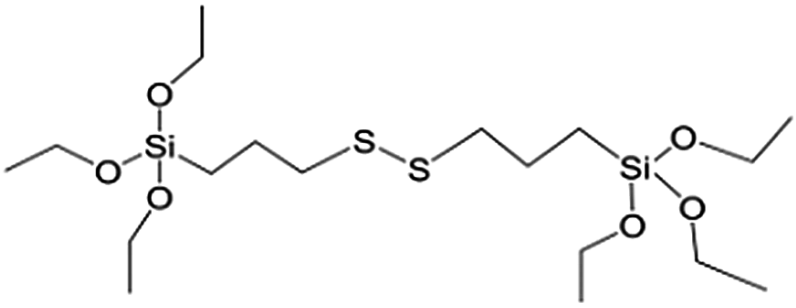

Figure 13.2 Bis(triethoxysilylpropyl)disulfide

Hence, objective was to verify if the different curing system and the different silane should promote better tensile properties. Two different preparation procedures were applied. These are schematized in the Figure 13.3 and detailed in Figure 13.4.

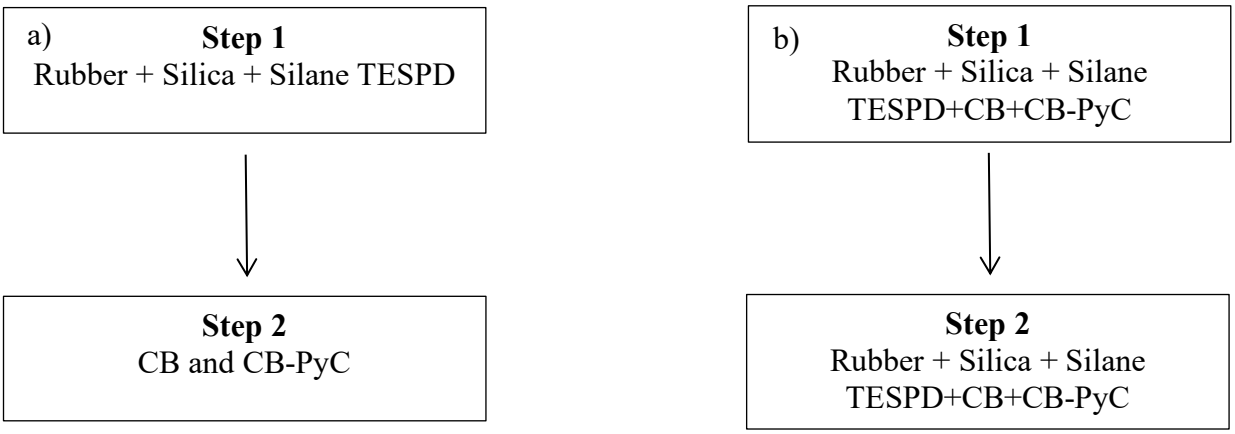

Figure 13.3 Procedures adopted for the preparation of the compounds.

The difference between these two preparation procedures relies on the interaction between CB or CB/TETAP and silica: in procedure a) carbon black interacts with a pre-silanized silica, while in b) CB/TETAP interacts with silica together with the silane TESPD. In particular, the interaction of a basic substance, such as CB/TETAP, with un-silanized silica could promote a better filler-polymer interaction: CB/TETAP could interact with un-silanized silica, which, through the silane, can create a covalent bond with the rubber. On the other hand, it is possible that the presence of CB/TETAP could badly influence silica silanization, leading to the presence of un-silanized silica in the compound. Therefore, this activity also aims to understand the influence of the preparation procedure on the compound's properties.

Composites were vulcanized for 10 minutes at 170°C (with RPA 2000 instrument). Characterization was made by means of dynamic-mechanical and tensile measurements. Dynamic-mechanical properties were investigated through shear strain-sweep experiments and in traction compression-mode, allowing the determination of G', G'', E', E'' and Tan Delta. Tensile properties were determined by means of quasi static experiments, measuring the stresses at different elongations on a universal tensile testing machine (Zwick/Roll 2010) at a strain rate of 1 mm/min.

13.2 Formulations

A carbon black-silica ratio equal to 50/50 (in volume) was used for the composites' preparation. The same amount of carbon black was present in all the samples: 30 phr of carbon black. When the adduct was used, 30 phr of carbon black were replaced by 15.6 and 7.8 phr of CB/TETAP, considering TETAP as an extra ingredient. The amount of pyrrole derivative present on the carbon black surface was derived from thermogravimetric analysis and it was approximately equal to 4% by mass with respect to CB.

Recipes of the elastomeric composites are reported in Table 13.1:

Table 13.1 NR/BR-based composites filled with silica and CB or CB/TETAP as fillers.

Recipes in phr	**CB-Silica**	**CB/TETAP 25%**	**CB/TETAP 50%**	**CB/TETAP 50% Different mixing**
	[phr]	**[phr]**	**[phr]**	**[phr]**
BR	60	60	60	60
NR (SIR 20)	40	40	40	40
CB N326	30	22.5	15	15
CB/TETAP	0	7.8	15.6	15.6
CB		7.5	15	15
TETAP		0.3	0.6	0.6
Silica	35	35	35	35
TESPD	2.8	2.8	2.8	2.8
Sulphur	2	2	2	2

Other ingredients used for each composite: Stearic acid 2, ZnO 4, 6PPD 2, TBBS 1.8

Differentiating from the previous studies, a "different mixing" (DM) compound was present and was characterized, as the name suggests, by a different brabender® preparation's procedure. In Figure 13.4 are shown the mixing procedures employed for: A) CB-Silica, CB/TETAP 25% and CB/TETAP 50% composites, B) DM compound. A brabender® type internal mixer with a 50-cc chamber and 0.85 (85%) as fill factor was used.

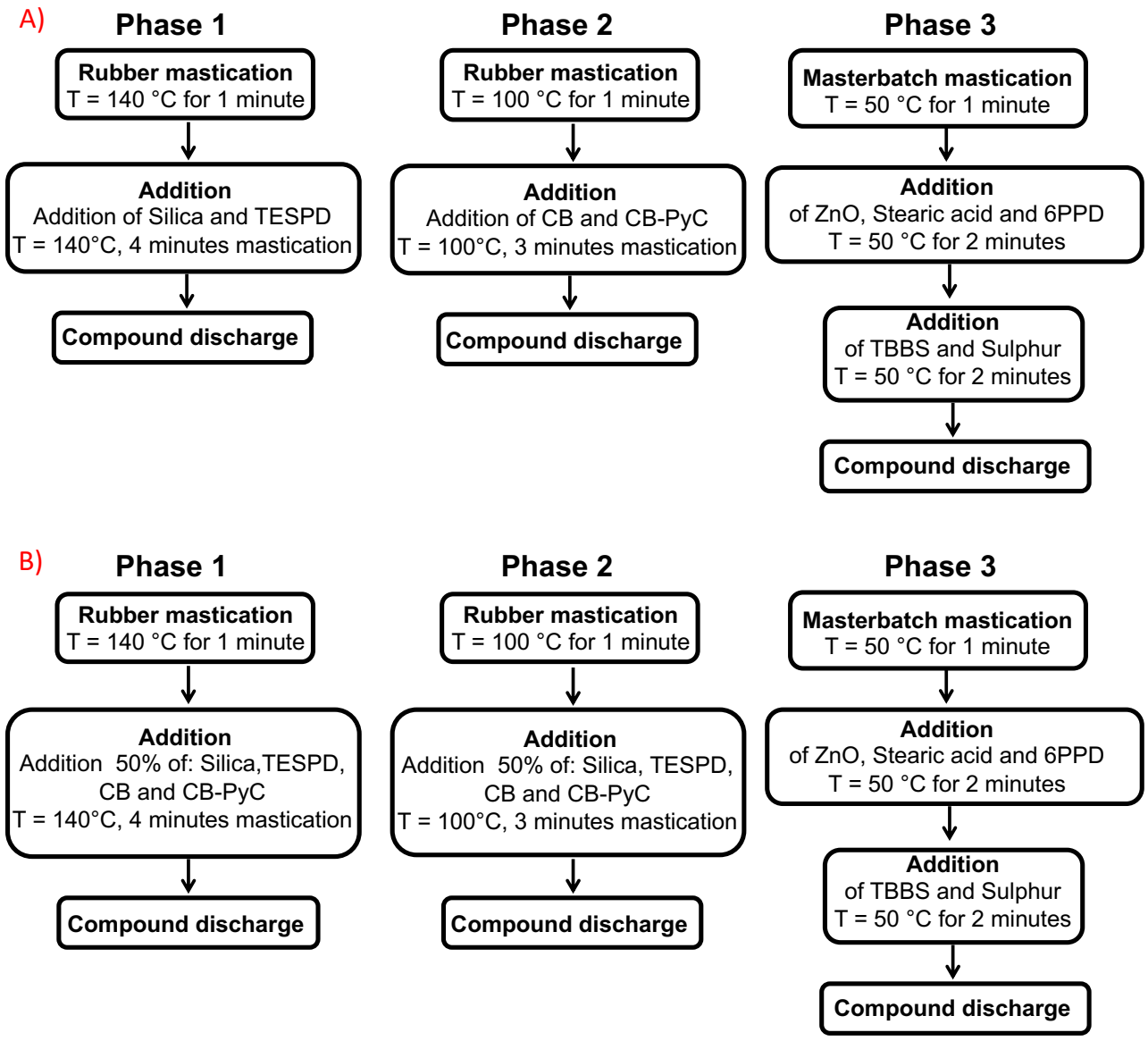

Figure 13.4 Procedure for the composites preparation: A) CB-Silica, CB/TETAP 50%, CB/TETAP 25% composites B) "different mixing" compound.

Composites can thus be divided on the basis of the preparation procedure:

- Produced with a pre-silanized silica: a masterbatch was made with rubber, silica, organosilane (TESPD) and this was then used for the composite's preparation (Figure 13.4-A).
- Produced performing silanization in situ: rubber, silica, TESPD and CB or CB/TETAP were mixed in the same step. (Figure 13.4-B). This was the "Different Mixing" (DM) sample.

13.2.1. *Vulcanization*

The elastomeric composites were cured with a sulfur-based system at 170°C. Rheometric curves and vulcanization data are respectively shown in Figure 13.5 and Table 13.2.

Table 13.2 Torque values, induction times and times to achieve the optimum level of vulcanization obtained for rubber composites.

	CB-Silica	CB/TETAP 25%	CB/TETAP 50%	CB/TETAP 50% DM
M_L [dNm]	4.46	4.92	5.73	5.58
M_H [dNm]	18.45	19.03	19.97	20.12
$M_H - M_L$ [dNm]	13.99	14.11	14.24	14.54
T_{90} [min]	5.59	4.96	4.64	4.60
T_{S1} [min]	2.53	2.34	2.25	2.12

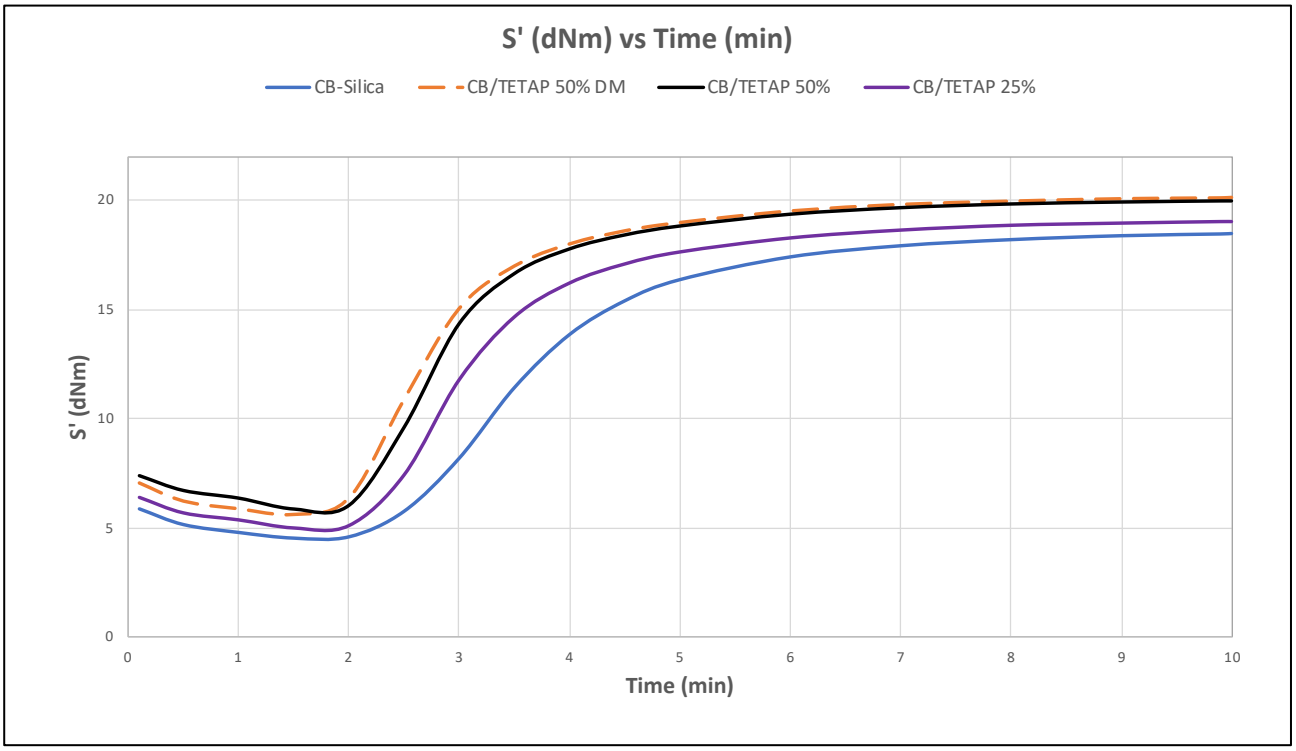

Figure 13.5 Rheometric curves of CB/TETAP compounds: Torque vs time.

Rheometric results were in line with those reported in the previous studies: CB/TETAP brought about a speed-up of the vulcanization process and higher torque values with respect to the reference CB-Silica compound can be seen.

Similar results were obtained for CB/TETAP 50% and DM composites, indicating that the different mixing procedure did not alter significantly the curing behavior.

13.2.2 *Dynamic-mechanical properties from strain sweep experiments*

Strain-sweep experiments were performed at 50°C on crosslinked samples to analyze the filler networking phenomenon. The detailed procedure is reported in the experimental section. In Figure 13.6 are reported: A) the dependence of G' vs strain, B) the G plot (G'' vs G'), C) the dependence of G'' vs strain, D) the dependence of Tan δ vs strain. Results from strain-sweep experiments are

summarized in Table 13.3. Tan Delta is the ratio between G'' and G', and ΔG' is the difference between the highest and the lowest G' values at 0.1 and 25% as strain amplitude, respectively (see experimental details).

Table 13.3 Dynamic-mechanical properties obtained through strain-sweep experiments.

Parameters	CB-Silica	CB/TETAP 25%	CB/TETAP 50%	CB/TETAP 50% DM
G' $_{\gamma min}$ (MPa)	3.25	3.25	3.25	3.14
G' $_{\gamma max}$ (MPa)	1.36	1.38	1.41	1.38
ΔG' (MPa)	1.89	1.87	1.84	1.76
ΔG'/G' $_{\gamma min}$	0.58	0.58	0.57	0.56
G'' $_{max}$ (MPa)	0.40	0.41	0.42	0.38
Tan Delta max	0.20	0.20	0.20	0.19

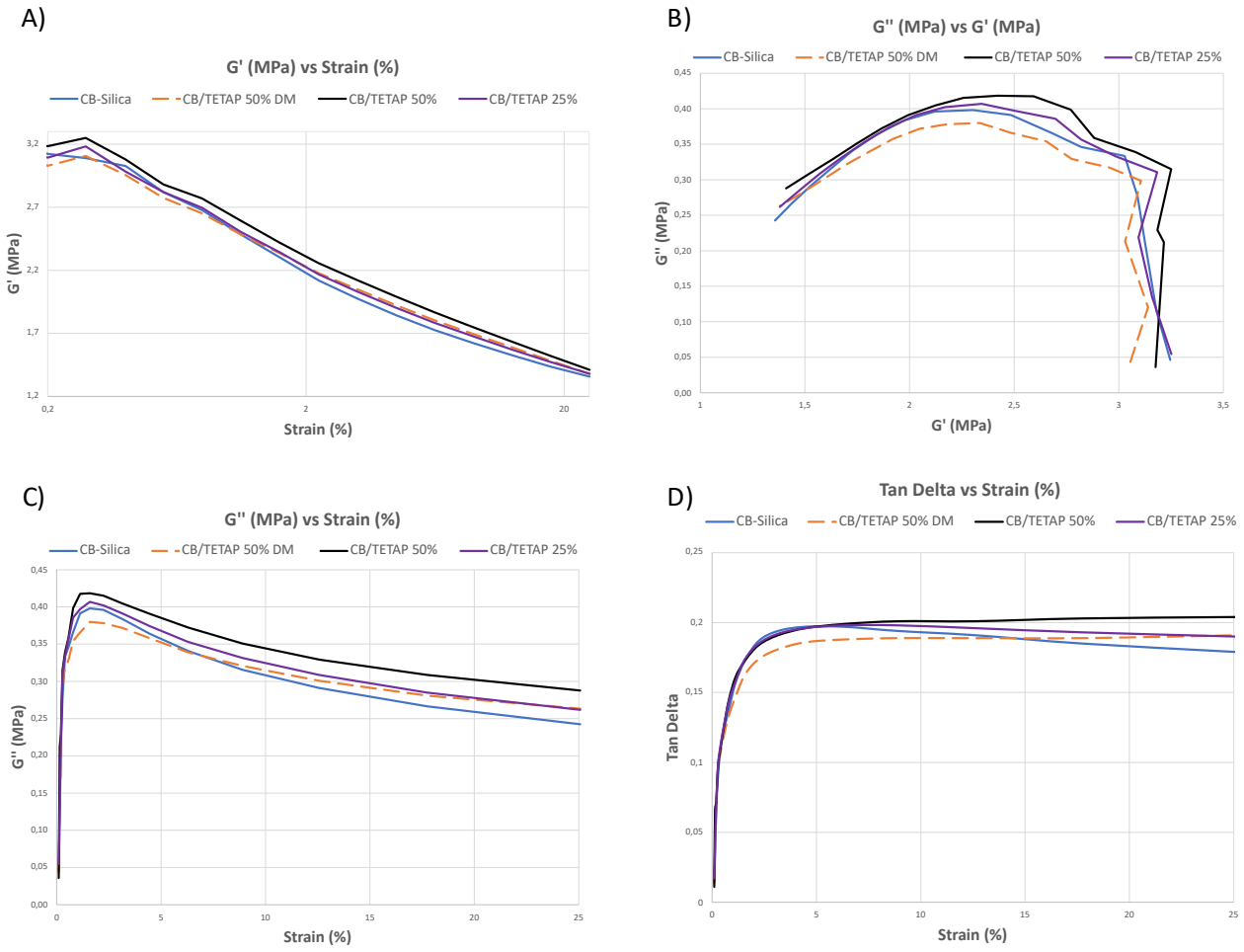

Figure 13.6 A) G' vs strain B) G plot (G'' vs G') C) G'' vs strain D) Tan δ vs strain.

Procedure A: a slight decrease in Payne effect, related to ΔG' values, was associated to CB/TETAP composites compared to the reference CB-Silica. However, higher loss modulus (Figure 13.6 B and C) characterized these composites, leading to slightly higher Tan δ values (Figure 13.6 D)). The decrease of Payne effect but not in the hysteresis can be related to the interaction of functionalized carbon black with the silica but not with the polymer. This is just a hypothesis and confirmations are needed.

Procedure B: this composite showed the lowest ΔG', G'' max and Tan Delta max values (Table 13.3) and thus a reduction in Payne effect and in hysteresis. The reduction of the filler network can be seen also in the G plot (Figure 13.6 B)): for a given level of storage modulus (G'), DM showed the lowest loss modulus (G'').

While CB/TETAP 50% compound was characterized by a lower Payne effect and higher Tan Delta values compared to CB-Silica, DM showed a reduction in both filler network and hysteresis compared to all the other samples. The following hypothesis can be made to explain these experimental findings:

a) CB/TETAP can interact with an unsilanized silica and, through TESPD, silica can establish a chemical bond with the polymer chains.
b) CB/TETAP can act as a catalyst for the silanization reaction. As reported in literature, the nitrogen presence in the pyrrole ring can speed up the silanization reaction. [1]

Nevertheless, further studies have to be performed to properly understand the nature of CB/TETAP and unsilanized silica interaction.

13.2.3 *Dynamic-mechanical properties from axial compression tests*

Axial-dynamic mechanical properties were measured in compression, as reported in the experimental section. In Figure 13.7 the dependence of the dynamic storage modulus (A) and of Tan Delta (B) with the temperature are shown. Dynamic-mechanical results are summarized in the Table below:

Table 13.4 Axial dynamic-mechanical properties of composites described in Table 13.1.

	CB-Silica	CB/TETAP 25%	CB/TETAP 50%	CB/TETAP 50% DM
E' (10°C)	9.29	10.22	11.00	10.33
E'' (10°C)	1.98	2.09	2.22	2.04
Tan Delta (10°C)	0.21	0.20	0.20	0.20
E' (23°C)	8.59	9.56	10.25	9.61
E'' (23°C)	1.77	1.92	2.03	1.85
Tan Delta (23°C)	0.21	0.20	0.20	0.19
E' (70°C)	7.49	8.08	8.70	8.35
E'' (70°C)	1.45	1.59	1.71	1.55
Tan Delta (70°C)	0.19	0.20	0.20	0.19
ΔE' (E' 10°C –E' 70°C)	1.80	2.14	2.3	1.98

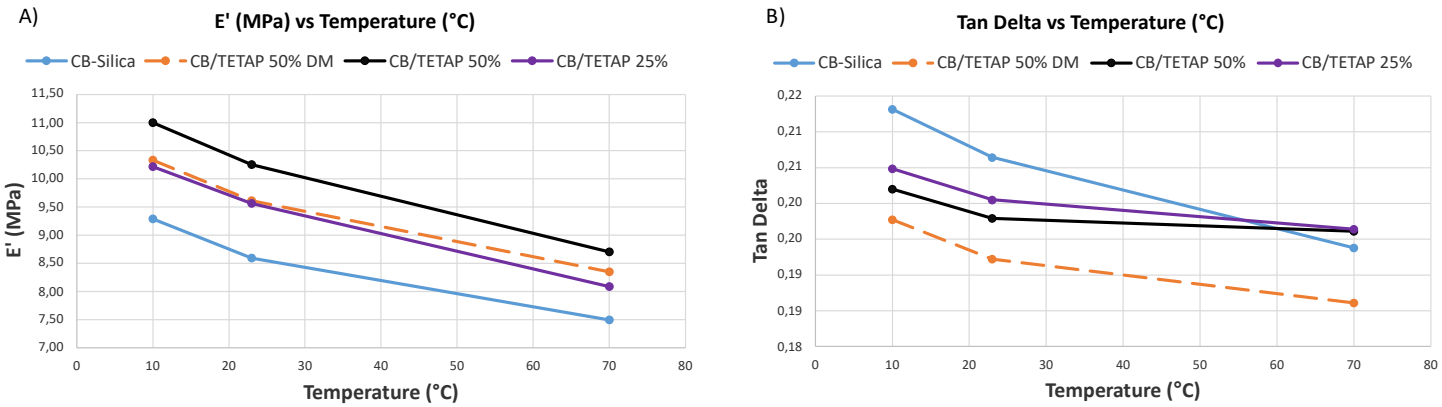

Figure 13.7 A) E' vs T B) Tan Delta vs T.

Procedure A: Higher E' and ΔE' values for all the tested temperatures characterized CB/TETAP composites compared to the reference CB-Silica. Hence, the higher stiffness of CB/TETAP, which arose in the precedent studies, was still confirmed. No significant changes in Tan δ can be seen.

Procedure B: E' and ΔE' values were lower than CB/TETAP 50% but higher than CB-Silica. Therefore, the different preparation procedure used for the DM sample seems to reduce the stiffness of the composite. The composite showed the lowest Tan δ values, confirming the hysteresis reduction already seen from strain-sweep experiments.

13.2.4. *Tensile properties*

Tensile properties were measured through quasi-static measurements. Stresses at 100 and 300% of elongation (σ_1 and σ_3), stresses at break (σ_B), elongations at break (ε_B) and the fracture energy are reported in Table 13.5:

Table 13.5 Tensile properties of compounds described in Table 13.1.

Parameters	CB-Silica	CB/TETAP 25%	CB/TETAP 50%	CB/TETAP 50% DM
σ_1 (MPa)	2.2	2.7	2.5	2.5
σ_3 (MPa)	9.2	10.3	10.2	9.9
σ_B (MPa)	19.2	14.2	12.7	15.2
ε_B (%)	527.1	379.4	359.5	413.2
Energy (J/cm^3)	44.5	24.7	20.4	27.6

Procedure A: results were in line with those of the previous studies: lower stresses, elongation and energy at break characterized CB/TETAP composites compared to the reference CB-Silica. Nevertheless, it is worth to underline that values of elongation at break were still above 350%. These behaviors were more pronounced in CB/TETAP 50% rather than CB/TETAP 25%, pointing out a positive correlation between the effect on the mechanical properties and the amount of functionalized carbon black.

Procedure B: higher stresses, elongation and energy at break were associated to DM compared to CB/TETAP 50% sample. DM composite showed better ultimate properties compared also to CB/TETAP 25%, in which a lower amount of functionalized carbon black was used (see Table 13.1). These experimental findings confirmed what hypothesized in strain-sweep experiments: it seems that the different preparation method can promote better filler-polymer interactions. However, the tensile properties of DM were still worse than CB-Silica: both fracture energy, elongation and stress at break were lower.

13.3 Comparison between NR/BR-based composites filled with both CB and Silica

In this section the effect of TETAP bound to the CB surface in a hybrid filler system was studied as a function of the recipe of the vulcanization system, so basically as a function of the sulphur/accelerator ratio. The comparison was done between CV CB-Silica and CB/TETAP 50% (Chapter 12) and SEV CB-Silica and CB/TETAP 50% (Chapter 13). Compounds' data, coming from the rheometric curves and describing dynamic-mechanical and tensile properties, are compared *vis a vis* in the following Tables.

13.3.1 *Vulcanization*

Rheometric data of CB-Silica and CB/TETAP 50% are reported in Table 13.6. Data of CB-Silica compound were taken as reference (set at 100) for the calculation of the other composite's values.

Table 13.6 Torque values, induction times (T_{S1}) and times to achieve the optimum level of vulcanization (T_{90}) obtained for rubber composites.

	Conventional vulcanization system		**Semi-efficient vulcanization system**	
	CB-Silica	**CB/TETAP 50%**	**CB-Silica**	**CB/TETAP 50%**
M_L [dNm]	100	118.8	100	128.5
M_H [dNm]	100	113.0	100	108.2
$M_H - M_L$ [dNm]	100	111.5	100	101.8
T_{90} [min]	100	76.9	100	83.0
T_{S1} [min]	100	85.6	100	88.9

Results are in line with those reported in the precedent comparison (Chapter 11): slightly lower T_{S1} and higher M_H values are associated to the conventional vulcanization system. In particular, the higher M_H values of the conventional vulcanization system are associated to the higher amount of Sulphur, which promotes a higher crosslinking density.

13.3.2 *Dynamic-mechanical properties from strain sweep experiments*

Results from strain-sweep experiments are compared in the Table below.

Table 13.7 Dynamic-mechanical properties obtained through strain-sweep experiments.

	Conventional vulcanization system		**Semi-efficient vulcanization system**	
Parameters	**CB-Silica**	**CB/TETAP 50%**	**CB-Silica**	**CB/TETAP 50%**
G' γ_{min} (MPa)	100	112.0	100	100.0
G' γ_{max} (MPa)	100	108.6	100	103.7
ΔG' (MPa)	100	114.6	100	97.4
ΔG'/G' γ_{min}	100	103.6	100	98.3
G'' $_{max}$ (MPa)	100	95.3	100	105.0
Tan Delta max	100	90.2	100	110.0

Similar values of loss modulus are associated to CV and SEV compounds, while higher storage modulus and lower loss factors characterize conventional vulcanization system. Analyzing normalized $\Delta G'/G'_{\gamma min}$ values, very similar results are reported, pointing out that the vulcanization system does not influence significantly the filler network.

13.3.3. *Dynamic-mechanical properties from axial compression tests*

The comparison between dynamic-mechanical properties of conventional and semi-efficient vulcanization system is reported in Table 13.8.

Table 13.8 Axial dynamic-mechanical properties of CV and SEV composites.

	Conventional vulcanization system		**Semi-efficient vulcanization system**	
	CB-Silica	**CB/TETAP 50%**	**CB-Silica**	**CB/TETAP 50%**
E' 10°C	100	103.5	100	118.4
E'' 10°C	100	93.6	100	112.1
Tan Delta 10°C	100	90.5	100	95.2
E' 23°C	100	104.4	100	119.3
E'' 23°C	100	94.0	100	114.7
Tan Delta 23°C	100	90.0	100	95.2
E' 70°C	100	104.0	100	116.1
E'' 70°C	100	93.8	100	117.9
Tan Delta 70°C	100	89.7	100	105.3
ΔE' (E' 10°C-E' 70°C)	100	100.8	100	127.8

As in the previous comparison between CV and SEV compounds (Chapter 11), higher E' values are associated to the conventional vulcanization system. For both vulcanization systems, a hysteresis decrease is related to the presence of functionalized carbon black. However, this reduction is more pronounced in the CV system.

13.3.4. *Tensile properties*

Tensile properties of CV and SEV compounds are illustrated in Table 13.9

Table 13.9 tensile properties of CV and SEV composites.

	Conventional vulcanization system		**Semi-efficient vulcanization system**	
Parameters	**CB-Silica**	**CB/TETAP 50%**	**CB-Silica**	**CB/TETAP 50%**
σ_1 (MPa)	100	137.0	100	113.6
σ_B (MPa)	100	92.2	100	66.1
ε_B (%)	100	75.0	100	68.2
Energy (J/cm^3)	100	73.8	100	45.8

Tensile properties were strongly influenced by the curing system. As a consequence of the higher amount of Sulphur, lower elongation and worsen tensile properties were displayed by conventional vulcanization system. It is also important to underline that different organo-silane were employed in these two studies: in CV compounds bis(3-triethoxysilylpropyl)tetrasulfide (TESPT) was used while SEV composites were prepared with bis(3- triethoxysilylpropyl)disulfide (TESPD). Differently from the previous comparison, in which the same organo-silane was used in compounds, in this case the difference in Sulphur content was furthermore accentuated.

13.4. Conclusions

NR/BR-based compounds filled with a hybrid filler system carbon black and silica were discussed in this section. Two different preparation's procedures were exploited which differ on the interaction between carbon black (pristine or functionalized) and silica.

Vulcanization properties were not influenced significantly by the preparation procedure, while differences arose with the analysis of dynamic-mechanical and tensile properties. CB/TETAP compounds obtained with a pre-silanized silica showed a reduction in Payne effect, a slightly higher hysteresis and higher stiffness compared to the reference compound. Tensile properties were in line with those of the previous experiments: a worsening in ultimate properties was registered.

Different mixing compound showed a reduction in both Payne effect and hysteresis and a lower stiffness compared to CB/TETAP composites. Better tensile properties were still displayed by DM compound with respect to CB/TETAP. These experimental findings suggest that better filler-polymer interactions could be promoted performing the latter procedure. Further studies have to be executed to understand which kind of interactions are related to the CB-Silica-polymer-silane system.

The comparison between conventional and semi-efficient vulcanization was in line with the one reported in Chapter 11: lower hysteresis, higher storage modulus and lower tensile properties were displayed by CV composites. All these results were attributed to the different amount of Sulphur, accentuated even more by the use of different organo-silanes.

References

[1] Hayichelaeh C, Reuvekamp LAEM, Dierkes WK, Blume A, Noordermeer JWM, Sahakaro K. Enhancing the Silanization Reaction of the Silica-Silane System by Different Amines in Model and Practical Silica-Filled Natural Rubber Compounds. *Polymers (Basel)*. 2018.

Section III – Experimental part

Chapter 14
Experimental Part

14.1. Materials

14.1.1. *Carbon Black*

Carbon Black (CB) N326 was from Birla Carbon S.p.a..

14.1.2. *Reagents and solvents*

The following reagents were purchased by Sigma-Aldrich and were used for the pyrrole-derivatives synthesis: 2,5-hexanedione, 2-aminoethanol (EA), 1,4-phenylenediamine (p-PDA) and *N,N'*-Bis(2-aminoethyl)ethane-1,2-diamine (TETA). All the listed reagents were used without further purification, with the only exception of 1,4-phenylenediamine, which required a recrystallization.
Deuterated chloroform ($CDCl_3$) was used to perform NMR tests.
Xylene, tetrahydrofuran (THF), 2-propanol, methanol, distilled water, acetone, hexane, and ethyl acetate (all from Sigma-Aldrich, used as received) were used for the dispersions' tests.

14.1.3. *Rubbers*

Synthetic poly (1,4-butadiene) (BR) was neocis BR 40 from Versalis, with a 43 Mooney Viscosity (ML(1+4)100°C). Poly(1,4-*cis*-isoprene) from *Hevea brasiliensis* (NR) (EQR-E.Q. Rubber, BR-THAI, Eastern GR. Thailand – Chonburi) had trade name SIR20 and 73 Mooney Units (MU) as Mooney viscosity (ML(1+4)100°C).

14.1.4. *For rubber compounds preparation*

Silica was Zeosil 1165 (industrial grades for tire applications) from Solvay. The following ingredients were used as received: bis(3-triethoxysilylpropyl)tetrasulfide (TESPT) (Si69 Evonik), bis(3-triethoxysilylpropyl)disulfide (TESPD), ZnO (Zinc Oxide), Stearic acid (Sogis), (1,3-dimethyl butyl)-N'-Phenyl-p-phenylenediamine (6PPD) (Crompton), sulphur (Solfotecnica), N–tert-butyl-2-benzothiazyl sulfenamide (TBBS).

14.2. Synthesis of pyrrole compounds

14.2.1. *Synthesis of 2-(2,5-dimethyl-1H-pyrrol-1-yl)ethanol (EAP)*

A mixture of 2,5-hexanedione (3.9 g; 0.0342 mol) and ethanolamine (2.1g; 0.0342 mol) was poured inside a 250 mL round bottomed flask equipped with a magnetic stirrer and heated at 130°C for 2h. The product of the reaction was then cooled at room temperature. The final product obtained was a viscous liquid which weighed 4.012 g.

14.2.2. *Synthesis of 4-(2,5-dimethyl-1H-pyrrol-1-yl)aniline (p-PDAP)*

A recrystallization in water of p-Phenylenediamine was performed before the p-PDAP synthesis in order to purify the chemical which appeared partially oxidized.

3.8 g (0.035 mol) of Paraphenylenediamine and 4g (0.035 mol) of 2,5-hexanedione were poured in a 250 mL round bottomed flask equipped with a magnetic stirrer and a condenser. The temperature was set at 150°C and the mixture was left under stirring for 1h 30 min. Then, the reaction proceeded for 30 min at the same temperature without the condenser. Due to the high viscosity of the pyrrole and to its tendency to solidify almost instantaneously, acetone was used to recover the pyrrole from the bottom of the flask. Then it was boiled off and dried overnight. The final product was a brown/red solid and weighed 6.089 g.

14.2.3. *Synthesis of N^1-(2-aminoethyl)-N^2-(2-(2,5-dimethyl-1H-pyrrol-1-yl)ethyl)ethane-1,2-diamine (TETAP)*

2.92 g (0.02 mol) of triethylenetetramine and 2.29 g (0.02 mol) of 2,5-hexanedione were poured in a 250 mL round bottomed flask equipped with a magnetic stirrer and a condenser. The mixture was left to stir for 1h 30min at 150°C. After that time, the condenser was removed and the mixture was left under stirring at the same temperature for 30min to let the water evaporation. Then, the product was cooled at room temperature. The reaction product obtained was an amber viscous liquid weighing 3.6 g.

14.3. Functionalization of carbon black with pyrrole derivatives

14.3.1. *General procedure*

In a 250 mL round bottom flask carbon black N326 and a pyrrole derivative were dispersed in acetone and sonicated for 20 minutes at room temperature with a 2 L ultrasonic bath (260 W). Solvent was removed under reduced pressure using a rotary evaporator at 40°C and the macroscopic powders were grinded with a mortar.

The resulting grinded powder was added to a 3-neck round bottom flask. A thermocouple was inserted in the first neck to measure the temperature inside the flask. The second neck was provided with a rubber plug equipped with a glass needle for the air flux. A condenser was inserted in the third neck. The flask, equipped with a magnetic stirrer, was immersed in an oil bath at 180 °C or 160°C and it was left under stirring for 2 hours at 300 rpm under air flux.

After that time, the obtained powders were inserted inside a cotton thimble and a solvent extraction, using a Soxhlet apparatus, took place in order to remove the fraction of unreacted pyrrole derivative and impurities. Extraction was complete when the solvent near the thimble was clear.

This general procedure was applied to 10.00 g of CB N326 without any pyrrole derivative too. In this case a Soxhlet extraction was not needed, and it was done to make comparisons with the others adducts. CB N326 that was subjected to this procedure was designed as CB N326*.

In the Table below are reported the materials and the reaction conditions of each CB-PyC adducts synthesis reaction:

Table 14.1 Reagents and reactions conditions for the synthesis of CB-PyC adducts.

Adducts		**Reagents**	**Weight/g**	**Temperature[a]**	**Reaction time**	**Stirring**
1°	**CB/EAP**	CB N326	10.56	180°C	2h	300 rpm
		EAP	1.50			
	CB/p-PDAP	CB N326	10.20			
		p-PDAP	1.502			
	CB/TETAP	CB N326	19.99	160°C		
		TETAP	2.99			
2°	**CB/EAP**	CB N326	30.00			
		EAP	2.60			
	CB/p-PDAP	CB N326	30.00			
		p-PDAP	2.60			
	CB/TETAP	CB N326	30.00			
		TETAP	2.60			

a) Temperature of the oil bath.

14.3.2. *Soxhlet extraction*

A Soxhlet Extractor is characterized by three main sections: a percolator (boiler and reflux) where the solvent circulates, a thimble (usually made of thick filter paper), which retains the solid to be washed, and a siphon mechanism, that periodically empties the thimble.

Acetone was used as solvent and was heated to reflux at 80°C or 90 °C. The solvent vapor travels up to a distillation arm, and floods into the chamber containing the thimble of solid. The condenser ensures that any solvent vapor cools down, and drips back into the chamber containing the solid material. The chamber containing the solid material slowly fills with warm solvent. Some of the desired compound dissolves in the warm solvent. When the Soxhlet chamber is almost full, the chamber is emptied by a siphon. The solvent is returned to the distillation flask.

Extraction was carried out until no traces of PyC were detected in the Soxhlet apparatus. This means that the solvent in the extraction chamber was colourless since at least three extraction cycles. Soxhlet extraction required times which were variable between 14 and 18 hours.

The Soxhlet purification is schematized in the Figure below:

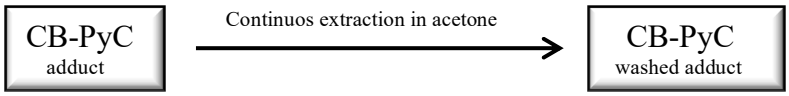

Figure 14.1 Schematic representation of a Soxhlet extraction.

14.4. Dispersions of CB-PyC adducts

14.4.1. *Water dispersions*

Aqueous dispersions of CB-PyC adducts and of CB N326* were prepared inserting 50 mg of powder in a test tube with 20 mL of distilled water. Each dispersion was sonicated for 30 min using an ultrasonic bath (260 W). After the sonication, the dispersions were stored for 72h at rest.

Stability of aqueous dispersions were qualitatively studied by visual inspections immediately after the sonication and 72 hours later. An aqueous dispersion was defined as stable when it was homogenous and unstable when the powder settled down.

14.4.2. *Solvents' dispersions*

The following solvents were tested: xylene, tetrahydrofuran (THF), 2-propanol, methanol, distilled water, acetone, hexane and ethyl acetate. Dispersions of CB-PyC adducts, CB N326* and pristine carbon black were prepared in glass tubes with a concentration of 1 mg/mL. Each dispersion was sonicated for 40 min using an ultrasonic bath (260 W). After the sonication, the dispersions were stored for one week at rest.

Qualitative evaluation of the dispersions' stability was performed through visual inspection immediately after the sonication and one week later. A dispersion was defined as stable when it was homogeneous and unstable when settling occurred.

14.5. Characterization Techniques

14.5.1. *Thermogravimetric analysis*

TGA under flowing N_2 (60 mL/min) were performed with a Mettler TGA SDTA/851 instrument according to the standard method ISO9924-1. Samples were heated from 30 to 300 °C at 10 °C/min, kept at 300 °C for 10 min, and then heated up to 550 °C at 20 °C/min. After being maintained at 550 °C for 15 min, they were further heated up to 900 °C at 10°C/min and kept at 900 °C for 30 min under flowing air (60 mL/min).

14.5.2. *Nuclear magnetic resonance*

One-dimensional H and C NMR spectra were measured at 400 and 100 MHz, respectively, using a Bruker AV 400 equipped with a 5 mm multinuclear probe with reverse detection. The solvent was chloroform deuterated and the temperature was 298 K. The experimental time for C NMR spectra was typically 15 min (corresponding to 1400 scans). Data were processed using TOPSPIN 1.1 or MestReNova.

14.5.3. *Gas Chromatography*

About 0.1 µL of the liquid mixture sample was dissolved in 1 mL of acetone. The resulting solution was injected into the gas chromatograph, GC-2010 Plus ATF (SHIMADZU). The column type was 95% dimethyl- and 5% diphenylpolycyloxane (phenomenex, ZB-5(phase)), with a length of 30 m. Helium (He) was the carrier gas at a constant flow rate of 1.2 mL/min. The GC was interfaced with 5973N Mass Selective Detector, G2577A Model, mass detector, from Agilent Technologies, operated under the EI mode (70 eV) using an autotune file.

14.5.4. pH determination of primary amines and pyrrole derivatives

100 mg of primary amines or pyrrole derivatives were dispersed in 10 mL of distilled water. The pH measurements were determined by inserting the sensor in the solution until the value was stable.

14.5.5. pH determination of pristine and modified carbon black

Aqueous dispersions of CB-PyC adducts, CB N326 and CB N326* were prepared dispersing 1.5 g of powder in 20 mL of distilled water. The mixture was stirred at room temperature at 300 rpm. The

pH measurements were determined by inserting the sensor in the heterogenous solution, left under stirring, until the value was stable.

14.5.6. Sonication

2 L ultrasonic bath (power 260 W) Soltec Sonica Ultrasonic Cleaner.

14.5.7 Elemental analysis

The analysis was carried out using a Costech ECS Mod. 4010 Elementary Analyzer which allows the simultaneous determination of C, H, N, S. The result is the arithmetic mean of the values resulting from the analysis of 3 specimens for each sample.

14.6. Characterization of rubber compounds

14.6.1. *Curing*

Curing reaction was performed at 170 °C for 10 min. A Monsanto oscillating disc rheometer (MDR 2000) (Alpha Technologies, Swindon, UK) was used, determining the minimum modulus M_L, the maximum modulus M_H, the modulus M_{final} at the end of the crosslinking reaction, the time T_{s1} required to have a torque equal to $M_L + 1$, the time T_{90} required to achieve 90 % of the maximum modulus M_H, and therefore to achieve the optimum of crosslinking.

14.6.2. *Stress-Strain tests*

The stress-strain behavior of the cured composites was investigated on a universal tensile testing machine (Zwick Roell Z010) following the Standard ISO 37/UNI 6065 with a clamp rate of 1 mm/min. The samples were fixed in pneumatic grips and stretched at constant feed until tensioned to failure. Ultimate tensile strength, modulus at 10% and 20% elongation and elongation at break were determined.

14.6.3. *Dynamic-mechanical test: Strain Sweep*

Tests were performed with a Monsanto R.P.A. 2000 rheometer in the torsion mode. The following procedure was applied: RPA was charged with 5.0 g of crude compound. A first strain sweep (0.1 - 25% shear strain amplitude) was performed at 50 °C and 1 Hz. Then, the sample was crosslinked at 170°C for 10 min at 17 Hz of frequency and, at the end of crosslinking, it was kept at 50°C for 10 minutes. Shear-dynamic mechanical properties were finally measured applying a 0.1-25% strain sweep at 10 Hz. Rubbers' dynamic-mechanical properties were evaluated calculating G', G'' and consequently Tan δ.

14.6.4. *Axial compression tests*

An Instron dynamic device was used to measure dynamic-mechanical properties in traction-compression mode. A cured test piece with a cylindrical shape (length=25 mm; diameter=12 mm) was kept at a prefixed temperature (10°C, 23°C and 70°C) for the whole test's duration. The sample underwent to compression-preloaded up to a 25% longitudinal deformation with respect to the initial length and then it was submitted to a dynamic sinusoidal strain with an amplitude of ±3.5% with respect to the length under pre-load, with a 100 Hz frequency. The rubber's dynamic-mechanical properties in compression were calculated in terms of dynamic storage modulus (E'), dynamic loss modulus (E'') and consequently loss factor (Tan Delta) values.

14.6.5 *Total crosslinking density*

In order to allow reagents' diffusion, samples were swollen in n-heptane for two days under nitrogen atmosphere. N-heptane was then drained and samples were washed with petroleum ether and dried under reduced pressure overnight at room temperature. Then samples, in a glass tube flashed with nitrogen and closed with a cap, were immersed in 200 mL of toluene. They were left in the dark for 72 hours to reach the equilibrium swelling state. Later samples were taken from the glass tube, removing the solvent by blotting the samples with a filter paper. Then, these were rapidly placed in a container and weighed. To remove the solvent, samples were dried for 24 hours under vacuum at 70 °C and weighed again, to obtain the weight of the dry network and the amount of absorbed solvent. In order to calculate the crosslink density, Flory-Rehner equation was used.

14.6.6 *Mono and di-sulfidic crosslinks measurement*

100 mg of the crosslinked composite and 100 mL of heptane were poured, in sequence, in a 200 mL beaker. The sample was left in heptane for 24 hours, without stirring. Then, 4 mL of piperidine and 3.8 mL of propanethiol were added and this mixture was left at room temperature. After 2 hours, the mixture was washed with 50 mL of heptane for three times and then it was filtered. The solid was left again in 50 mL of heptane. 24 hours later, the solvent was removed and the solid was washed with 50 mL of petroleum ether for three times. Then, it was filtered using a vacuum pump. The solid obtained was left in petroleum ether (50 mL) for 2 hours, then was filtered and dried under vacuum for 24 hours. In order to achieve the equilibrium swelling state, the resulting sample was immersed in 200 mL of toluene for 72 hours.

14.7. Composite preparation

14.7.1. *Rubber compounds filled with only CB*

40 phr of Natural Rubber and 60 phr of poly(1,4-butadiene) (BR) were inserted into the internal mixer brabender® at T = 100°C for 1 minute. Then CB (pristine or modified with pyrrole derivatives) was added and mixed for 3 min at 100°C and 60 rpm. The composite was then discharged at T = 100°C.Then, the internal mixer's temperature was lowered at 50°C. The composite obtained in the previous step was added and mixed for 1 min at 60 rpm. After that, stearic acid, zinc oxide and 6PPD (N-(1,3-dimethylbutyl)-N'-phenyl-p-phenylenediamine, an antioxidant agent) were added and mixed for 2 min at 50°C and 60 rpm. Then TBBS (N-tert-butyl-2-benzothiazyl sulfenamide) and sulfur were added and mixed for 2 min (50°C, 60 rpm). Finally, the compound was discharged at 50°C.

14.7.2. *Rubber compounds filled with both CB and silica*

60 phr of poly(1,4-butadiene) (BR) and 40 phr of Natural Rubber were fed into a brabender® internal mixer and masticated at 130°C (or 140°C for SEV composites) for 1 minute. Silica and silane were added and mixed for 4 minutes. The obtained compound was unloaded at 130°C (or 140°C for SEV). Then, the temperature was set at 80°C (100°C in case of SEV compounds) and the obtained composite was fed into the internal mixer and masticated for 1 minute. Carbon black (pristine or modified with pyrrole derivatives) was added and mixed for a further 3 minutes, then unloaded at 80°C (100°C for SEV). This composite was fed again into the internal mixer at 50°C, adding ZnO, stearic acid and 6PPD and mixed for 2 minutes. Sulfur and TBBS (N-tert-butyl-2-benzothiazyl sulfenamide) were then added, mixing for a further 2 minutes. The composite was unloaded at 50°C.

14.7.3. *Rubber compounds filled with both CB and silica: different mixing*

A brabender® internal mixer was charged with 60 phr of poly(1,4-butadiene) (BR) and 40 phr of Natural Rubber. Elastomers were masticated at 140°C for 1 minute. 50% of silica, silane TESPD and carbon black (pristine or functionalized) were added and mixed. The obtained compound was unloaded at 140°C after 4 minutes. The temperature was now set at 100°C and the obtained composite was fed into the internal mixer and masticated for 1 minute. The remaining 50% of silica, silane TESPD and carbon black (pristine or modified with pyrrole derivatives) was fed and mixed for a further 3 minutes, then unloaded at 100°C. Then, the temperature was set at 50°C and the compound was fed again into the internal mixer, adding ZnO, stearic acid and 6PPD and mixed. After 2 minutes, sulfur and TBBS (N-tert-butyl-2-benzothiazyl sulfenamide) were added, mixing for a further 2 minutes. The composite was finally discharged at 50°C.

Chapter 15

Conclusions

Objective of this thesis was the preparation of elastomeric composites with an improved crosslinking efficiency, a better compatibility between carbon black and silica and a lower dissipation of energy, thanks to the use of a functionalized carbon black.

Carbon black was functionalized with new pyrrole compounds (PyC) and CB/PyC adducts were prepared. In particular, pyrrole compounds able to bring bases onto the surface of CB were selected. Pyrrole derivatives were synthesized through the Paal-Knorr reaction between a primary amine and 2,5-hexanedione. In particular, the following pyrrole compounds were synthesized: triethylenetetramine pyrrole (TETAP), p-phenylenediamine pyrrole (p-PDAP), mono-ethanolammine pyrrole (EAP). These are represented in Figure 15.1.

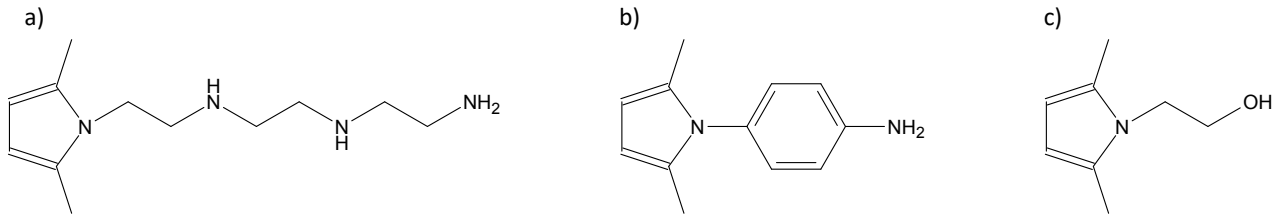

Figure 15.1 a) triethylenetetramine pyrrole (TETAP), b) p-phenylenediamine pyrrole (p-PDAP), c) mono-ethanolammine pyrrole (EAP).

TETAP and p-PDAP were used in the light of the above mentioned objective: to have bases on carbon black. EAP was used for the sake of comparison.

CB/PyC adducts were obtained by simply mixing and providing thermal energy, adopting the principles of green chemistry: both for the adducts and for the pyrroles' derivatives synthesis, solvents or catalysts were not used.

CB/PyC adducts were investigated by means of pH measurements in water dispersions and through the evaluation of Hansen solubility parameters. A basic pH was measured for CB/TETAP and an appreciable modification of the adducts' solubility parameter was found. These findings lead to suppose that CB/PyC are able to establish different interactions with the rubber compound surroundings with respect to the pristine carbon black.

Elastomeric compounds, based on diene elastomers and CB/PyC adducts were prepared. Natural rubber and butadiene rubber were selected as elastomers. A furnace carbon black (CB N326) and silica Zeosil 1165 were used as the reinforcing fillers.

The behavior of functionalized carbon black was studied in total or partial replacement of the pristine CB, in compounds with CB as the only filler or with the hybrid CB/silica filler system.
Rubber composites were prepared through melt blending, were crosslinked with a sulfur-based system and were characterized through dynamic-mechanical and tensile tests. Two types of vulcanization systems were used: conventional (with higher sulphur/accelerator ratio) or semi-efficient (with lower sulphur/accelerator ratio).

NR/BR-based composites with carbon black as the only filler
CB, pristine or functionalized with TETAP, was used as filler. The pyrrole derivative was also fed as such in a compound in order to investigate the effect of the immobilization on the CB surface. Two different vulcanization systems were used: conventional and semi-efficient.
Faster vulcanization kinetics, higher torque values, reduction of Payne effect, lower hysteresis, higher stiffness and lower ultimate properties, with respect to the composite with pristine CB, were obtained in compounds with CB/TETAP.
The compound with the pyrrole derivative fed as such showed faster crosslinking kinetics, lower Payne effect, higher hysteresis and lower stiffness compared to the reference composite. Larger elongations and energy at break were also measured with respect to compounds with functionalized fillers.
Differences between conventional and semi-efficient curing system were observed. The effect of CB/TETAP appears to be larger in presence of a larger amount of sulphur.

NR/BR-based composites with CB/silica as the hybrid filler system. Conventional vulcanization system
Three different adducts were used, functionalized with the pyrrole derivatives reported in Figure 15.1. CB/TETAP leaded to faster vulcanization kinetics, larger dynamic-mechanical rigidity and lower hysteresis. Lower effects were found when CB/p-PDAP and, in particular, CB/EAP were used.

NR/BR-based composites with CB/silica as the hybrid filler system. Semi-efficient vulcanization system
Two different preparation procedures were applied. In one case, CB/PyC was added to a rubber masterbatch that contained a silanized silica. In the other case, CB/PyC was fed together with silica and the silane. The preparation procedure did not influence the vulcanization properties and the Payne effect, while hysteresis reduction, a decrease in stiffness and better tensile properties were favored by the CB-unsilanized silica interaction.

In a nutshell

CB functionalized with a pyrrole compound with a basic nature has clear effect on the properties of a rubber compound, based either on CB as the only filler or on CB/Silica as the hybrid filler system. The key role is played by the anchoring of the pyrrole compound onto the CB surface.

Main results were: increased viscosity, to indicate the tendency of the adducts to interact and form agglomerates, faster vulcanization kinetics, higher stiffness, and poor ultimate properties. Payne effect's reduction and lower hysteresis were also observed: CB/PyC can be used in compounds for lower fuel consumption and CO_2 emissions.

Two hypotheses can be made:

(i) the effect of the base occurs in the proximity of CB and a dense crosslinking network frames the filler, emphasizing its reinforcing effect.

(ii) sulphur, activated by the presence of the base, reacts with the surface of carbon black, creating a hybrid crosslinking network which involves the filler and achieving the ultimate goal for a filler, the covalent bond with the rubber chains.

Appendix

HSP.m

```
% A Simple Program To Calculate Hansen Solubility Parameters
% Farhad Gharagheizi & Mahmood Torabi Angaji, % Department of Chemical Engineering,
% Faculty of Engineering, University of Tehran.
% 30 September, 2005.
clc
clear all
Solvents_Database;
delta_d1⁄4(data(:,1))';
delta_p1⁄4(data(:,2))';
delta_h1⁄4(data(:,3))';
solubility1⁄4(data(:,4))';
a(1)1⁄4mean(delta_d);
a(2)1⁄4mean(delta_p);
a(3)1⁄4mean(delta_h);
a(4)1⁄4sqrt(a(1)^2þa(2)^2þa(3)^2);
guess=a;
options=optimset('Display','off');
res=1;
while res>1e-4;
[delta res]=fminsearch(@QF,guess,options,delta_d, delta_p,delta_h,. solubility,n);
guess=delta;
end
d_d1=delta(1); d_p=delta(2); d_h=delta(3); R_o=delta(4); R_a=sqrt(4*(d_d-delta_d).^2 +(d_p-
delta_p).^2 + (d_h-delta_h).^2);
RED=(R_a/R_o);
clc
disp('***********************************************************')
disp('Delta_d Delta_p Delta_h Solub RED')
disp('***********************************************************')
disp([delta_d' delta_p' delta_h' solubility' RED'])
disp('Data Fit ==')
Data_Fit=1+QF(delta,delta_d,delta_p,delta_h, solubility,n);
```

```
disp(Data_Fit)
disp('Delta_d Delta_p Delta_h R_o')
disp([d_d d_p d_h R_o])
```

QF.m

```
function y=QF(x,delta_d,delta_p,delta_h,solubility,n)
d_d=x(1);
d_p=x(2);
d_h=x(3);
R_o=x(4);
R_a=sqrt(4*(d_d-delta_d).^2 + (d_p-delta_p).^2 +(d_h-delta_h).^2);
for i=1:n,
if                                                                    R_a(i)>R_o;
if solubility(i)==0;
A(i)=1;
else
A(i)=exp(R_o-R_a(i));
end
else                                                                  R_a(i)<R_o;
if solubility(i)==0;
A(i)1⁄4exp(R_a(i)-R_o);
else
A(i)=1;
end
end
end
y=abs(((prod(A))^(1/n))1);
```

Solvent_Database.m

```
%Numbr of Solvents n = 41;
% delt_d delta_p delta_h Solub
[18.0 12.3 7.2 1.0;
17.4 13.7 11.3 1.0;
19.6 8.6 3.7 1.0;
18.2 6.3 6.1 1.0;
```

18.4 16.4 10.2 0;
19.0 16.6 7.4 1.0;
19.0 7.4 4.1 0;
16.6 8.2 7.4 0;
19.2 6.3 3.3 0;
16.8 5.7 8.0 0;
15.8 8.2 10.8 0;
16.0 9.0 5.1 0;
15.5 10.4 7.0 0;
16.2 12.1 4.1 0;
16.2 9.2 14.3 0;
20.0 18.0 4.1 0;
17.4 4.1 13.5 0;
17.8 3.1 5.7 0;
18.0 3.1 5.3 0;
19.0 1.8 7.4 0;
15.8 5.3 7.2 0;
16.0 5.1 12.3 0;
19.0 4.3 2.0 0;
16.0 15.5 4.5 0;
16.2 9.2 16.4 0;
15.8 3.7 6.3 0;
16.0 5.7 15.8 0;
15.3 6.1 4.1 0;
15.8 18.8 5.1 0;
18.0 1.4 2.0 0;
15.8 8.8 19.4 0;
16.6 12.0 20.7 0;
18.4 0 2.0 0;
14.5 2.9 5.1 0;
17.0 15.5 21.2 0;
17.8 0 0.6 0;
16.8 9.4 23.3 0;
15.1 12.3 22.3 0;

14.9 0 0 0;

17.0 11.0 26.0 0;

17.2 26.2 19.0 0;]